Title

OBSERVATION OF FORWARD PEAKS IN n+n ->K|Y*+(l385) AND IN RELATED SINGLE-MESON-EXCHANGE-PORBIDDEN REACTIONS

Author

Hoch, Paul L.

Publication Date

1972-10-01

LBL-1052

OBSERVATION OF FORWARD PEAKS IN $\pi^+ n \to K^0 Y^{*+}(1385)$ AND IN RELATED SINGLE-MESON-EXCHANGE-FORBIDDEN REACTIONS

Paul L. Hoch
(Ph. D. Thesis - Part 2)

October 16, 1972

Prepared for the U.S. Atomic Energy Commission under Contract W-7405-ENG-48

LBL-1052

DISCLAIMER

OBSERVATION OF FORWARD PEAKS IN $\pi^+ n \to K^0 Y^{*+}(1385)$ AND IN RELATED SINGLE-MESON-EXCHANGE-FORBIDDEN REACTIONS

[This report is Chapter 3 of a Ph. D. thesis,]
[the other parts of which are LBL Reports LBL-1051 and LBL-1053.]

CONTENTS

[Continued]

[Contents - continued]

OBSERVATION OF FORWARD PEAKS IN $\pi^+ n \to K^0 Y^{*+}(1385)$ AND IN RELATED SINGLE-MESON-EXCHANGE-FORBIDDEN REACTIONS

Paul L. Hoch

Lawrence Berkeley Laboratory
University of California

ABSTRACT

We have studied the production of decuplet-baryon resonances [$Y_1^*(1385)$, $\Xi^*(1530)$, and $\Delta(1236)$] in reactions which cannot proceed by the exchange of any single known meson. We have examined these exotic exchange reactions at incident momenta ranging from 1.8 to 4 GeV/c, using data from several bubble chamber exposures. In all but one of the reactions studied, there is significant "forbidden" forward peaking. At roughly 2 to 3 GeV/c, the cross section in the forward direction is 2 to 7 μb/sr for $\pi^- p \to K^+ Y^{*-}$ and $K^- p \to K^+ \Xi^{*-}$, ≈20 μb/sr for $K^- p \to \pi^+ Y^{*-}$, and ≈100 μb/sr for $\pi^- p \to \pi^+ \Delta^-$; no peak is seen in $K^- p \to K^0 \Xi^{*0}$. A decrease with energy is evident. The data is presented at length, to establish the existence of the forbidden peaking in final states which are dominated by other features; production and decay distributions are given.

Various possible explanations of forbidden peaking are reviewed. We argue that Berger's model does not explain away the peaking as a kinematic reflection. Recent work suggests that two-meson exchange may provide an explanation. We also consider the possible roles of exchange of a single (exotic) meson and of direct-channel resonance formation.

3.1 INTRODUCTION

3.11 GENERAL REMARKS

This report is essentially an expanded version of two published Letters, in which we reported forward peaking in $\pi^+ n \rightarrow K^0 Y^{*+}$ and in other decuplet-baryon production reactions whose t-channel quantum numbers forbid the exchange of any known (i.e., non-exotic) meson.[91,92] The data analysis which has been done since those papers were completed has not altered the results. This chapter does present the analysis in considerably more detail, and includes many additional figures. In Section 3.3 we have expanded the discussion of various possible interpretations of the effect, taking note of recently published experimental and theoretical work. Our opinion on the most probable explanation has changed somewhat; two-meson exchange now seems most likely to explain this phenomenon. For a summary of the data presented here, the reader is referred to Section 3.4.

3.12 HISTORICAL BACKGROUND

The one-particle-exchange model has been remarkably successful in describing two-body and quasi-two-body reactions at moderate and high energies. The most prominent feature of many such reactions is a c.m. production cosine distribution that is markedly forward peaked. In naive terms, the one-meson-exchange model suggests that the target or beam emits a virtual meson which is captured by the other particle. The corresponding amplitude has a propagator with a pole where the transferred four-momentum is equal to the mass of the exchanged particle; this leads to peaking in the forward direction (i.e., at small momentum transfer). (Backward peaking can similarly be associated with baryon exchange.)

Especially when modified by absorption corrections, this model has provided a good description of the production distribution of many reactions. Decay correlations of resonances produced by one-particle-exchange (OPE) can be interpreted in terms of the spin and angular momentum information carried by the exchanged particle. The OPE model has been extended to cover the exchange of Regge trajectories, corresponding to families of particles; the properties of the trajectories have been deduced from their exchanges. Duality arguments have allowed the use of exchange models to describe (at least in an average sense)

reactions which appear to be dominated by, and can be described simply in terms of, direct-channel resonances. Finally, we note that one can use extrapolation techniques to extract information on real particle scattering from an exchange-dominated reaction, with the virtual exchanged particle acting as a target.

The simple OPE model is applicable in a negative sense to reactions where the quantum numbers in a crossed channel prohibit the exchange of a single particle. For example, the reaction $\pi^- p \rightarrow K^+\Sigma^-$ is, in the t-channel, $p\bar{\Sigma}^+ \rightarrow K^+\pi^+$. Since the exchange process conserves charge, strangeness, and baryon number, one-meson exchange would require a particle or resonance with the quantum numbers of a $K^+\pi^+$ resonance (S=1, B=0, Q=2); none such is known to exist. When we began our study, the reported evidence on such single-meson-exchange-forbidden reactions was essentially confined to reactions, such as this one, where a member of the $J^P = 1/2^+$ baryon octet is produced. Experimentally, forward peaking in such reactions was known to be very small or absent. This was occasionally cited as indirect evidence that the mesons which would have to be exchanged, and had not been observed directly, in fact did not exist.[93]

We studied the counterpart of the reaction $\pi^- p \rightarrow K^+\Sigma^-$ with a member of the $3/2^+$ baryon decuplet produced,

$$\pi^- p \dashrightarrow K^+ Y^{*-}(1385)$$

and its charge-symmetric equivalent

$$\pi^+ n \dashrightarrow K^0 Y^{*+}(1385).$$

We have also studied additional decuplet-production reactions, using data from old Berkeley bubble chamber experiments. Attention had been focused on other, more prominent, features of the final states fed by these reactions, and little consideration had been given to the possibility of forbidden forward peaking.

Since the publication of our results and other experimental studies, it is recognized that, at the very least, the evidence against the exchange of these unknown mesons is weak. There is now quite a bit of interest in exotics. This report attempts to provide an up-to-date (but not necessarily complete) review of recent theoretical models for these forbidden reactions. The experimental situation has been summarized in a review by Rosner.[94] We note that the reaction $\pi^- p \rightarrow K^+ Y^{*-}$ has now been studied by other researchers; it and other forbidden decuplet-production reactions have been looked for at energies higher than ours.[95-99]

3.13 TERMINOLOGY AND DEFINITIONS

If the above-mentioned reactions were to proceed by one-meson exchange, the mesons would have to be members of a multiplet with S = 1 and I = 3/2. (That is, "K^{*++}", "K^{*+}", "K^{*0}", and "K^{*-}" (not "$\bar{K}^{*-}$").) Such mesons are generally referred to as exotic. Since the hypothesized quark q has quantum numbers I = 1/2, S = 0 or I = 0, S = 1, this multiplet can not be constructed out of $q\bar{q}$. All established mesonic states can be put into the $\underline{1}$ and $\underline{8}$ representations of SU(3); those are the representations generated by $q\bar{q}$. The states which in this chapter we refer to as exotic would require a larger SU(3) multiplet and would have to be constructed out of $qq\bar{q}\bar{q}$.

Rosner distinguishes two additional types of exotic mesons.[94] "Type 2 exotics" have J^{PC} which cannot be accounted for by $q\bar{q}$ with orbital angular momentum. "Type 3 exotics" would be "extra" low-mass states with allowed quantum numbers which do not fit into the established multiplets and whose existence would imply non-harmonic $q\bar{q}$ forces. We use "exotic" to mean Type 1.

Rosner's review covers the experimental evidence on all three types of exotics. Since no exotic mesons or baryons have been established in production or formation experiments, we call an exchange process "forbidden" if it is forbidden in the absence of type-1 exotics.

If exotics do exist and are exchanged, the process obviously should be referred to as "exotic meson exchange." However, we will avoid using "exotic exchange" as an abbreviation for this. One may argue that exchange of two known mesons in a reaction whose t-channel quantum numbers are exotic may be referred to as exotic exchange. As we shall see, although two-meson exchange is expected to occur, it is interesting enough so that the label "exotic" is not inappropriate.

We will use the abbreviations OME [OBE, OPE] for one-meson [baryon, particle] exchange, and DME for double-meson (i.e., two-meson) exchange.

Our production cosine will be the cosine of the angle between the beam and the outgoing meson in the overall c.m. frame. Thus, "forward" and "peripheral" correspond to meson-exchange diagrams, and "backward" corresponds to baryon exchange.

Unless otherwise specified, Y^*, Δ (or N^*), and Ξ^* refer to the members of the $3/2^+$ decuplet: $\Sigma(1385)$, $\Delta(1236)$, and $\Xi(1530)$.

3.14 LISTS OF REACTIONS AND FINAL STATES

For convenient reference, we list here all the reactions given more than passing mention in this chapter. First we present *all* OME-forbidden reactions of the form

$(\pi^{\pm}$ or $K^-)$ + (p or n) ---> (0^- octet meson) + ($3/2^+$ decuplet baryon).

We denote charge-symmetric pairs by (for example) "(1p)" and "(1n)"; references to "Reaction (1)" are to the pair considered together. The t-channel quantum numbers are indicated.

[b N ---> M B*]	$\lvert S_t \rvert$	$\lvert Q_t \rvert$	I_t	
$\pi^- p \longrightarrow K^+ Y^{*-}$	1	2	3/2	(1p)
$\pi^+ n \longrightarrow K^o Y^{*+}$	1	1	3/2	(1n)
$K^- p \longrightarrow \pi^+ Y^{*-}$	1	2	3/2	(2)
$K^- p \longrightarrow K^+ \Xi^{*-}$	2	2	1	(3)
$K^- p \longrightarrow K^o \Xi^{*o}$	2	1	0,1	(4)
$K^- n \longrightarrow K^o \Xi^{*-}$	2	1	0,1	(5)
$\pi^- p \longrightarrow \pi^+ \Delta^-$	0	2	2	(6p)
$\pi^+ n \longrightarrow \pi^- \Delta^{++}$	0	2	2	(6n)

We have not studied Reaction (5). We report on data from several LBL bubble chamber experiments for the other reactions.

Next we list the final states for each of the reactions on which we present data. A spectator proton is denoted by "(p)."

Reaction	Final State [M π B]	
(1p)	$\pi^- p \longrightarrow K^+ \pi^- \Lambda$	(7)
(1n)	$\pi^+ d \longrightarrow (p) K^o \pi^+ \Lambda$	(8)
(2)	$K^- p \longrightarrow \pi^+ \pi^- \Lambda$	(9)
(3)	$K^- p \longrightarrow K^+ \pi^o \Xi^-$	(10)
(3)	$K^- p \longrightarrow K^+ \pi^- \Xi^o$	(11)
(4)	$K^- p \longrightarrow K^o \pi^+ \Xi^-$	(12)
(6p)	$\pi^- p \longrightarrow \pi^+ \pi^- n$	(13)
(6n)	$\pi^+ d \longrightarrow (p) \pi^- \pi^+ p$	(14)

For comparison with our results, we will refer to the octet-baryon reactions corresponding to (1) through (5):

$\pi^- p \longrightarrow K^+ \Sigma^-$ (15p)

$\pi^+ n \longrightarrow K^o \Sigma^+$ (15n)

$$K^- p \longrightarrow \pi^+ \Sigma^- \quad (16)$$

$$K^- p \longrightarrow K^+ \Xi^- \quad (17)$$

$$K^- p \longrightarrow K^0 \Xi^0 \quad (18)$$

$$K^- n \longrightarrow K^0 \Xi^- \quad (19)$$

Finally, we take this opportunity to point out that there are other classes of accessible OPE-forbidden reactions. (See Ref. 94 for a survey of the data.) For example, these reactions are forbidden both forward (i.e., with the first final-state particle having low momentum transfer from the beam) and backward:

$$\bar{p} p \longrightarrow \bar{\Sigma}^+ \Sigma^-, \text{ or } \bar{\Xi}^+ \Xi^- \quad (20)$$

$$\bar{p} p \longrightarrow \bar{Y}^{*+} \bar{Y}^{*-}, \text{ or } \bar{\Xi}^{*+} \Xi^{*-}, \text{ or } \bar{\Delta}^+ \Delta^- \quad (21)$$

When our work was published, a small number of events had been reported in these reactions and the possibility of forbidden exchanges had been tentatively raised.[100-101]

The reaction

$$p n \longrightarrow \Delta^- \Delta^{++} \quad (22)$$

is forbidden with the Δ^- forward; in Section 3.322 we will comment on a recent study of this reaction.

The reactions

$$K^- p \longrightarrow p K^- \quad (23)$$

and

$$\bar{p} p \longrightarrow p \bar{p} \quad (24)$$

are dominated by allowed meson exchange mechanisms; however, with the first-written final-state particle going forward, exchange of an exotic baryon would be required.

3.2 DATA

3.21 SUMMARY OF THE BASIC RESULTS

In this section we identify our data samples, show plots establishing the existence of forbidden forward peaking in 4 of the 5 reactions, and present our results for the production angular distributions. In Section 3.22 we discuss in detail the sources of the data and the cuts applied, and explain in each case how we got the shape and normalization for the production distribution. Additional results are presented in Sections 3.23 and 3.24.

Table 3.1 gives the number of events in the uncut data for the 5 reactions we have studied, each at 2 or 3 beam momenta. The precise meaning of the momentum indicated (in GeV/c) for each of the 12 Samples is given in Section 3.22; generally several beam momenta have been combined. Our data comes from several different LBL experiments, all using the 72-inch bubble chamber at the Bevatron. Here we have combined charge-symmetric $\pi^- p$ and $\pi^+ n$ states, and the two $(\Xi\pi)^-$ states; results from these subsamples separately (which are generally consistent, as expected) are given in Section 3.24.

In order to refer to all the reactions together, we will denote them by "bN→MπB", where $B^* \to B\pi$ is the decuplet baryon resonance and the beam-to-meson production cosine is given by $\cos\theta_{pr} = (\hat{b}\cdot\hat{M})$. We will use "Fig. 3.n$^+$" to refer to Figures 3.n through 3.(n+11), corresponding to Sample (1) through Sample (12).

Our basic results are shown in Fig. 3.1$^+$ [3.1 through 3.12]. Fig. 1$^+$(a) is a plot of the Bπ effective mass against the production cosine. [Such a plot will be refered to as a Chew-Low-like plot. We have chosen to display m(Bπ) rather than $m^2(B\pi)$, and to show $\cos\theta_{pr}$ rather than the corresponding momentum transfer so that when several beam momenta are combined the backward direction lies on a single kinematic boundary.] Fig. 1$^+$(b) is the Dalitz plot for forward-produced events ($\cos\theta_{pr} > 0.7$). Fig. 1$^+$(c) gives the production angular distribution as obtained from a cut in m(Bπ), with a background subtraction using events in adjacent m(Bπ) bins.

We see that a B^* resonance band is present (for some values of $\cos\theta_{pr}$) in each sample, and that there is some B^* in the forward direction in most cases. The possible exceptions are Sample 9, where there is essentially no forward Ξ^{*o} production, and Samples 10 through 12, where Δ production is not readily distinguishable from a broad enhancement which crosses the plot from the region

Sample	UNCUT DATA Reaction	Events
1	P~2 $\pi^-p\to K^+\pi^-\Lambda$ (& $\pi^+n\to K^0\pi^+\Lambda$)	1958
2	P~3 $\pi^-p\to K^+\pi^-\Lambda$ (& $\pi^+n\to K^0\pi^+\Lambda$)	2089
3	P~4 $\pi^-p\to K^+\pi^-\Lambda$ (& $\pi^+n\to K^0\pi^+\Lambda$)	930
4	P=2.1 GeV/c $K^-p\to\pi^+\pi^-\Lambda$	4424
5	P~2.6 GeV/c $K^-p\to\pi^+\pi^-\Lambda$	6519
6	P=2.1 GeV/c $K^-p\to K^+\pi^{0,-}\Sigma^{-,0}$	348
7	P~2.6 GeV/c $K^-p\to K^+\pi^{0,-}\Sigma^{-,0}$	1024
8	P=2.1 GeV/c $K^-p\to K^0\pi^+\Sigma^-$	379
9	P~2.6 GeV/c $K^-p\to K^0\pi^+\Sigma^-$	697
10	P<1.8 $\pi^+n\to\pi^-\pi^+p$	9676
11	P~2.2 $\pi^-p\to\pi^+\pi^-n$ (& $\pi^+n\to\pi^-\pi^+p$)	19453
12	P=3.2 $\pi^-p\to\pi^+\pi^-n$	2545

Number of Events in Samples 1 through 12 (Raw Data)

Table 3.1

P~2 GeV/c $\pi^-p \to K^+\pi^-\Lambda$ (& $\pi^+n \to K^0\pi^+\Lambda$) (Sample 1)

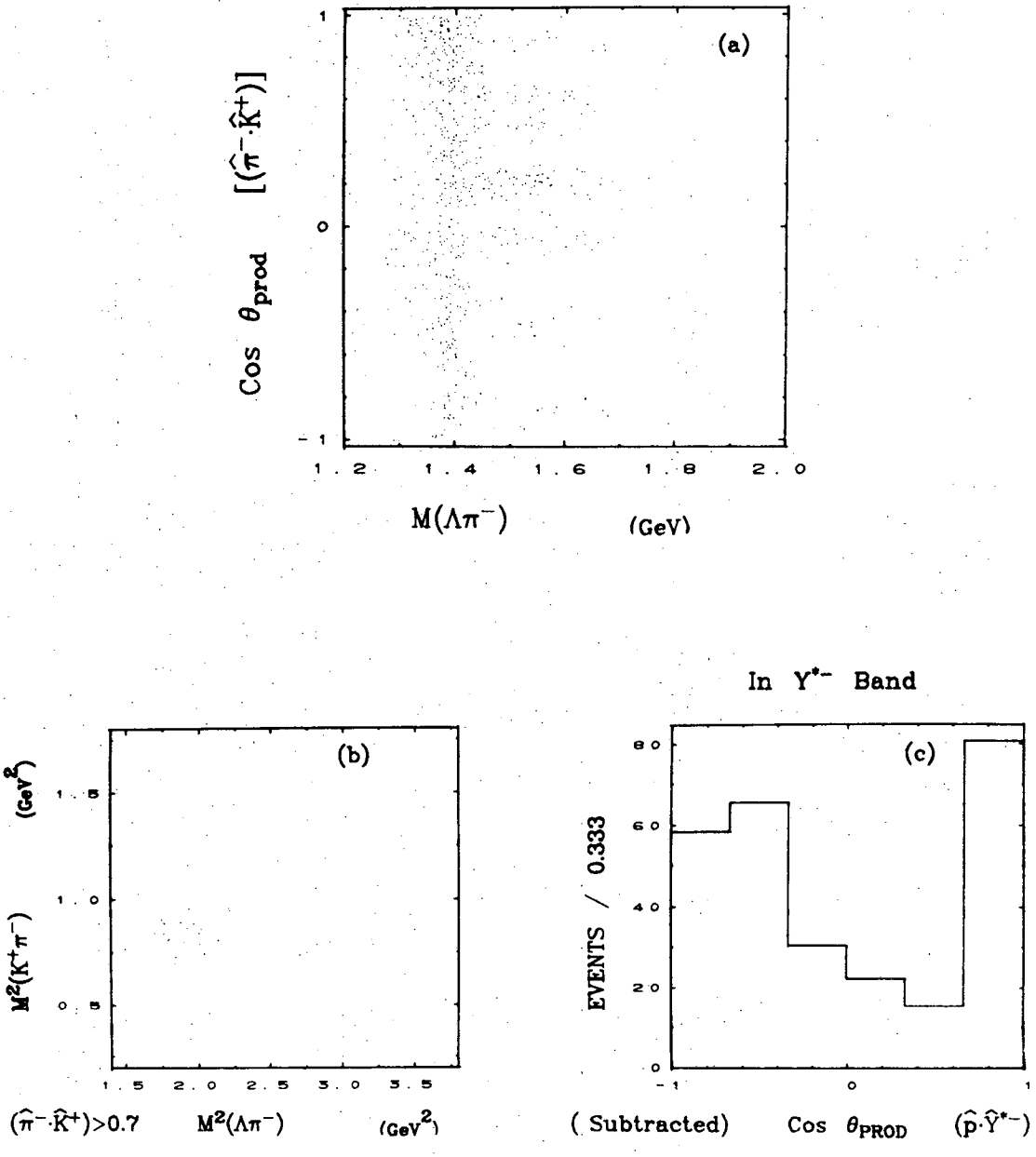

XBL 729-1713

Fig. 3.1

P~3 GeV/c $\pi^- p \to K^+ \pi^- \Lambda$ (& $\pi^+ n \to K^0 \pi^+ \Lambda$) (Sample 2)

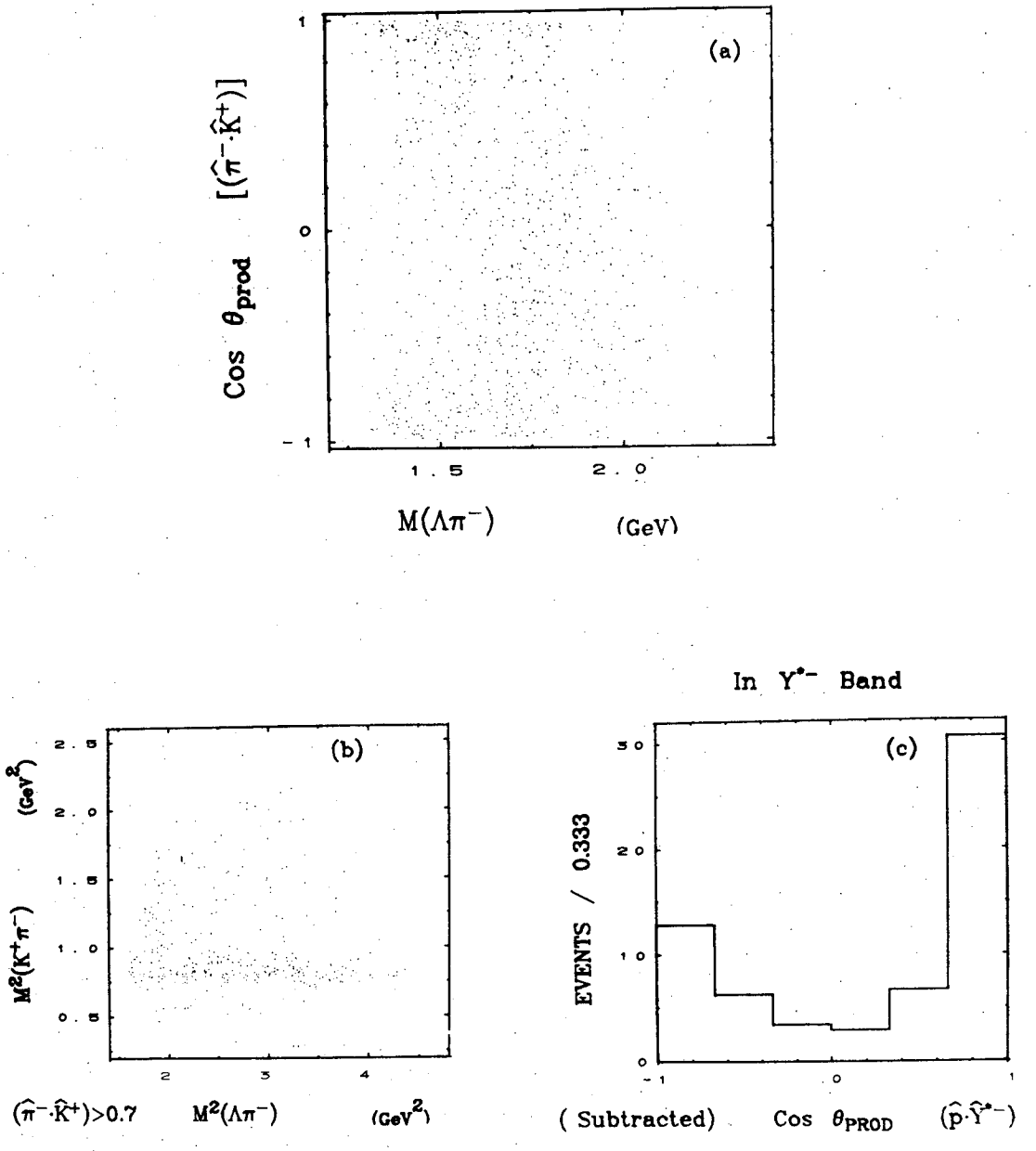

XBL 729-1714

Fig. 3.2

P~4 GeV/c $\pi^-p \to K^+\pi^-\Lambda$ (& $\pi^+n \to K^0\pi^+\Lambda$) (Sample 3)

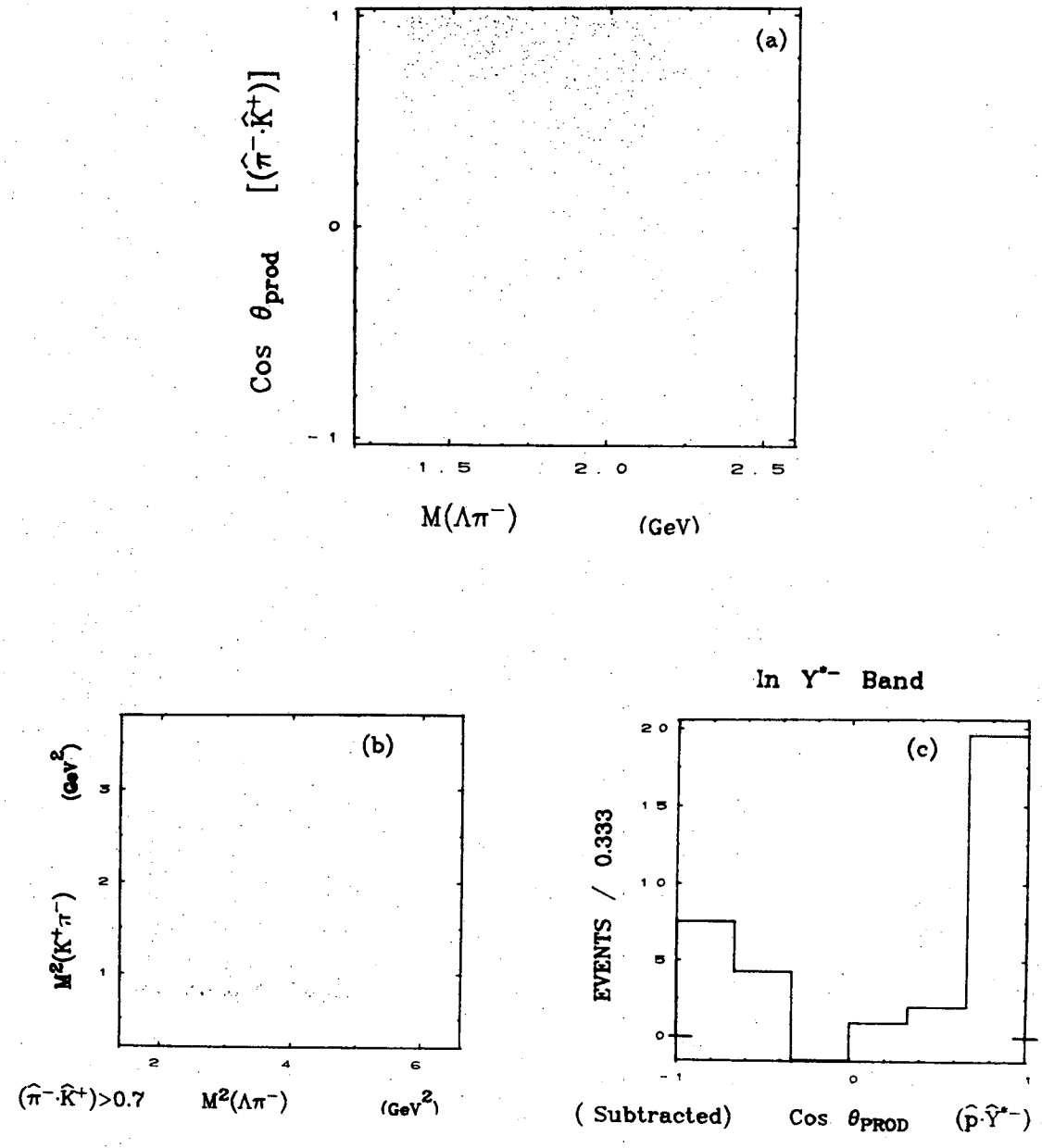

XBL 729-1715

Fig. 3.3

P=2.1 GeV/c $K^-p \to \pi^+\pi^-\Lambda$ (Sample 4)

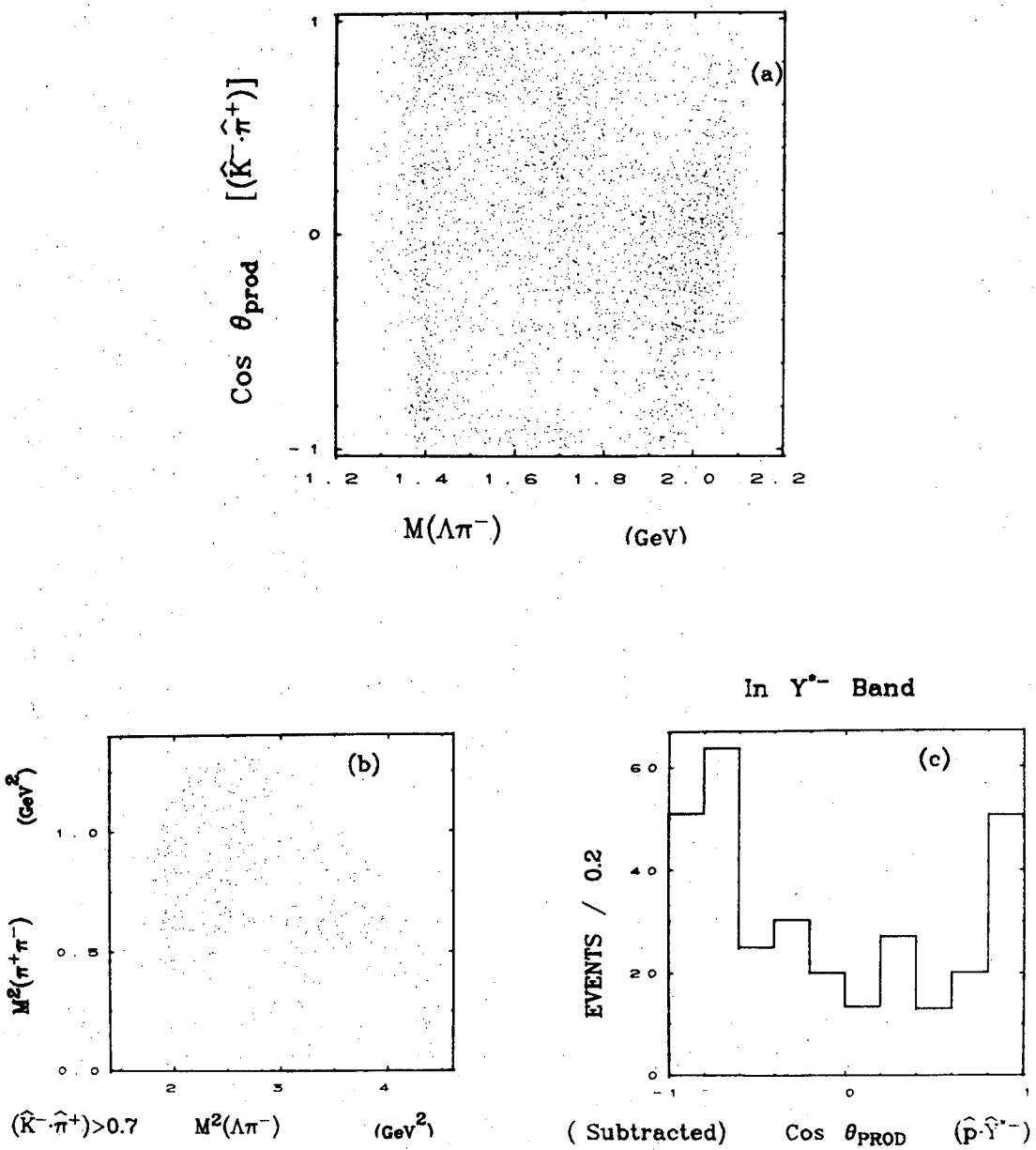

XBL 729-1716

Fig. 3.4

P~2.6 GeV/c $K^-p \to \pi^+\pi^-\Lambda$ (Sample 5)

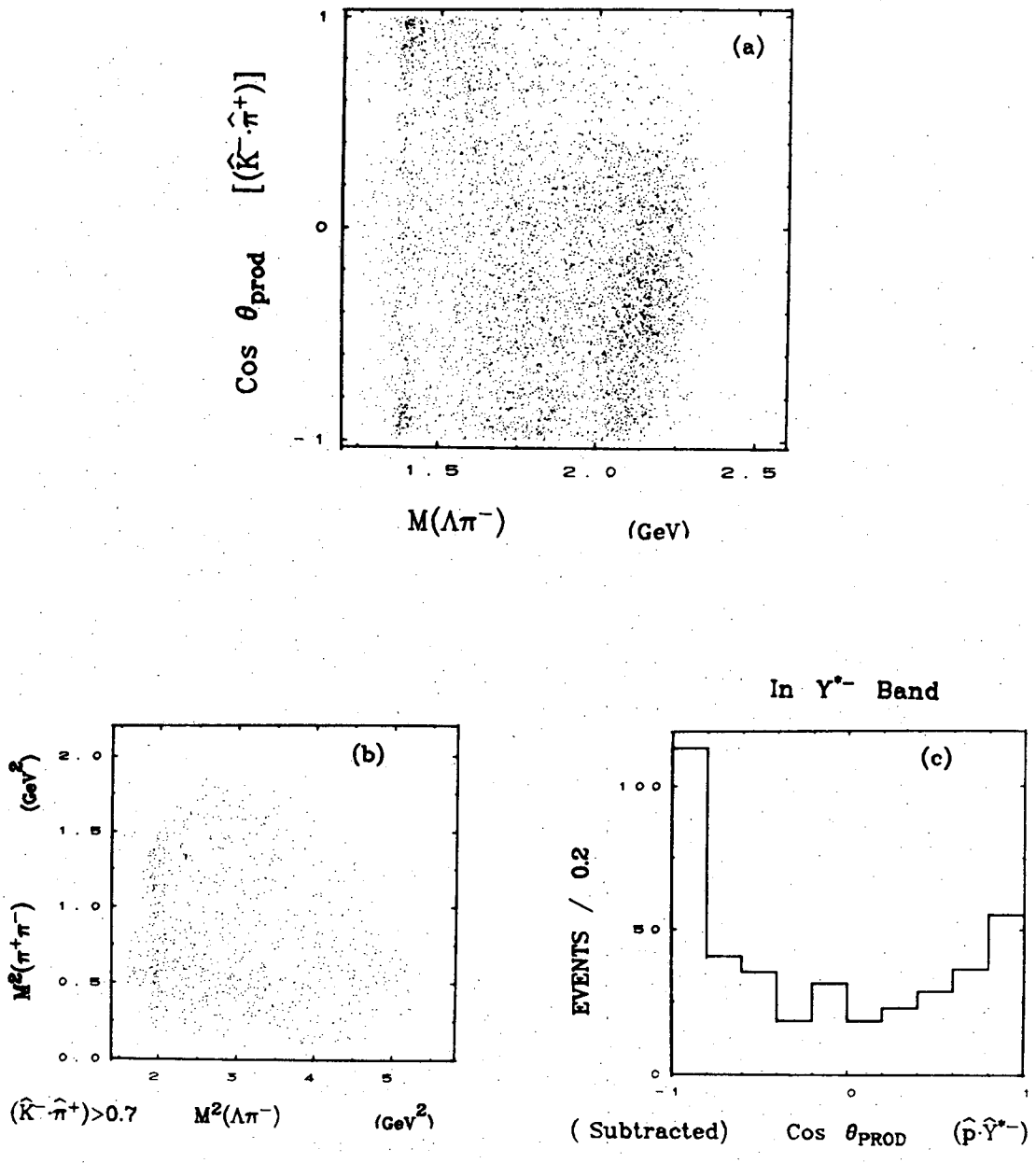

XBL 729-1717

Fig. 3.5

P=2.1 GeV/c $K^-p \to K^+\pi^{0,-}\Xi^{-,0}$ (Sample 6)

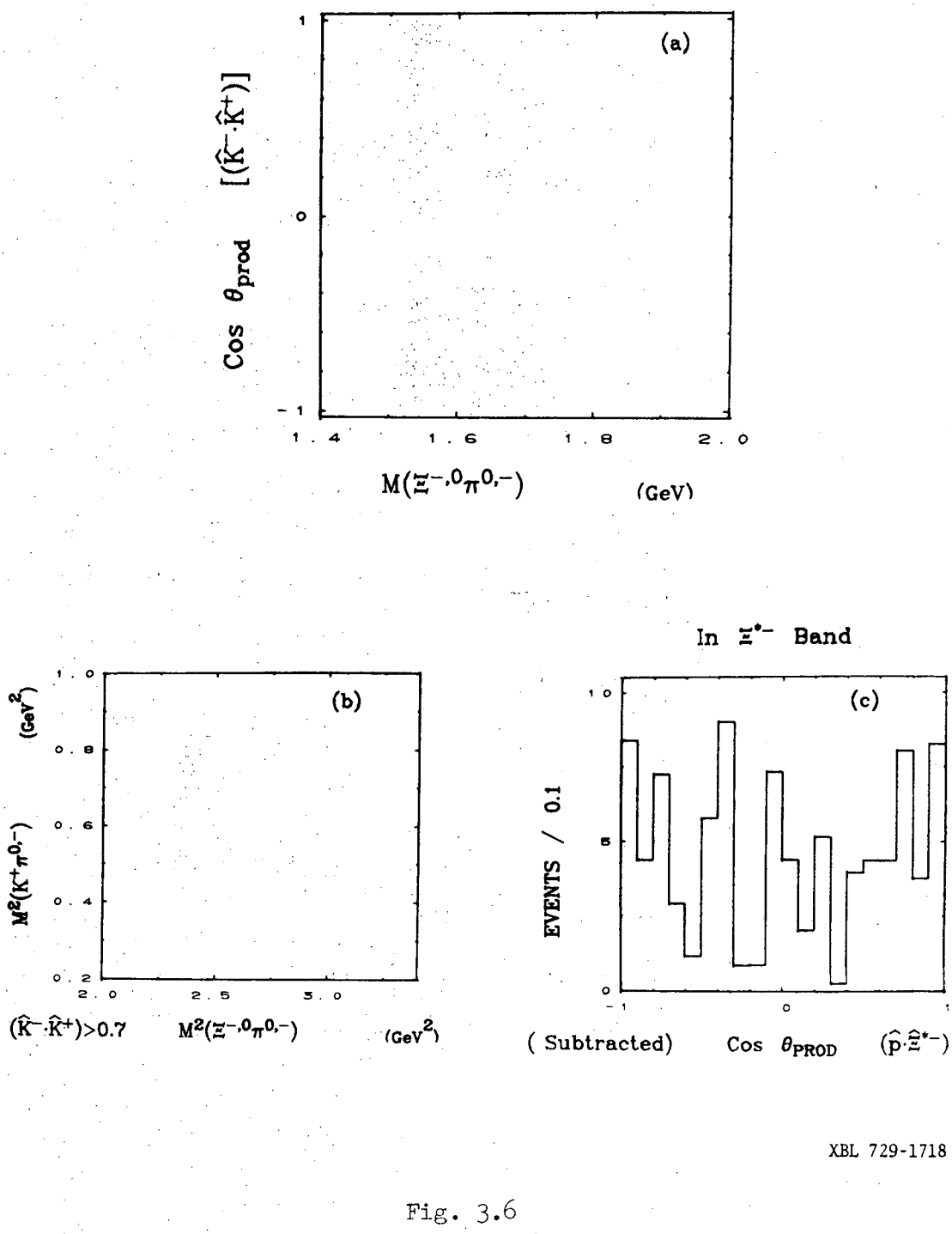

XBL 729-1718

Fig. 3.6

P~2.6 GeV/c $K^-p \to K^+\pi^{0,-}\Xi^{-,0}$ (Sample 7)

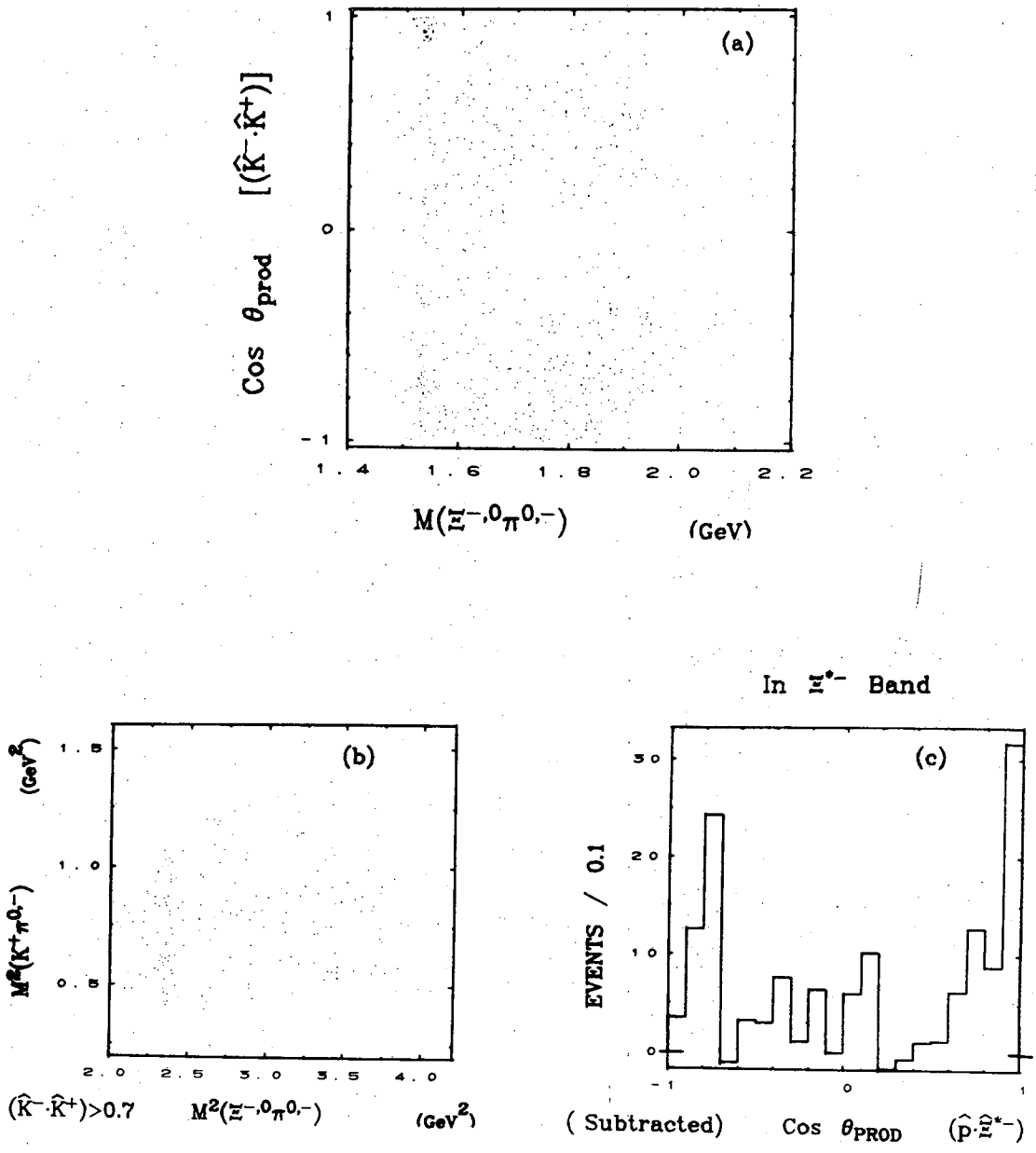

XBL 729-1719

Fig. 3.7

P=2.1 GeV/c $K^-p \to K^0\pi^+\Xi^-$ (Sample 8)

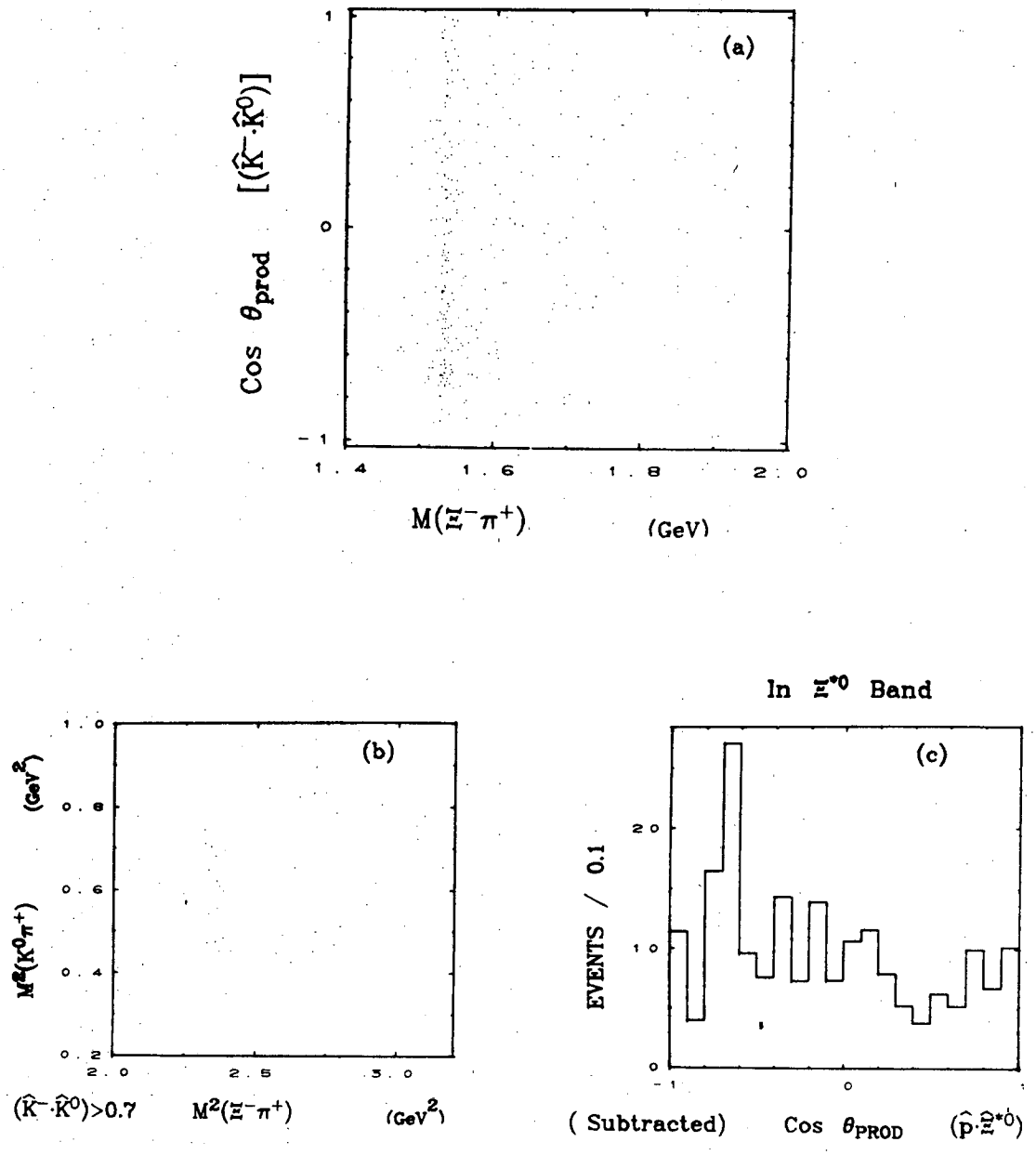

XBL 729-1720

Fig. 3.8

P~2.6 GeV/c $K^-p \to K^0\pi^+\Xi^-$ (Sample 9)

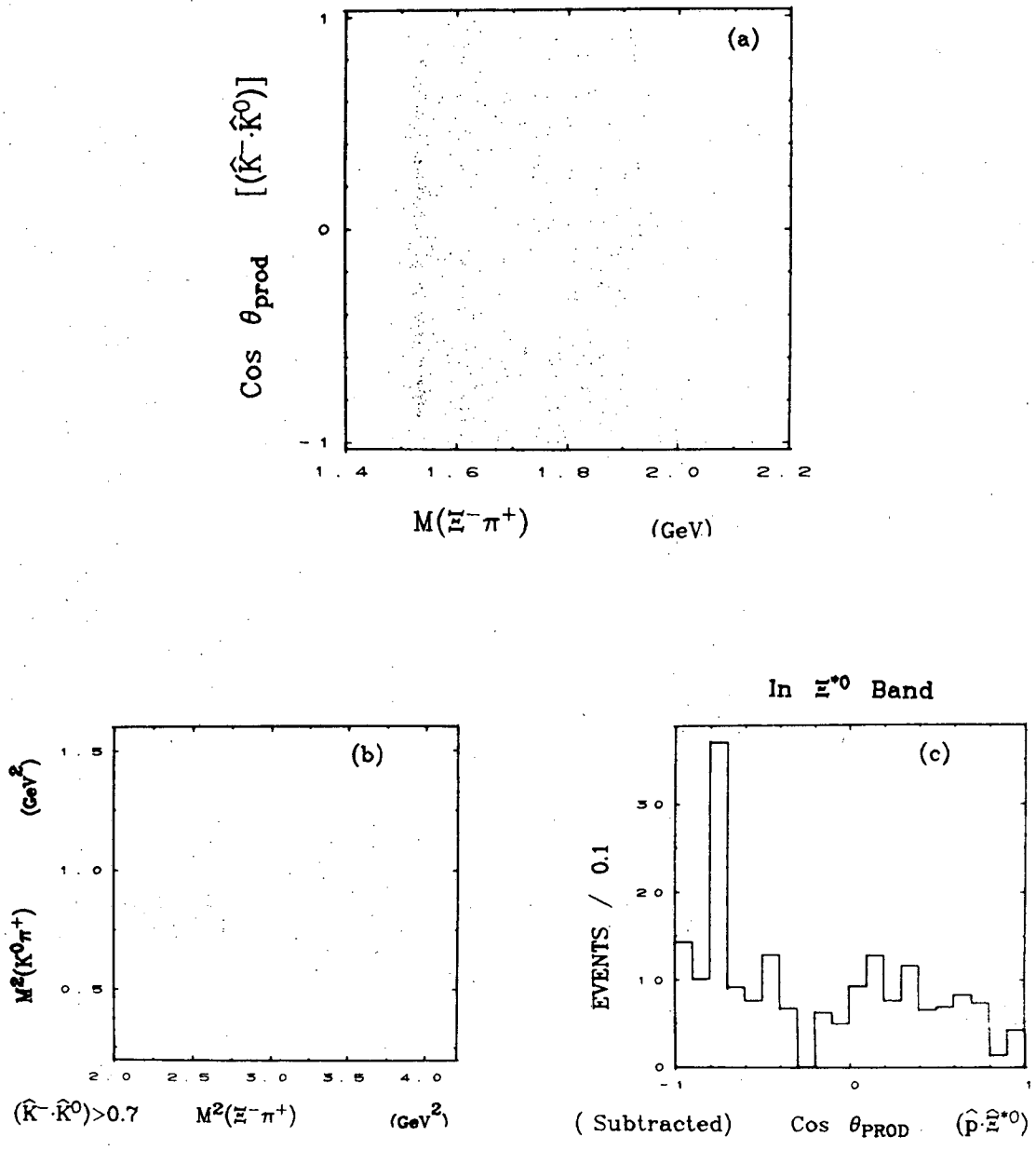

XBL 729-1721

Fig. 3.9

P<1.8 GeV/c $\pi^+n\to\pi^-\pi^+p$ (Sample 10)

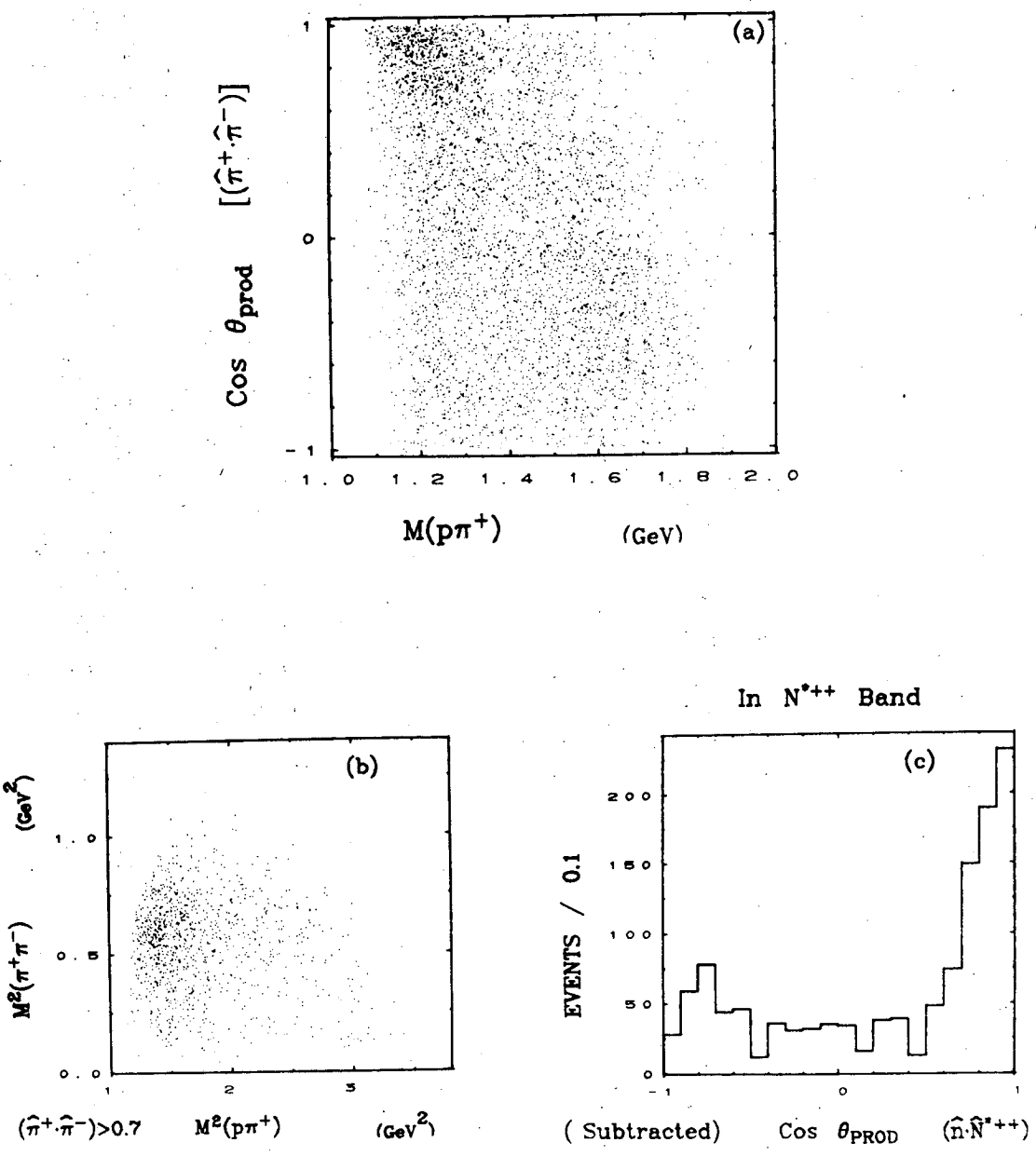

XBL 729-1722

Fig. 3.10

P~2.2 GeV/c $\pi^-p \to \pi^+\pi^-n$ (& $\pi^+n \to \pi^-\pi^+p$) (Sample 11)

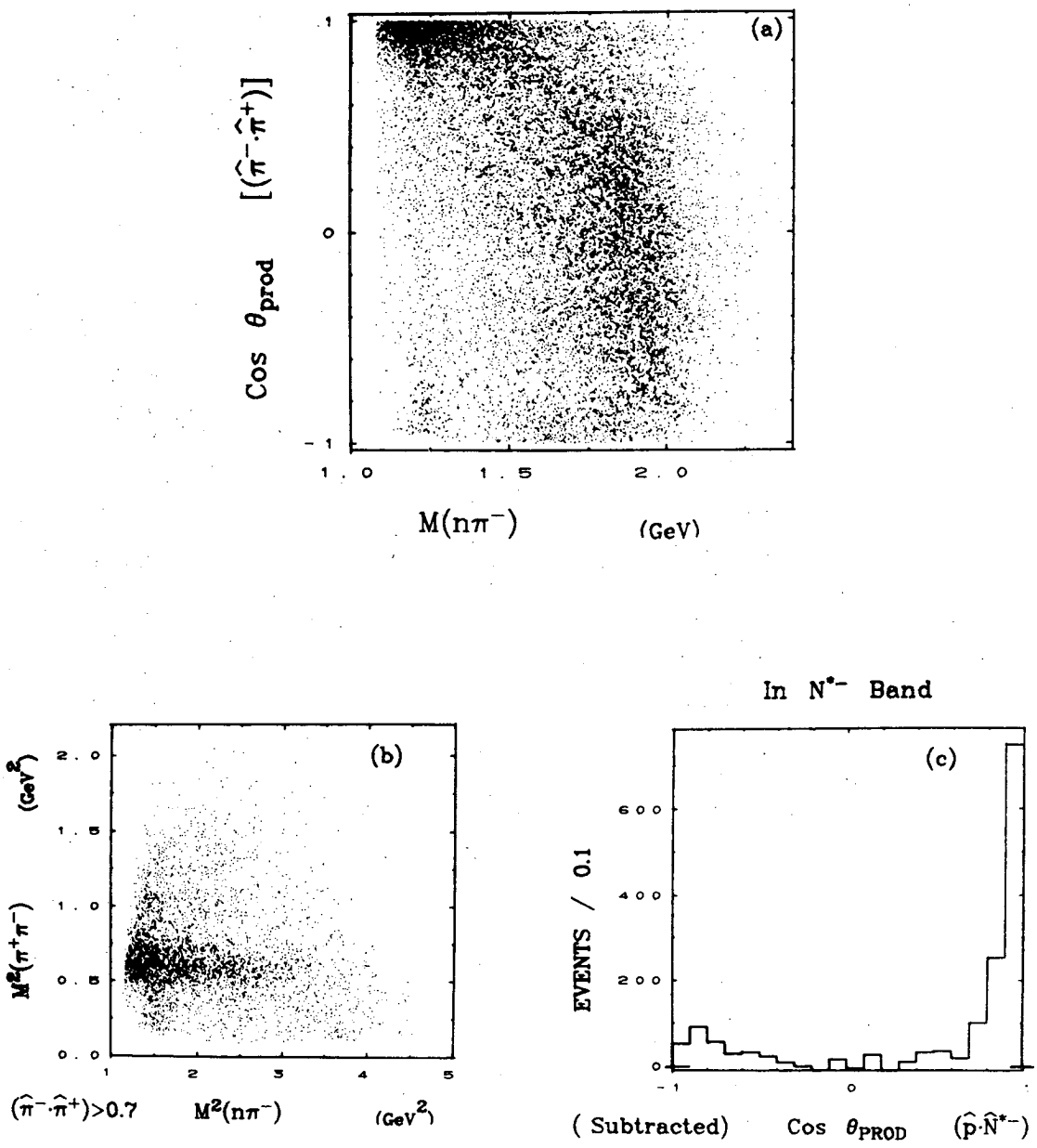

XBL 729-1723

Fig. 3.11

P=3.2 GeV/c $\pi^-p\to\pi^+\pi^-n$ (Sample 12)

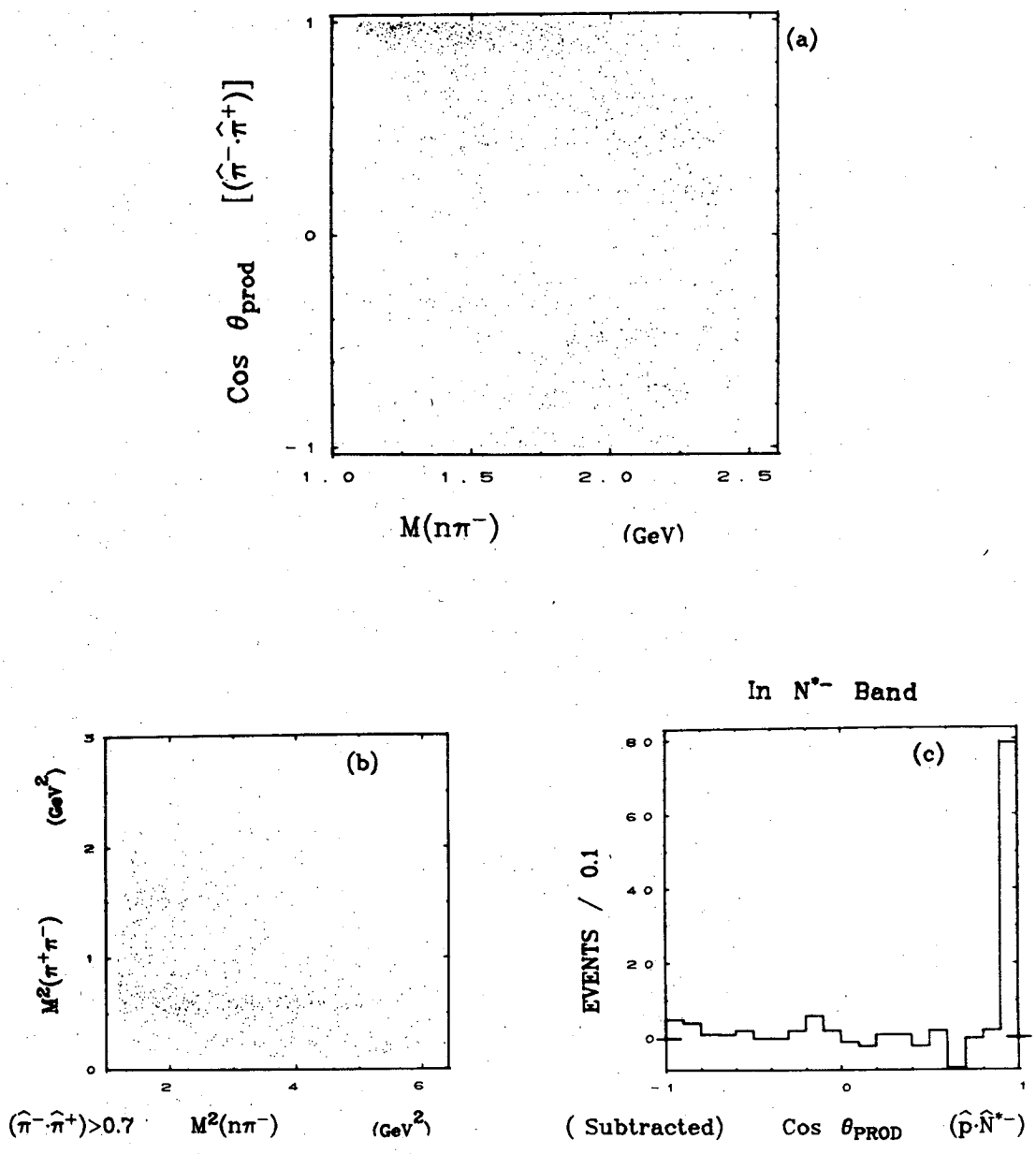

XBL 729-1724

Fig. 3.12

of high $n\pi^-$ mass and $\cos\theta_{pr} \approx -1$ to the low-mass, forward production region. This enhancement is a kinematic reflection of peripheral $\pi\pi$ production; in the forward region it results in broad bands in the Δ region which look quite a bit wider than the Δ. [The Δ band, $(m_o^2 \pm m_o\Gamma)$, is (1.53 ± 0.14) GeV^2.] We discuss below (Sections 3.24, 3.321) our claim that there is in fact Δ production on top of this enhancement.

From Fig. 1^+(a) and (c), we see that the production distribution of events in the B^* band has forward peaking in all cases except Ξ^{*o} production (Samples (8)-(9)), and perhaps Ξ^{*-} production at 2.1 GeV/c (Sample (6)). Note that in Y^* and Ξ^{*-} production there are backward peaks comparable in size to the forward peaks; in Δ production the backward peaks are small; in Ξ^{*o} production there are backward peaks with a pronounced dip in the extreme backward direction.

The forward Dalitz plots show competing M^* production in the $M\pi$ system (that is, ρ or K^*) in most cases. For Samples (1)-(3) and (10)-(12), M^* production in this region is stronger than B^* production; for Samples (4)-(5) it is comparable in size. In Samples (6)-(9), K^* production is OME-forbidden and is not evident in the B^*-forward region. In all cases, Fig. 1^+(b) shows that the forward B^* production is not predominantly connected with the B^*-M^* overlap region.

In Figures 3.13 and 3.14 we give our best estimates for the shapes and sizes of the production angular distributions. They were obtained in various ways which, we hope, take into account the peculiarities of each sample. The distributions for Samples (1)-(5) come from maximum-likelihood fits for the amount of B^* production made in each region of production cosine. The Ξ^* distributions come from the data with a simple mass cut. There is no distribution shown for Sample (10). Those for Samples (11) and (12) come from an eyeball estimate of the number of Δ events in the $N\pi$ spectrum for each cosine interval. These distributions were normalized to total B^* cross sections obtained from a variety of sources. We feel that the uncertainties in our procedures, especially for $\pi^\pm N \to KY^*$ and for Δ production, have given us good estimates for the size of the forward peak rather than careful measurements. Our primary interest was in studying the existence of authentic forward peaking, not in determining its magnitude. The error bars do not include any of the systematic uncertainties in the normalization.

We see that the differential cross section in the forward bin ranges in size from about 1 μb/sr to about 150 μb/sr. (The forward cross sections, with normalization uncertainties included, will be summarized in Table 3.12 below.) In

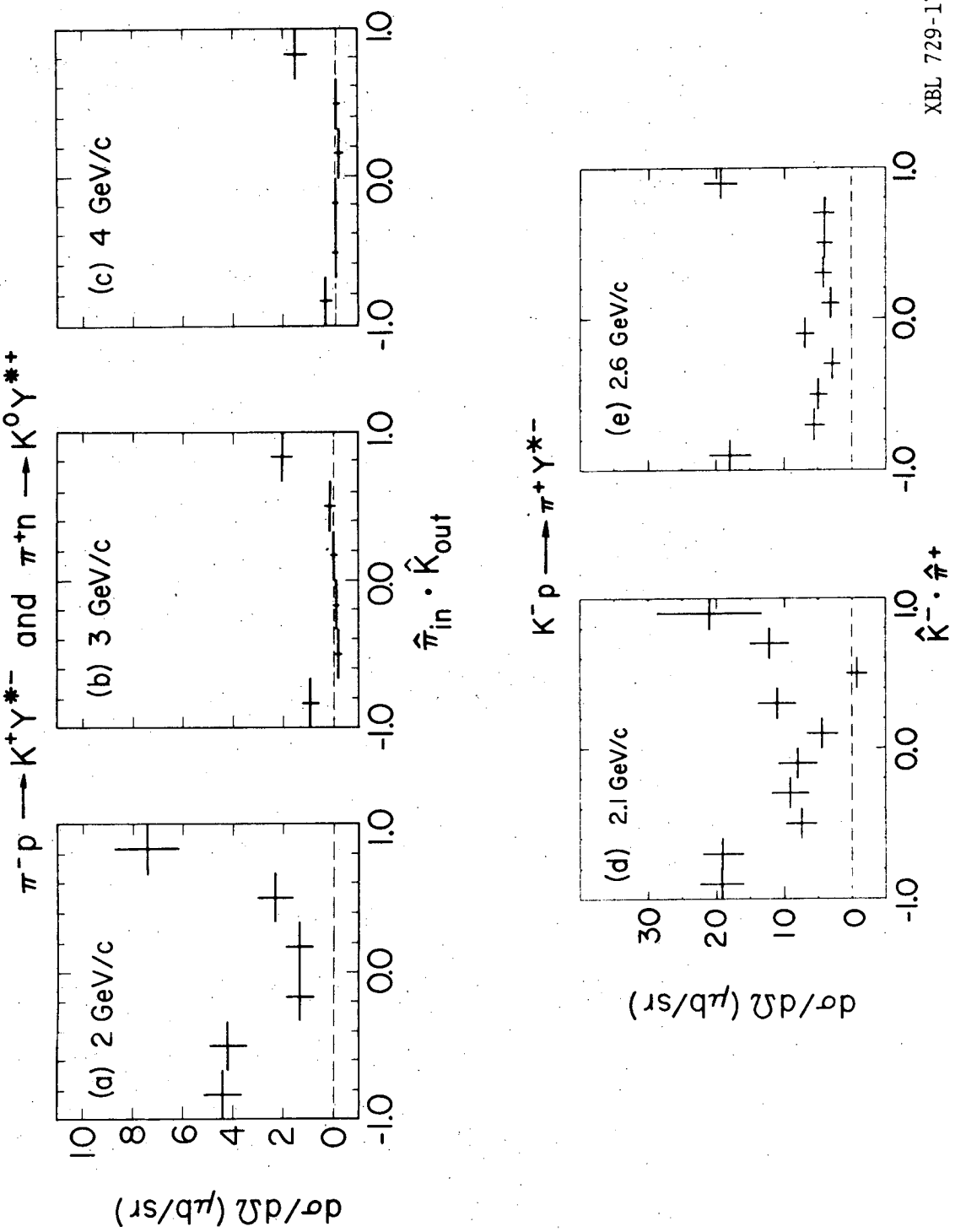
$\pi^- p \longrightarrow K^+ Y^{*-}$ and $\pi^+ n \longrightarrow K^0 Y^{*+}$
(a) 2 GeV/c
(b) 3 GeV/c
(c) 4 GeV/c
$d\sigma/d\Omega$ (μb/sr)
$\hat{\pi}_{in} \cdot \hat{K}_{out}$
$K^- p \longrightarrow \pi^+ Y^{*-}$
(d) 2.1 GeV/c
(e) 2.6 GeV/c
$\hat{K}^- \cdot \hat{\pi}^+$
XBL 729-1791

Fig. 3.13

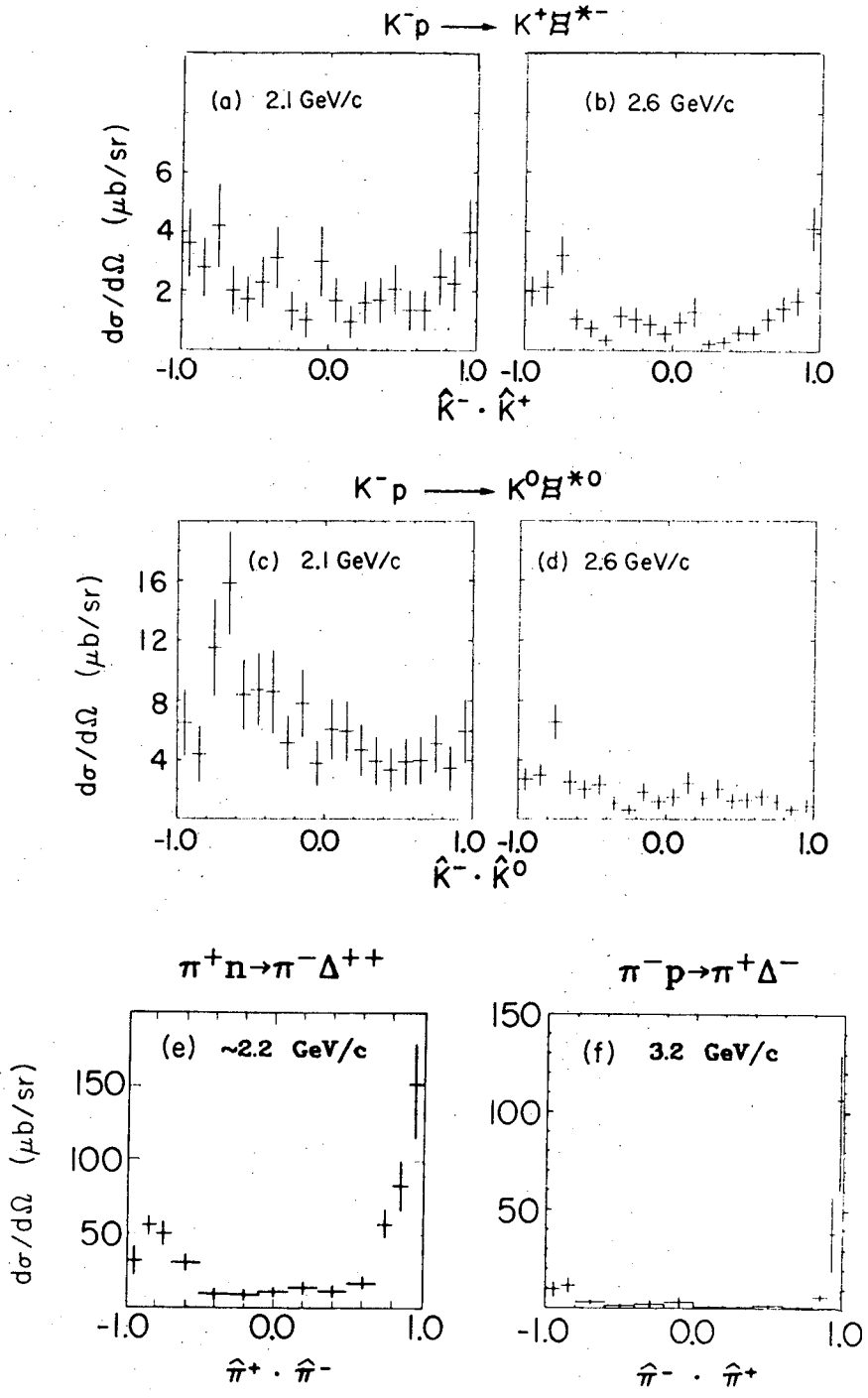

XBL 729-1792

Fig. 3.14

the cases where we have data above 3 GeV/c, a rapid decrease with energy is apparent.

3.22 DETAILS OF THE BASIC RESULTS

For each reaction in turn, we first identify the source of the data and define the cuts applied. Then we describe how the shape of the B^* production distribution was obtained, and tabulate the numerical results for reference. Finally we discuss our determination of the B^* production cross section, to which the angular distribution was normalized in Fig. 3.13-14.

In Figure 3.15 we give the $E_{c.m.}$ distribution for each sample, with the usual weights and fiducial and spectator cuts (as specified below) applied. For the 4 samples consisting of π^+n and π^-p data, the $E_{c.m.}$ distributions for each subsample are given in Figure 3.16. We have defined 20 subsamples, consisting of charge-symmetric reaction pairs, the two $(\Xi\pi)^-$ states, and odd- or even-pronged proton-spectator events. These subsamples are tallied in Table 3.2.

Table 3.3 lists the resonance masses and widths used to define the resonance bands for cuts. The bands were wide ones, $(m\pm\Gamma)$. We used the masses and widths from the Particle Data Group Compilation,[102] except for the Δ mass (where the peak in our data is slightly lower than the accepted mass) and the Ξ^* width (which is small compared to our resolution).

3.221 REACTION (1), $\pi N \rightarrow KY^*$

Description of the Data Sample

For reaction (1p), $\pi^-p \rightarrow K^+Y^{*-}$, we have used the data of the Pi63 experiment (run in 1963), as described in theses by R. Hess[103] and L. Hardy.[104] We have denoted by "P~2" the data taken at various beam momenta from 1.6 to 2.2 GeV/c (totaling 13.6 ev/μb). "P~3" and "P~4" correspond respectively to 12.8 ev/μb at 2.9 to 3.3 GeV/c and 5.6 ev/μb at 3.8 to 4.2 GeV/c.[105] We used a final data-summary tape left by the Pi63 experimenters, which included some events from an earlier exposure at 1.5 to 2.4 GeV/c in the "P~2" sample. [For unknown reasons, the number of events on this tape did not agree exactly with the numbers given in Ref. 104; however, our results for the fractions of resonance production at all $\cos\theta_{pr}$ were almost all within one standard deviation of the results of a similar fit reported in Ref. 104.] Hardy noted that Y^{*-} was

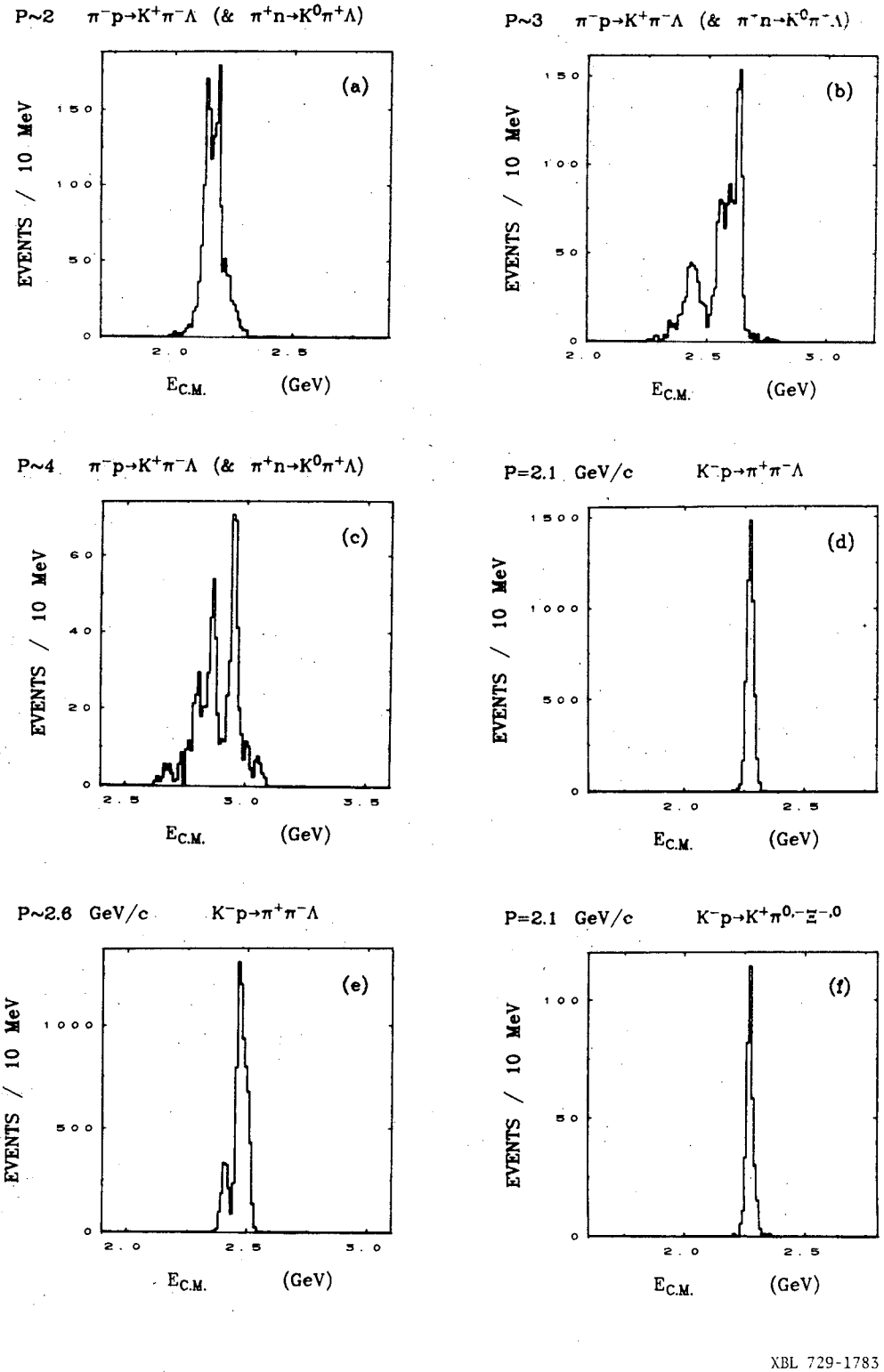

Fig. 3.15 (Page 1)

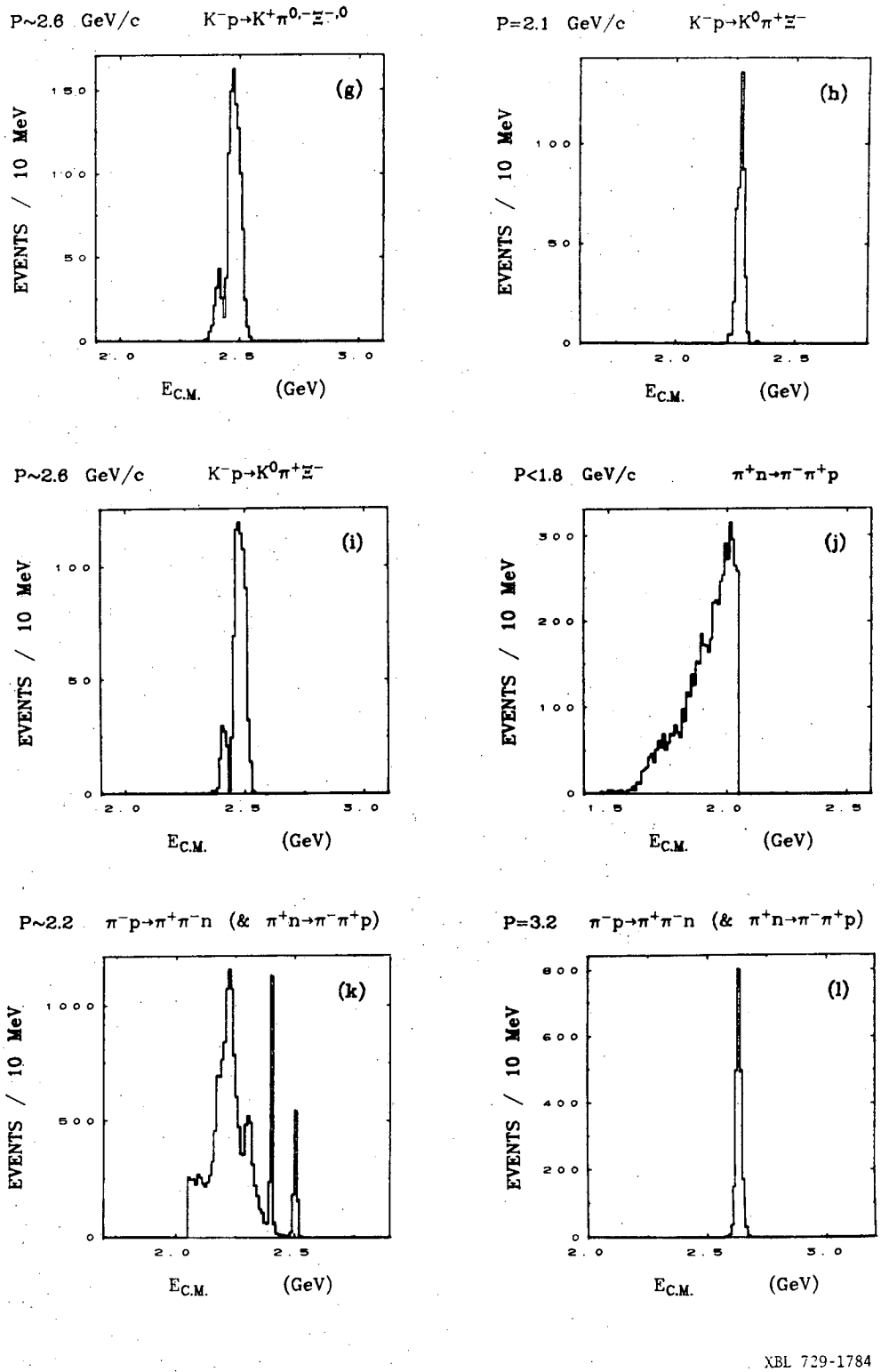

Fig. 3.15 (Page 2)

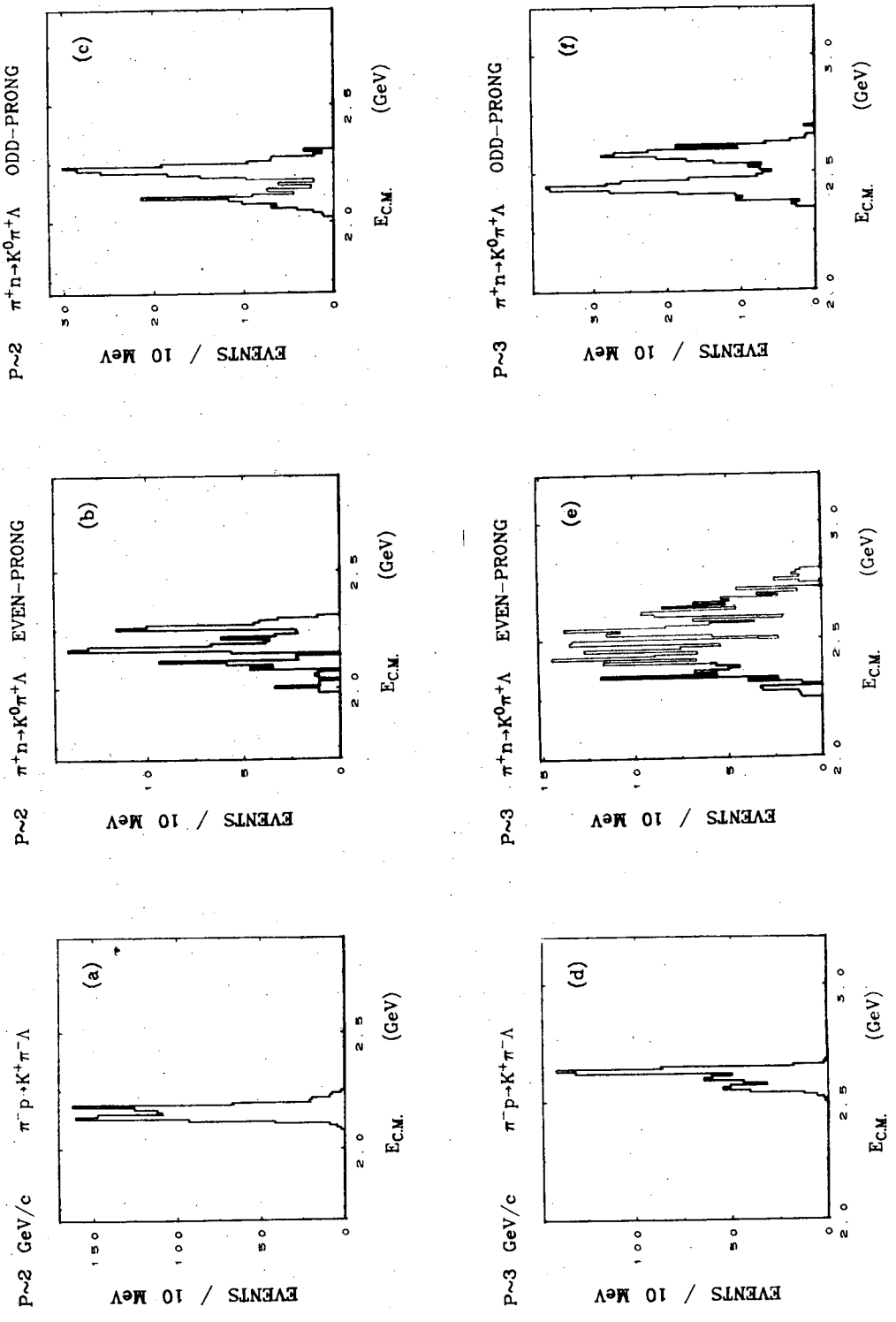

XBL 729-1785

Fig. 3.16 (Page 1)

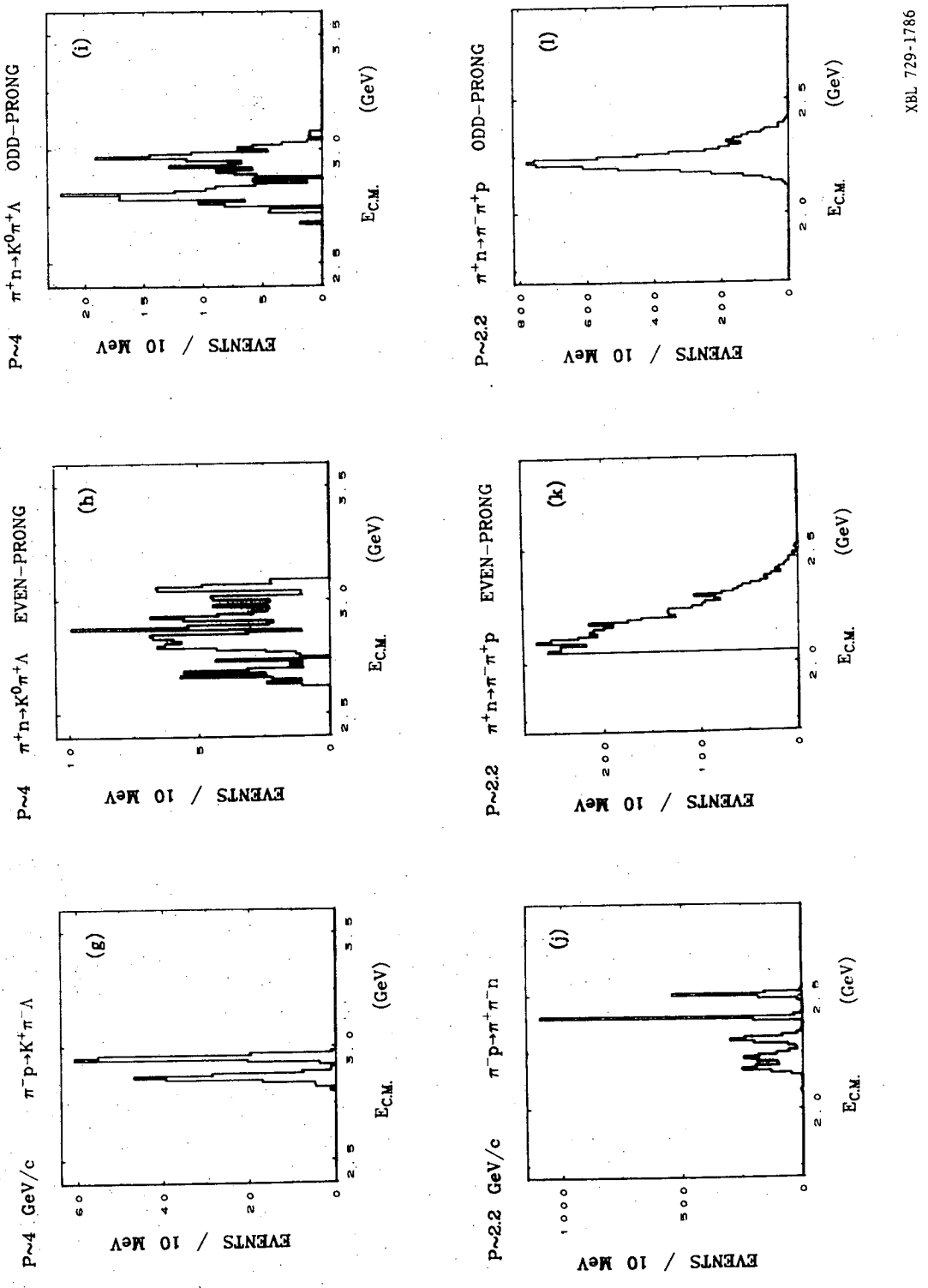

Fig. 3.16 (Page 2)

Sample	UNCUT DATA Reaction		Events
13	P~2 GeV/c	$\pi^- p \to K^+ \pi^- \Lambda$	1275
14	P~3 GeV/c	$\pi^- p \to K^+ \pi^- \Lambda$	966
15	P~4 GeV/c	$\pi^- p \to K^+ \pi^- \Lambda$	331
16	P~2 GeV/c	$\pi^+ n \to K^0 \pi^+ \Lambda$	683
17	P~3 GeV/c	$\pi^+ n \to K^0 \pi^+ \Lambda$	1123
18	P~4 GeV/c	$\pi^+ n \to K^0 \pi^+ \Lambda$	599
19	P=2.1 GeV/c	$K^- p \to K^+ \pi^0 \Sigma^-$	120
20	P~2.6 GeV/c	$K^- p \to K^+ \pi^0 \Sigma^-$	359
21	P=2.1 GeV/c	$K^- p \to K^+ \pi^- \Sigma^0$	228
22	P~2.6 GeV/c	$K^- p \to K^+ \pi^- \Sigma^0$	665
23	P~2.2 GeV/c	$\pi^- p \to \pi^+ \pi^- n$	5242
24	P~2.2 GeV/c	$\pi^+ n \to \pi^- \pi^+ p$	14211
25	P~2	$\pi^+ n \to K^0 \pi^+ \Lambda$ EVEN-PRONG	350
26	P~3	$\pi^+ n \to K^0 \pi^+ \Lambda$ EVEN-PRONG	641
27	P~4	$\pi^+ n \to K^0 \pi^+ \Lambda$ EVEN-PRONG	341
28	P~2	$\pi^+ n \to K^0 \pi^+ \Lambda$ ODD-PRONG	333
29	P~3	$\pi^+ n \to K^0 \pi^+ \Lambda$ ODD-PRONG	482
30	P~4	$\pi^+ n \to K^0 \pi^+ \Lambda$ ODD-PRONG	258
31	P~2.2	$\pi^+ n \to \pi^- \pi^+ p$ EVEN-PRONG	6978
32	P~2.2	$\pi^+ n \to \pi^- \pi^+ p$ ODD-PRONG	7233

Number of Events in Subsamples (Raw Data)

Table 3.2

Resonance	m (MeV)	Γ (MeV)
Y^{*+}	1382.2	36
Y^{*-}	1388	38
Ξ^{*o}	1528.9	30[a]
Ξ^{*-}	1533.8	30[a]
$\Delta^{++,-}$	1206[b]	120
K^{*o}	897.7	49.7
K^{*+}	891.4	49.7
ρ^{o}	764	120

(a) This was used to take our resolution into account. The actual widths are [respectively] ≈9 [≈16] MeV for the Ξ^{*o} [Ξ^{*-}].

(b) The accepted value of the Δ mass is ≈1236 MeV; our Δ peaks were a bit lower.

Parameters Used for Resonance Band Definition

Table 3.3

produced but did not study the production distribution.

The data for reaction (1n), $\pi^+ n \to K^o Y^{*+}$, was obtained from the LBL Pi66A experiment. The processing of the data from this 72-inch bubble chamber exposure of ≈20 ev/μb at 3 and 4 GeV/c has been described in Chapter 2 of this thesis.[106] When we did this study of exotic exchange we had processed essentially all the events, but we used a preliminary scheme for the separation of hypotheses.[107] We are confident that our results would be essentially the same with our final data sample. (See Section 3.24.)

Around 2 GeV/c, we have examined the $\pi^+ n$ data from the Pi66B exposure.[108] When we did the fits to get $d\sigma/d\Omega$ [Fig. 3.13(a)] these events were not included. However, they are in most of the other figures.

After a preliminary examination showed that the data for the $\pi^+ n$ and $\pi^- p$ reactions appeared consistent, as predicted by charge symmetry, we did most of our studies using all the events combined.

The number of events in the raw data samples is given in Tables 3.1 and 3.2. We generally applied the usual fiducial-volume cuts, with the corresponding weights, and (in the $\pi^+ d$ exposure) a spectator-momentum cut (p_{sp}<300 MeV/c). For the fits described in the next subsection, we had to exclude a fairly small number of events in the tails of the distribution of effective c.m. energy. (The fitting program could handle only a limited c.m. energy range.) For consistency, this same cut was applied to all the plots in this chapter (except where the raw data was used). Overall, about 70% of the events on the data tapes (i.e., about 5000 events) survived all these cuts. The number of events used in the figures is given in Table 3.14 below.

Shape of the Production Distribution

The combination of small production cross sections and relatively large non-Y^* background (as indicated by Figures 3.1-3.3(a-b)) has made accurate estimation of the angular distributions difficult. The Y^* production angular distributions (Fig. 3.13) were obtained by dividing the events into six intervals in $\Lambda\pi$ production cosine and, for each interval, calculating the number of Y^* events present. This work was done before it became clear to us that one could get a good idea of the distribution by simpler methods (a Y^* mass cut and background subtraction, or an eyeball estimate of the number of Y^* events in each production interval); in view of the complications of this fitting method we emphasize that the existence of the forward peaking is best seen directly in the Chew-Low-like

plots in Fig. 3.1+(a).

The fraction of each evident resonance process and of phase space was obtained by using the maximum-likelihood fitting program MURTLEBERT.[109] The results of the fits are given in Table 3.4. (In one interval with a small number of events, no fit was found, and an eyeball estimate of the number of Y^* events was used.) We used simple (S-wave) Breit-Wigner forms for the 3 resonant processes, with the indicated "wallet card" resonance parameters. It was assumed that these resonant processes and phase space did not interfere.

We found that the results were not particularly sensitive to the details of the model. In Table 3.5 we present the fits (for all production angles combined) with various changes in the model, and for π^+n (Pi66) and π^-p (Pi63) separately. (We did not repeat the fits for each $\cos\theta_{pr}$ interval in all these cases.) It can be seen that the overall amount of Y^* production is not greatly changed by changing the resonance masses or widths, allowing them to vary, adding a weakly produced resonance, or using non-simple Breit-Wigner shapes.

At 2 and 3 GeV/c, the use of noninterfering processes is justified by the absence of obvious interference effects in the Dalitz plots. (In Section 3.323, we comment on a model which describes the forward peaking in terms of interference effects in the K^*-Y^* crossing region. Such an effect seems to be present, at least at 4 GeV/c; we had not noticed this when we did the fits.)

In general, the fits gave good agreement with the mass projections. In each interval, the number of Y^* events given by the fit was checked for consistency with the $m(\Lambda\pi)$ spectrum. Also, we obtained the angular distributions in a more conventional manner: we looked at events in a wide $[m\pm\Gamma]$ Y^* band, subtracting, as background, events in bands of width Γ on either side of the Y^* band. The resulting production distributions (in six bins, so that they can be compared with Figs. 3.13(a)-(c)) are given in Figs. 3.1-3.3(c). We also tried cutting out events in a wide $K^*(890)$ band; the resulting distributions, similar in shape, are given in Figs. 3.42-3.44(d) below. The qualitative agreement is quite good; certainly the forward peak is present in all cases.

After our results on Y^* production were published,[91] we started working on the other reactions. In the case of Δ production, we paid special attention to the low-mass enhancement in $m(B\pi)$ that results from the strong peripheral production of the dimeson $M\pi$. We then decided that the amount of Y^* production in the forward bin at 2 GeV/c had probably been overestimated by about 20% because of this enhancement. Thus, the forward peak was reduced by this amount

Cos θ Bin[a]	Events N	ΣWt	Resonance Fractions (%) Y* (m,Γ)=(1385,38)	K*(890) (892,49.2)	K*(1420) (1440,80) [MeV]	Number of Y* Events
P ≈ 2 GeV/c:						
1	186	186.7	33.9 ± 5.3	41.0 ± 6.0	-	63.3 ± 10.9
2	152	157.3	38.6 ± 6.1	46.6 ± 7.3	-	60.7 ± 10.7
3	125	123.6	15.6 ± 6.6	53.3 ± 8.9	-	19.3 ± 8.4
4	158	160.0	12.1 ± 4.9	62.6 ± 7.6	-	19.4 ± 7.9
5	171	174.5	19.1 ± 5.6	54.6 ± 7.3	-	33.4 ± 10.0
6	292	291.1	44.9 ± 5.0	40.3 ± 5.6	-	130.8 ± 16.4
All	1084	1093.1	29.3 ± 2.4	48.8 ± 3.0	-	[Sum=326.9]
P ≈ 3 GeV/c:						
1	297	303.6	8.5 ± 2.8	6.9 ± 2.9	-	25.9 ± 8.6
2	162	173.4	-2.9 ± 2.1	13.8 ± 4.4	-	-5.0 ± 3.6
3	108	109.8	-2.2 ± 2.4	17.3 ± 6.4	-	-2.5 ± 2.6
4	144	138.5	0.0 ± 2.7	40.5 ± 8.5	-	0.0 ± 3.8
5	227	238.8	1.9 ± 2.2	59.0 ± 5.0	-	4.6 ± 5.1
6	549	582.4	10.0 ± 2.1	68.3 ± 3.0	-	58.5 ± 12.2
All	1487	1546.5	4.3 ± 1.1	40.6 ± 1.9	-	[Sum= 81.5]
P ≈ 4 GeV/c:						
1	116	128.5	4.9 ± 3.0	3.8 ± 3.2	28.8 ± 7.0	6.3 ± 3.9
2	65	71.4	-0.2 ± 2.6	2.9 ± 3.9	46.7 ± 10.6	-0.1 ± 1.9
3	42	46.4	No fit obtained; Estimate:			0 ± 2
4	43	45.9	-4.4 ± 6.4	10.2 ± 7.8	-3.4 ± 9.0	-2.0 ± 2.9
5	103	113.7	-0.2 ± 1.7	55.2 ± 6.0	19.7 ± 6.5	-0.2 ± 2.0
6	324	348.3	8.2 ± 2.2	72.6 ± 3.6	1.9 ± 2.0	28.4 ± 7.7
All	693	754.2	3.2 ± 1.3	40.3 ± 2.7	12.5 ± 2.6	[Sum= 32.4]

(a) Each bin covers an interval of 0.33 in Cos θ_{pr} [$\equiv(\hat{\pi}^- \cdot \hat{K}^+)$]; bin 1 is $-1 <$ Cos $\theta_{pr} < -2/3$.

Resonance-Production Fits in $\pi^- p \rightarrow K^+\pi^-\Lambda$ (and $\pi^+ n \rightarrow K^0\pi^+\Lambda$)

Table 3.4

#	Features	Note	Y^* Fraction (%)		
			P≈2	P≈3	P≈4 GeV/c
1	Basic Fits	(a)	29.3 ± 2.4	4.3 ± 1.1	3.2 ± 1.3
2	Pi66 (π^+n) only	-	-	3.8 ± 1.5	3.6 ± 1.7
3	Pi63 (π^-p) only		[29.3 ± 2.4]	4.6 ± 1.9	2.6 ± 1.7
4	m and Γ varied	(b)	29.7 ± 2.8	3.7 ± 0.9	No solution
	[Results for m (MeV):]		[1388.9 ± 2.2]	[1381.1 ± 4.2]	-
	[Results for Γ (MeV):]		[37.8 ± 4.7]	[16.8 ± 5.6]	-
5	$\Gamma(Y^*)$ = 43 MeV	-	30.5 ± 2.5	4.4 ± 1.1	3.3 ± 1.3
6	With $N^*(1680)$	(c)	-	5.1 ± 1.6	-
7	Non-simple Breit-Wigners	(d)	30.2 ± 2.5	4.7 ± 1.1	3.5 ± 1.4

Notes:

(a) These are the fits given in detail in Table 3.4

(b) In all the fits except #4, the resonances masses and widths were fixed. Since this work was done before we decided what values to use in the final fits, there was some variation. For the Y^*, we used (m,Γ) = (1385 or 1382, 37 or 38), and Γ=43 for Fit #5; for the $K^*(890)$, we used (m,Γ) = (892.0 or 892.4, 49.2 or 49.8); for the $K^*(1420)$, which was included only at 4 GeV/c, we used (m,Γ) = (1440 or 1418.6, 80 or 89.1).

(c) For Pi66 at 3 GeV/c only, we tried a fit with this N^*, with Γ=130 MeV; the result was (18 ± 3)% N^*.

(d) P-wave dependence included (D-wave for the $K^*(1420)$).

Y^* Fraction in Fits with Modifications

Table 3.5

(after the normalization described in the next subsection).

Cross-Section Normalization

As discussed in detail here, we estimated the cross section for $\pi^- p \to K^+ Y^{*-}$, $Y^{*-} \to \Lambda\pi^-$ to be 42.8 [5.5, 3.5] μb at 2 [3, 4] GeV/c [respectively]. The production distributions were normalized to these numbers (increased by 11% to take into account the $\Sigma\pi$ decay mode of the Y^*). The result is given in Fig. 3.13 and in Table 3.6. The indicated errors are statistical only. The correction for the low-mass enhancement in the forward bin at 2 GeV/c is a reduction of 19%, corresponding to a decrease of the total Y^* production cross section by 8%.

At 2 GeV/c, we simply used the Pi63 result for the $\Lambda K^+\pi^-$ cross section, (42.8 ± 4.0) μb.[110] At 3 and 4 GeV/c, we have combined the Pi63 result with an estimate of the cross section observed in Pi66. We wanted to take into account the fact that our Pi66 ($\pi^+ n$) data was subject to misassigment problems which had not yet been examined closely. Table 3.7 indicates the rather involved way we got those estimates; the details of the calculation are in the notes.

In Pi66, the $\Lambda K^0\pi^+$ final state can be detected in 3 ways: with both or either strange particle decaying via a charged mode. The ratio of "all : 2V" should be $(\Lambda+K^0+\Lambda K^0)/\Lambda K^0 = (4+1+2)/2$. In our (uncut) data, the ratio $R_X = n_{tot}/[(7/2)n_{2V}]$ is not 1 but 1.4 at 3 GeV/c and 2.1 at 4 GeV/c. We expected that since the 2V state is a 4-production-constraint fit, and the others (being 1C) are more subject to misassignment, we probably had an excess of 1V events and roughly the right number of 2V events. We argued that the excess 1V events would probably not contribute to the Y^* peak if they were not real $\Lambda K^0\pi^+$ events. If all that were true, it would have been proper to increase the $\Lambda K^0\pi^+$ cross section according to the 1V excess and hope that the Y^* fraction (from the fit) was compensatingly low. So, we multiplied the "one-vee excess" ratio R_X by the $\Lambda K\pi$ cross section from Pi63, giving the indicated Pi66 $\Lambda K\pi$ cross sections. The Y^*K cross section is then calculated from the Y^* fraction given by our fits, and averaged with the Y^*K cross section found by Pi63.

Now that we have calculated the Pi66 cross sections, it appears that our assumption that we had an excess of one-vee events was in error, and that we have a deficiency of 2V events. Here are the results from Chapter 2 for $\sigma(\Lambda K^0\pi^+)$ (with the visibility factors for the vees multiplied in):[111]

$\cos\theta_{pr}$ $[\hat{\pi}\cdot\hat{K}]$	Number of Y^* events	$d\sigma/d\Omega$ (μb/sr)
P≈2 GeV/c:		
-1.00 to -0.67	63.3 ± 10.9	4.40 ± 0.76
-0.67 to -0.33	60.7 ± 10.7	4.22 ± 0.74
-0.33 to 0.00	19.3 ± 8.4	1.34 ± 0.58
0.00 to 0.33	19.4 ± 7.9	1.34 ± 0.55
0.33 to 0.67	33.4 ± 10.0	2.32 ± 0.70
0.67 to 1.00	[130.8 ± 16.4]	[9.08 ± 1.14]
Corrected:	106.0 ± 20.0	7.36 ± 1.39
Totals: N = 302.2 [327.0 before correction], $\sigma \pm \partial\sigma$ = (44.0 ± 4.4) [47.6 ± 4.4] μb. ($\partial\sigma/\sigma$ = 10%)		
P≈3 GeV/c:		
-1.00 to -0.67	25.9 ± 8.6	0.93 ± 0.31
-0.67 to -0.33	-5.0 ± 3.6	-0.18 ± 0.13
-0.33 to 0.00	-2.5 ± 2.6	-0.09 ± 0.09
0.00 to 0.33	0.0 ± 3.8	0.00 ± 0.14
0.33 to 0.67	4.6 ± 5.1	0.17 ± 0.18
0.67 to 1.00	58.5 ± 12.2	2.09 ± 0.44
Totals: N = 81.5, $\sigma \pm \partial\sigma$ = (6.1 ± 1.7) μb. [$\partial\sigma/\sigma$ = 27%]		
P≈4 GeV/c:		
-1.00 to -0.67	6.3 ± 3.9	0.36 ± 0.23
-0.67 to -0.33	-0.1 ± 1.9	-0.01 ± 0.11
-0.33 to 0.00	0.0 ± 2.0	0.00 ± 0.11
0.00 to 0.33	-2.0 ± 2.9	-0.12 ± 0.17
0.33 to 0.67	-0.2 ± 2.0	0.01 ± 0.11
0.67 to 1.00	28.4 ± 7.7	1.63 ± 0.44
Totals: N = 32.4, $\sigma \pm \partial\sigma$ = (3.9 ± 2.3) μb. [$\partial\sigma/\sigma$ = 58%]		

The normalization uncertainty, $\partial\sigma/\sigma$, is not included in the errors on $d\sigma/d\Omega$.

Production Distributions for $\pi^-p \rightarrow K^+Y^{*-}$ (and $\pi^+n \rightarrow K^oY^{*+}$)

Table 3.6

			P≈3 GeV/c	P≈4 GeV/c
From $\pi^- p \rightarrow \Lambda K^+ \pi^-$:		(Units)		
(1)	$f(Y^*)$		0.05 ± 0.01	0.02 ± 0.02
(2)	$\sigma_p(Y^{*-}K^+)$	μb	5.0 ± 1.0	1.9 ± 1.9
(3)	$\sigma(\Lambda K^+ \pi^-)$	μb	110 ± 20	95 ± 15
From $\pi^+ n \rightarrow \Lambda K^o \pi^+$:				
(4)	$N(\Lambda_V K^o{}_V \pi^+)$	ev	265.2 ± 16.3	92.8 ± 9.6
(5)	$N_{Tot.}(\Lambda K^o \pi^+)$	ev	1289.1 ± 35.9	677.3 ± 26.0
(6)	R_X		1.39 ± 0.09	2.09 ± 0.23
(7)	$N_{Cut}(\Lambda K^o \pi^+)$	ev	749.8 ± 27.4	441.7 ± 21.0
(8)	"$\sigma(\Lambda K^o \pi^+)$"	μb	153 ± 30	198 ± 38
(9)	$f(Y^*)$		(3.8 ± 1.5)%	(3.6 ± 1.7)%
(10)	$\sigma_p(Y^*K)$	μb	5.81 ± 2.55	7.13 ± 3.64
Net:				
(11)	$\sigma_p(Y^*K)$	μb	5.5 ± 1.5	3.5 ± 2.0
(12)	$\sigma(Y^*K)$	μb	6.1 ± 1.7	3.9 ± 2.3

Table 3.7 (Page 1)

Notes:

(1) Y^* fraction, from fit. From Ref. 104, Table 9.

(2) Cross section for Y^*K in the $\Lambda K\pi$ final state. From Ref. 104, Table 10. [The value at 4 GeV/c is reported there as (0 ± 1.9) μb; we have changed it to agree with Row (1). There is some Y^* in $m(\Lambda\pi)$ in the π^-p data alone (See Fig. 3.87(a)); our own fit on that data alone gave (2.6 ± 1.7)% Y^*.]

(3) Cross section for the final state. [Row (2)/Row (1)]; at 3 GeV/c, we used (110 ± 20) μb rather than (100 ± 20) μb, to get better agreement with the value of $\sigma(\Lambda K^+\pi^-)$ given in Table 7 and Fig. 9 of Ref. 104.

(4) Number of events with 2 vees (in the uncut data).

(6) One-vee-excess ratio. {Row (5)/[Row (4)*(7/2)]}.

(7) Number of events used in the fits.

(8) Effective final-state cross section, [Row (3) * Row (6)].

(9) Y^* fraction from fit. (Table 3.5, Fit #2)

(10) [Row (8) * Row (9)]

(11) Average of Row (2) and Row (10). (We used these estimated averages; the weighted averages are respectively (5.1 ± 0.9) μb and (3.0 ± 1.7) μb.]

(12) From Row (11), corrected for $Y^* \rightarrow \Sigma\pi$.

Cross-Section Estimates for $\pi^+n \rightarrow K^0Y^{*+}$ (or $\pi^-p \rightarrow K^+Y^{*-}$)

Table 3.7 (Page 2)

	$n_{tot}/$ [(7/2)*n_{2V}]	Decays: ΛK^0	$\sigma(\Lambda K^0\pi^+)$ (μb) K^0	Λ	$\sigma(\Lambda K^+\pi^-)$ From Pi63
P~3	1.27	83.7 ± 7.9	145.4 ± 14.0	105.9 ± 8.0	110 ± 20
P~4	1.99	49.4 ± 8.1	146.3 ± 21.7	92.6 ± 12.4	95 ± 15

Thus, it would appear that we have too few 2V events and too many with a K^0 decay.

At 3 GeV/c, our estimate for $\sigma(Y^*K)$ came out to be consistent with the Pi63 value. The result at 4 GeV/c is perhaps the most important, since the question of the persistence of the forbidden forward peaking with increasing energy is crucial to the interpretation. From Pi66 alone we estimate the Y^* cross section at 4 GeV/c to be (7.1 ± 3.6) μb, compared to the Pi63 result of (1.9 [or 0] ± 1.9) μb. This discrepancy reflects the fact that there does seem to be more Y^* production in our data, as well as the high value for $\sigma(\Lambda K\pi)$ obtained in Pi66. We decided to use (3.5 ± 2.0) μb; the large error reflects our conclusion that the normalization in Fig. 3.13(c) may be off by ≈50% in either direction.

3.222 REACTION (2), $K^-p \rightarrow \pi^+Y^{*-}$

We used the final data tape from the Berkeley K63 experiment, as processed by Dan Siegel. Our determination of the shape of the production distribution is taken directly from his thesis.[112] Here we summarize the relevant information from that report.

The experiment was an exposure of the 72-inch chamber to K^- beams at 5 incident momenta.[113] In our plots, "P=2.1" denotes a 6.6 ev/μb sample at 2.10 GeV/c, and "P~2.6" denotes the other 4 exposures, from 2.47 to 2.73 GeV/c. [However, Siegel's fit at 2.6 GeV/c, which we used in Fig. 3.13(e), did not include the relatively small sample at 2.47 GeV/c.]

Siegel achieved good separation of the 4-production-constraint $\Lambda\pi^+\pi^-$ final state, yielding about 11000 events. Weights for the Λ decay were calculated, and a fiducial cutoff was defined. (The data tape did not include any of the events which failed the fiducial test, so what we refer to as our "raw data" consists of the same events as the cut data.)

Siegel's maximum-likelihood fits for various resonant processes are presented in his Chapter 5. The number of events and the fraction of $Y^{*-}\pi^+$ in each of 10 intervals of $\cos\theta_{pr}$ [$\equiv \hat{K}^-\cdot\hat{\pi}^+$] are given in his Table 18. From his Table 15, we take the cross section for $K^-p \rightarrow Y^{*-}\pi^+ \rightarrow \Lambda\pi^-\pi^+$ to be (135 ±

$\cos\theta_{pr}$ $[\hat{K}^- \cdot \hat{\pi}^+]$	Number of Y^{*-} Events	$d\sigma/d\Omega$ (μb/sr)
P=2.1 GeV/c:		
-1.0 to -0.8	74.4 ± 12.8	19.15 ± 3.30
-0.8 to -0.6	73.7 ± 11.6	18.99 ± 2.99
-0.6 to -0.4	28.9 ± 8.7	7.44 ± 2.23
-0.4 to -0.2	35.3 ± 10.8	9.09 ± 2.78
-0.2 to 0.0	30.9 ± 11.1	7.94 ± 2.86
0.0 to 0.2	17.0 ± 9.1	4.38 ± 2.34
0.2 to 0.4	42.9 ± 10.7	11.04 ± 2.75
0.4 to 0.6	-2.9 ± 5.8	-0.75 ± 1.50
0.6 to 0.8	47.4 ± 11.1	12.19 ± 2.85
0.8 to 1.0	[116.1 ± 37.5]	[29.89 ± 9.66]
Corrected:	82.0 ± 30.0	21.11 ± 7.73
Totals: N = 429.6 [463.6 before correction], $\sigma \pm \partial\sigma$ = (139 ± 17) [150 ± 17] μb. ($\partial\sigma/\sigma$ = 12%)		
P≈2.6 GeV/c:		
-1.0 to -0.8	127.6 ± 22.6	17.83 ± 3.16
-0.8 to -0.6	39.3 ± 10.8	5.49 ± 1.51
-0.6 to -0.4	35.0 ± 9.0	4.89 ± 1.26
-0.4 to -0.2	20.5 ± 8.5	2.86 ± 1.19
-0.2 to 0.0	49.1 ± 9.6	6.85 ± 1.35
0.0 to 0.2	22.5 ± 9.3	3.14 ± 1.30
0.2 to 0.4	29.7 ± 8.7	4.16 ± 1.21
0.4 to 0.6	28.4 ± 8.7	3.97 ± 1.22
0.6 to 0.8	28.9 ± 11.3	4.04 ± 1.58
0.8 to 1.0	137.9 ± 17.1	19.27 ± 2.39
Totals: N = 519.0, $\sigma \pm \partial\sigma$ = (91.1 ± 10.0) μb. [$\partial\sigma/\sigma$ = 11%]		

The normalization uncertainty, $\partial\sigma/\sigma$, is not included in the errors on $d\sigma/d\Omega$.

Production Distributions for $K^-p \rightarrow \pi^+ Y^{*-}$

Table 3.8

15) μb at 2.1 GeV/c and (82 ± 9) μb at 2.6 GeV/c. Taking note of the $\Sigma\pi$ decay mode of the Y^* (10%), we have normalized the result of his fits to $\sigma(Y^{*-}\pi^+)$ = 150.0 μb at 2.1 GeV/c and 91.1 μb at 2.6 GeV/c. The results are given in Fig. 3.13(d,e) and Table 3.8

As we did for Y^* production in πN at 2 GeV/c, we have corrected the forward bin at 2.1 GeV/c to take into account the effect of peripheral $\pi\pi$ production. (This problem is discussed in detail in Section 3.32.) After an examination of the $m(\Lambda\pi^-)$ spectrum for $\cos\theta_{pr} > 0.8$, we decreased the number of Y^* events by 29%. However, we did not renormalize, with the result that the total Y^* cross section indicated in Fig. 3.13(d) and Table 3.8 is 7% lower than Siegel's value.

Note that the distributions in Fig. 3.13(d-e) are in qualitative agreement with those obtained from a mass cut with background subtraction [Fig. 3.4(c), 3.5(c)].

3.223 REACTIONS (3) AND (4), Ξ^* PRODUCTION

This data came from the K63 experiment, as did that for reaction (2). Dauber *et al.* have reported on Ξ production in that exposure.[114] We used the final data tapes, reflecting the processing described in Ref. 114. The usual fiducial cuts were applied, removing about 15% of the events. The final state $K^+\Xi^0\pi^-$ was believed to be quite contaminated (≈26%); Dauber *et al.* defined a purified subsample, consisting essentially of unambiguous events, which was believed to be only ≈7% contaminated.[115] We usually did not apply this purification cut, but did check that it had little effect on the production distribution.

Dauber *et al.* studied Ξ^* production, obtaining production and decay distributions by mass cuts.[116] We repeated that procedure to get the distributions given in Fig. 3.14(a-d). Because of the small background under the Ξ^*, no background subtraction was done. (The distributions with that subtraction are given in Figs. 3.47-3.50(c) below.) We have normalized to the cross sections given in Table 6 of Ref. 114. The results are given in Tables 3.9 and 3.10.

$\cos\theta_{pr}$ $[\hat{K}^- \cdot \hat{K}^+]$	Number of Ξ^{*-} Events	$d\sigma/d\Omega$ (μb/sr)
P=2.1 GeV/c:		
-1.0 to -0.9	11.6 ± 3.7	3.61 ± 1.15
-0.9 to -0.8	9.0 ± 3.2	2.80 ± 1.00
-0.8 to -0.7	13.5 ± 4.5	4.20 ± 1.40
-0.7 to -0.6	6.5 ± 2.6	2.01 ± 0.83
-0.6 to -0.5	5.5 ± 2.5	1.72 ± 0.77
-0.5 to -0.4	7.3 ± 2.8	2.29 ± 0.87
-0.4 to -0.3	10.0 ± 3.4	3.12 ± 1.05
-0.3 to -0.2	4.2 ± 2.1	1.32 ± 0.66
-0.2 to -0.1	3.3 ± 1.9	1.02 ± 0.59
-0.1 to 0.0	9.6 ± 3.8	3.00 ± 1.19
0.0 to 0.1	5.4 ± 2.4	1.68 ± 0.76
0.1 to 0.2	3.1 ± 1.8	0.95 ± 0.55
0.2 to 0.3	5.1 ± 2.3	1.60 ± 0.72
0.3 to 0.4	5.4 ± 2.4	1.70 ± 0.76
0.4 to 0.5	6.6 ± 2.7	2.06 ± 0.84
0.5 to 0.6	4.4 ± 2.2	1.36 ± 0.69
0.6 to 0.7	4.3 ± 2.2	1.36 ± 0.68
0.7 to 0.8	8.0 ± 3.1	2.50 ± 0.95
0.8 to 0.9	7.3 ± 3.0	2.27 ± 0.93
0.9 to 1.0	12.8 ± 3.7	3.98 ± 1.16

Totals: N = 142.9, $\sigma \pm \partial\sigma$ = (28 ± 4) μb. [$\partial\sigma/\sigma$ = 14%]

The normalization uncertainty, $\partial\sigma/\sigma$, is not included in the errors on $d\sigma/d\Omega$.

Production Distributions for $K^-p \rightarrow K^+\Xi^{*-}$

Table 3.9 (Page 1)

$\cos\theta_{pr}$ $[\hat{K}^- \cdot \hat{K}^+]$	Number of Ξ^{*-} Events	$d\sigma/d\Omega$ (μb/sr)
P≈2.6 GeV/c:		
-1.0 to -0.9	17.6 ± 4.6	1.99 ± 0.52
-0.9 to -0.8	18.8 ± 5.3	2.12 ± 0.60
-0.8 to -0.7	28.2 ± 5.8	3.20 ± 0.66
-0.7 to -0.6	9.3 ± 3.3	1.05 ± 0.37
-0.6 to -0.5	6.5 ± 2.7	0.74 ± 0.30
-0.5 to -0.4	3.0 ± 1.7	0.34 ± 0.20
-0.4 to -0.3	10.2 ± 3.4	1.16 ± 0.39
-0.3 to -0.2	9.2 ± 3.9	1.04 ± 0.44
-0.2 to -0.1	7.8 ± 3.2	0.88 ± 0.36
-0.1 to 0.0	5.1 ± 2.6	0.57 ± 0.29
0.0 to 0.1	8.4 ± 3.2	0.96 ± 0.36
0.1 to 0.2	11.5 ± 4.3	1.30 ± 0.49
0.2 to 0.3	2.0 ± 1.4	0.23 ± 0.16
0.3 to 0.4	2.6 ± 1.8	0.29 ± 0.21
0.4 to 0.5	5.4 ± 2.4	0.62 ± 0.28
0.5 to 0.6	5.3 ± 2.4	0.61 ± 0.27
0.6 to 0.7	9.5 ± 3.4	1.08 ± 0.38
0.7 to 0.8	12.7 ± 3.9	1.44 ± 0.44
0.8 to 0.9	14.9 ± 4.2	1.69 ± 0.47
0.9 to 1.0	36.7 ± 6.5	4.15 ± 0.73

Totals: $N = 224.9$, $\sigma \pm \partial\sigma = (16 \pm 3)$ μb. $[\partial\sigma/\sigma = 19\%]$

The normalization uncertainty, $\partial\sigma/\sigma$, is not included in the errors on $d\sigma/d\Omega$.

Production Distributions for $K^-p \rightarrow K^+\Xi^{*-}$

Table 3.9 (Page 2)

Cos θ_{pr} $[\hat{K}^- \cdot \hat{K}^o]$	Number of Ξ^{*o} Events	$d\sigma/d\Omega$ (μb/sr)
P=2.1 GeV/c:		
-1.0 to -0.9	12.6 ± 4.4	6.53 ± 2.25
-0.9 to -0.8	8.5 ± 3.7	4.41 ± 1.91
-0.8 to -0.7	22.3 ± 6.2	11.51 ± 3.21
-0.7 to -0.6	30.6 ± 6.7	15.81 ± 3.45
-0.6 to -0.5	16.3 ± 4.5	8.41 ± 2.34
-0.5 to -0.4	16.9 ± 4.7	8.72 ± 2.43
-0.4 to -0.3	16.6 ± 5.4	8.58 ± 2.76
-0.3 to -0.2	10.0 ± 3.6	5.18 ± 1.83
-0.2 to -0.1	15.1 ± 4.4	7.82 ± 2.26
-0.1 to 0.0	7.3 ± 3.0	3.79 ± 1.55
0.0 to 0.1	11.8 ± 3.9	6.09 ± 2.04
0.1 to 0.2	11.6 ± 3.9	5.98 ± 1.99
0.2 to 0.3	9.1 ± 3.4	4.70 ± 1.78
0.3 to 0.4	7.7 ± 3.1	3.95 ± 1.61
0.4 to 0.5	6.5 ± 2.9	3.35 ± 1.50
0.5 to 0.6	7.6 ± 3.1	3.91 ± 1.60
0.6 to 0.7	7.8 ± 3.2	4.00 ± 1.63
0.7 to 0.8	10.0 ± 3.8	5.15 ± 1.96
0.8 to 0.9	6.7 ± 3.0	3.46 ± 1.55
0.9 to 1.0	11.6 ± 4.1	5.97 ± 2.12

Totals: N = 246.7, $\sigma \pm \partial\sigma$ = (80 ± 11) μb. [$\partial\sigma/\sigma$ = 14%]

The normalization uncertainty, $\partial\sigma/\sigma$, is not included in the errors on $d\sigma/d\Omega$

Production Distributions for $K^-p \rightarrow K^o\Xi^{*o}$

Table 3.10 (Page 1)

$\cos\theta_{pr}$ $[\hat{K}^- \cdot \hat{K}^o]$	Number of Ξ^{*o} Events	$d\sigma/d\Omega$ (μb/sr)
P≈2.6 GeV/c:		
-1.0 to -0.9	16.8 ± 4.7	2.70 ± 0.76
-0.9 to -0.8	18.6 ± 4.8	3.00 ± 0.77
-0.8 to -0.7	40.9 ± 7.4	6.57 ± 1.20
-0.7 to -0.6	15.7 ± 5.3	2.52 ± 0.85
-0.6 to -0.5	12.7 ± 4.0	2.04 ± 0.65
-0.5 to -0.4	14.5 ± 4.4	2.33 ± 0.70
-0.4 to -0.3	6.8 ± 3.1	1.09 ± 0.49
-0.3 to -0.2	3.9 ± 2.2	0.62 ± 0.36
-0.2 to -0.1	11.6 ± 3.9	1.86 ± 0.62
-0.1 to 0.0	7.5 ± 3.1	1.20 ± 0.49
0.0 to 0.1	9.3 ± 3.9	1.49 ± 0.62
0.1 to 0.2	15.4 ± 4.7	2.48 ± 0.76
0.2 to 0.3	8.8 ± 3.3	1.42 ± 0.54
0.3 to 0.4	12.9 ± 4.1	2.07 ± 0.65
0.4 to 0.5	7.8 ± 3.2	1.25 ± 0.51
0.5 to 0.6	8.2 ± 3.4	1.31 ± 0.54
0.6 to 0.7	9.5 ± 3.6	1.53 ± 0.58
0.7 to 0.8	7.3 ± 3.3	1.18 ± 0.53
0.8 to 0.9	4.1 ± 2.3	0.65 ± 0.38
0.9 to 1.0	5.6 ± 2.8	0.90 ± 0.45

Totals: $N = 237.6$, $\sigma \pm \partial\sigma = (24 \pm 3)$ μb. $[\partial\sigma/\sigma = 12\%]$

The normalization uncertainty, $\partial\sigma/\sigma$, is not included in the errors on $d\sigma/d\Omega$.

Production Distributions for $K^-p \rightarrow K^o\Xi^{*o}$

Table 3.10 (Page 2)

3.224 REACTION (6), $\pi N \rightarrow \pi\Delta$

Description of the Data Sample

For the reaction $\pi^+ d \rightarrow (p_{sp})\pi^-\pi^+ p$, we used data from the low momentum (1.1 to 2.4 GeV/c) part of the Pi66 experiment. This final state is discussed in detail in Jerry Manning's thesis.[117] We have divided the data into two intervals at an effective c.m. energy (for the $p\pi^+\pi^-$ system, excluding the spectator proton) of 2.05 GeV/c, which corresponds to a beam momentum of 1.75 GeV/c. These intervals are denoted by "P<1.8" and "P~2.2" respectively. In the P<1.8 sample we have only even-pronged events (i.e., those with a visible spectator proton); at P~2.2 we have both even-prongs (from the low-momentum beam settings) and odd-prongs. [The $E_{c.m.}$ spectra are in Fig. 3.15 and (for even- and odd-prongs separately) Fig. 3.16.] The spectator-momentum cut removes 41% of the ≈10000 events at 1.8 GeV/c and 15% of the ≈14000 events at ≈2.2 GeV/c.

The data for the reaction $\pi^- p \rightarrow \pi^+\pi^- n$ was provided to us by Larry Jacobs. It consists of events from the Pi72 experiment (run in 1962 on the 72-inch chamber) at 2.05, 2.17, and 2.36 GeV/c, and from the Pi63 exposure at 2.60, 2.86, and 3.22 GeV/c. The processing of this data is discussed in Jacobs' thesis.[118] The 5 lower momenta were grouped together (along with $\pi^+ n$ data) in the 'P~2.2" sample; the highest-momentum data forms Sample 12. The fiducial cut removes ≈10% of the ≈8000 events.

Shape of the Production Distribution

Because of the low c.m. energy, we did not take the trouble of making a determination of $d\sigma(\Delta\pi)/d\Omega$ from the data below 1.8 GeV/c. The production distribution obtained from cuts is given in Fig. 3.10; there is a forward peak in the N^* band but it is not immediately apparent how much is due to the broad kinematic enhancement. There is some N^* in the forward region, as shown by Figs. 3.27(b) and 3.63(b) below. [In this interval, $\sigma(\pi^+\pi^- p)$ is about 8 mb and falling rapidly;[117] that number corresponds to 2 μb/ev for the 4003 events in our cut sample.]

When we did our published determination of $d\sigma/d\Omega$ at 2.2 GeV/c, we had only the $\pi^+ n$ data. Here again we faced the problem of disentangling Δ production from the broad low-mass enhancement. We simply estimated the number of Δ events from plots of m(Nπ) in various intervals of $\cos\theta_{pr}$. Unfortunately, in the forward direction the enhancement peaks at just about the same $m(p\pi^+)$ as the Δ. In Figs. 3.17(a-b) we give the mass plots for the two most forward bins and our

$\cos\theta_{pr}$ $[\hat{\pi}\cdot\hat{\pi}]$	Number of Δ Events	$d\sigma/d\Omega$ (μb/sr)
P≈2.2 GeV/c, $\pi^+n \rightarrow \pi^-\Delta^{++}$ [Note unequal bin widths]:		
-1.0 to -0.9	48 ± 15	32 ± 10
-0.9 to -0.8	84 ± 11	56 ± 7
-0.8 to -0.7	76 ± 13	50 ± 9
-0.7 to -0.5	78 ± 17	26 ± 6
-0.5 to -0.3	30 ± 12	10 ± 4
-0.3 to -0.1	27 ± 9	9 ± 3
-0.1 to 0.1	33 ± 10	11 ± 3
0.1 to 0.3	42 ± 15	14 ± 5
0.3 to 0.5	36 ± 12	12 ± 4
0.5 to 0.7	52 ± 12	17 ± 4
0.7 to 0.8	85 ± 15	57 ± 10
0.8 to 0.9	126 ± 25	83 ± 17
0.9 to 1.0	230 ± 40	152 ± 27
Totals: N = 947, $\sigma \pm \partial\sigma$ = (395 ± 118) μb. [$\partial\sigma/\sigma$ = 30%]		
P=3.2 GeV/c, $\pi^-p \rightarrow \pi^+\Delta^-$ [Note unequal bin widths]:		
-1.0 to -0.9	5 ± 2	9.5 ± 3.8
-0.9 to -0.8	6 ± 2	11.4 ± 3.8
-0.8 to -0.6	3 ± 1	2.8 ± 0.9
-0.6 to -0.4	1 ± 1	0.9 ± 0.9
-0.4 to -0.2	2 ± 2	1.9 ± 1.9
-0.2 to 0.0	3 ± 3	2.8 ± 2.8
0.0 to 0.2	0 ± 1	0.0 ± 0.9
0.2 to 0.4	0 ± 1	0.0 ± 0.9
0.4 to 0.6	1 ± 1	0.9 ± 0.9
0.6 to 0.8	0 ± 1	0.0 ± 0.9
0.8 to 0.9	3 ± 1	5.7 ± 1.9
0.9 to 0.95	10 ± 5	37.9 ± 19.0
0.95 to 1.0	$28\ ^{+\ 6}_{-\ 12}$	$106.2\ ^{+\ 22.8}_{-\ 45.5}$
Totals: N = 62, $\sigma \pm \partial\sigma$ = (74 ± 12) μb. [$\partial\sigma/\sigma$ = 17%]		

The normalization uncertainty, $\partial\sigma/\sigma$, is not included in the errors on $d\sigma/d\Omega$.

Production Distributions for $\pi^-p \rightarrow \pi^+\Delta^-$ (and $\pi^+n \rightarrow \pi^-\Delta^{++}$)

Table 3.11

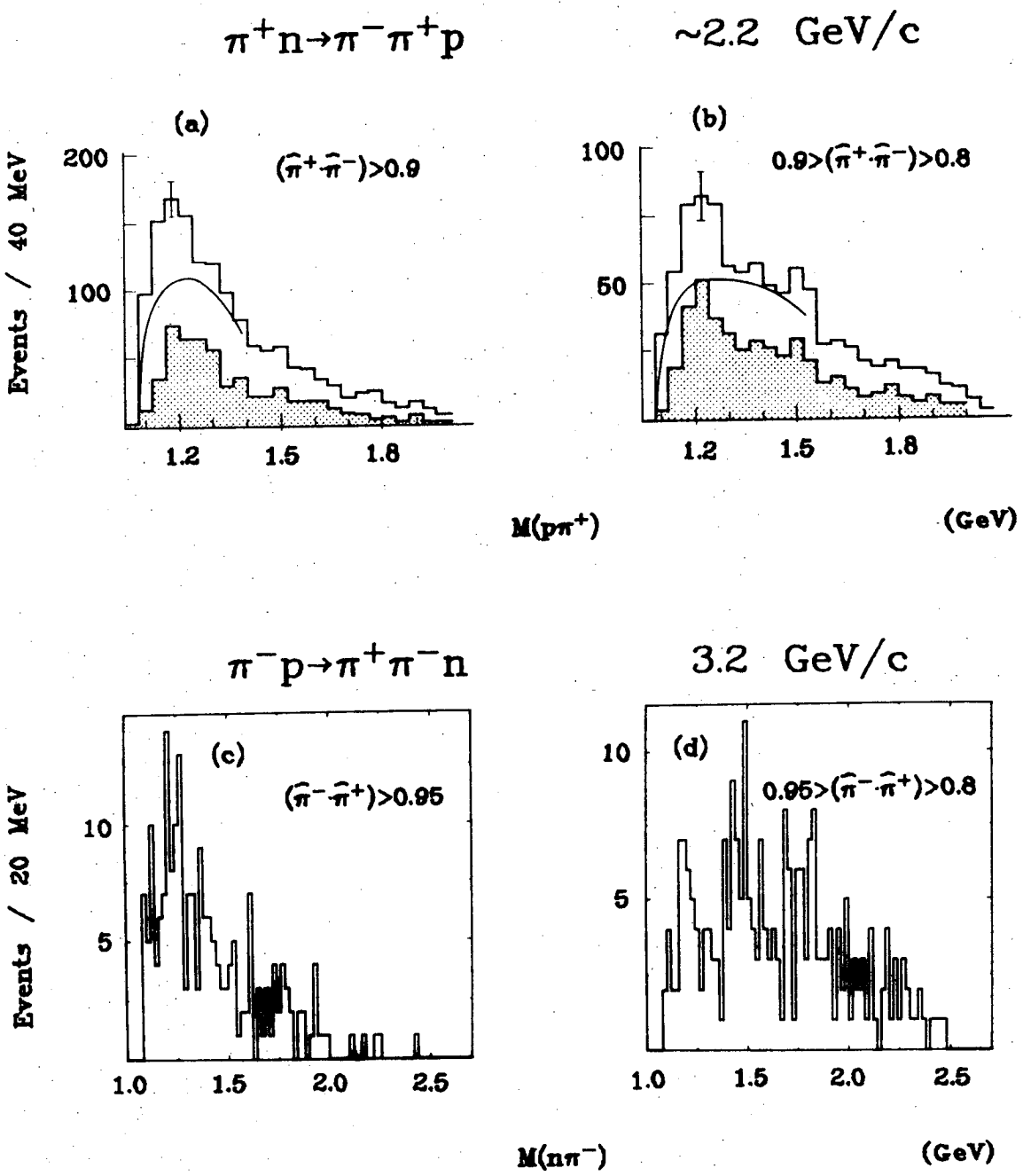

XBL 729-1793

Fig. 3.17

hand-drawn curves from which we got the number of Δ events. When the ρ band is removed (shaded histograms), the Δ is enhanced a little. The numbers of events (and the results of the normalization to $\sigma(\Delta\pi)$) are given in Table 3.11 and Fig. 3.14(e).

At 3.2 GeV/c, almost all the Δ events have $\cos\theta_{pr} > 0.8$. The $m(n\pi^-)$ spectra for the forward region are given in Fig. 3.17(c-d). There is Δ^- production for $\cos\theta_{pr}>0.95$, but it is hard to separate from the low-mass kinematic enhancement. For $0.8 < \cos\theta_{pr} < 0.95$, however, the Δ peak stands out more clearly above the background. We estimated the number of Δ events in each production interval from these mass spectra; the results (with the normalization) are given in Fig. 3.14(f) and Table 3.11.

Cross-Section Normalization

In the 2.2 GeV/c interval, we obtained $\sigma(N\pi\pi)$ both by extrapolating Jacobs' values[119] and by simply dividing the number of events in our uncut π^+n sample by the exposure size. We obtained [respectively] 5.9 [5.4, 4.2] mb at P = 1.9 [2.1, 2.4] GeV/c. We then estimated the Δ fraction by counting events in a plot of $m(N\pi)$ for all production angles, and got Δ production cross sections of 538 [434, 380] μb. Our plot of the production distribution for all these 3 parts of the "P~2.2" sample together is normalized to 395 μb; we estimate the error to be ±30%. This is in fact higher than Jacobs' determination of the Δ production cross section, which ranged from (350 ± 100) μb at P=2.05 GeV/c to (100 ± 50) μb at 2.86 GeV/c.[120] He obtained these values by counting Δ events. Although we feel that our eyeball estimate of the number of Δ events was conservative, we do note the possibility that our forward peak is overestimated by up to a factor of two.

At 3.2 GeV/c, we have normalized to $\sigma(\Delta^-\pi^+)$ = (74 ± 12) μb. This was obtained from our estimate of (62 ± 10) Δ events at all $\cos\theta_{pr}$, and Jacobs' path length value of 0.839 ev/μb ± 5%.[121] (Jacobs' own estimate, apparently also obtained by counting events, was (0.05 ± 0.02) mb.[120])

3.225 CROSS SECTION VALUES

In Table 3.12 we summarize our results for the B^* production cross section at all production angles and in the forward hemisphere, and the differential cross section in the forward bin. The information comes from Tables 3.6 and 3.8-3.11, which have just been discussed. In those tables, and in Figs. 3.13-3.14, we

Sample	Reaction	P_{bm} (GeV/c)	σ(total) (μb)	σ(cos θ_{pr}>0) (μb) (a)	Forward Bin cos θ_{pr}(min)	dσ/dΩ (μb/sr) (a)
1	$\pi^-p \to K^+Y^{*-}$ (b)	≈2	44.00 ± 4.44	23.12 ± 4.17	0.67	7.36 ± 1.58
2	"	≈3	6.11 ± 1.67	4.74 ± 1.66	0.67	2.09 ± 0.72
3	"	≈4	3.88 ± 2.26	3.15 ± 2.10	0.67	1.63 ± 1.05
4	$K^-p \to \pi^+Y^{*-}$	2.1	139.0 ± 16.7	60.3 ± 13.5	0.8	21.11 ± 8.13
5	"	≈2.6	91.1 ± 10.0	43.43 ± 6.56	0.8	19.27 ± 3.19
6	$K^-p \to K^+\Xi^{*-}$	2.1	28. ± 4.	12.23 ± 2.39	0.9	3.98 ± 1.29
7	"	≈2.6	16. ± 3.	7.77 ± 1.67	0.9	4.15 ± 1.07
8	$K^-p \to K^0\Xi^{*0}$	2.1	80. ± 11.	29.26 ± 5.37	0.9	5.97 ± 2.27
9	"	≈2.6	24. ± 3.	8.97 ± 1.59	0.9	0.90 ± 0.46
11	$\pi^+n \to \pi^-\Delta^{++}$	≈2.2	395. ± 118.5	245.3 ± 77.1	0.9	152.0 ± 53.0
12	$\pi^-p \to \pi^+\Delta^-$	3.2	74. ± 12.	50.1 ± 12.2	0.95	106.2 $^{+\ 28.6}_{-\ 48.7}$

(a) From Tables 3.6 and 3.8–3.11, with the error in σ(total) folded in.

(b) Includes data from the charge-symmetric reaction.

Summary of Forward Cross Sections

Table 3.12

presented the shape of the production distribution and gave only the error (statistical or estimated) on the number of events in each interval. In Table 3.12, however, we have included the normalization uncertainties in the error estimates.

3.23 ADDITIONAL FEATURES OF THE DATA

First we show some figures designed to convince the skeptical reader that there really are forbidden forward peaks. We point out other features of the final states, in many cases stronger than the process of interest; they do not obscure the forward peaking. To do this we look at Dalitz plots and their projections for various regions in $\cos\theta_{pr}$, and at production distributions obtained by mass cuts with various degrees of refinement. We examine the degree to which the forward peaking is associated with the competing meson resonance (M^*) production process.

Then we look at other features of the foward peaking: decay distributions, slopes in momentum transfer, and energy dependence.

We usually made each of these plots for all 12 data samples. To avoid confusion and preserve an adequate record we present all of the plots systematically here.[122] We comment only on the plots of special interest. We have not indicated the number of events in each figure; tallies containing this information are presented below (Table 3.14).

Forward-Production Dalitz Plots

In Fig. 3.18$^+$ [i.e., 3.18-3.29 for Samples (1)-(12)] we repeat the Dalitz plot for the forward production region, this time with all its projections. As is the case in all plots unless "raw data" is specified, we have made the usual cuts on fiducial volume and spectator momentum, and applied the fiducial weights in the histograms.

Strong M^* production is evident in the $m(M\pi)$ spectrum, Fig. 3.18$^+$(c), in most cases. The strong peripheral $M\pi$ production results in a low-mass enhancement in $m(B\pi)$ [Fig. 3.18$^+$(b)]. (In this interval of $\cos\theta_{pr}$, it also gives a high-mass enhancement in m(BM) [Fig. 3.18$^+$(d)].) The forbidden peaking is seen as a relatively narrow peak in the region of this enhancement in $m(B\pi)$. In Fig. 3.19 and 3.20, the narrow Y^* peak is evident; assuming that the resolution is not worse at lower beam momentum, one can see Y^* production in Fig. 3.18(b). (Recall

Fig. 11. Visible absorption spectra of three free base chlorins.

Chlorin (38) ————————————

Etiochlorin (54) . . . . . .

Pyromethyl pheophorbide a (38) - - - - - - - -

MCD of pyromethyl pheophorbide (9) (topmost dashed curve)

Fig. 12. Absorption spectra of three free base chlorins derived from chlorophyll a.(9,54,55) Compounds are numbered 11, 7, and 12, respectively, in Table I.

Fig. 13. Magnetic circular dichroism spectra of two free base chlorins.(9) Units of $[\theta]_M$ are deg mole^{-1} cm^3 at 41.7 kgauss.

Pyromethyl pheophorbide - - - - - - - - - - -

Chlorin e_6 ————————————

Fig. 14. Absorption and fluorescence polarization spectrum of chlorophyll a in castor oil.(65) Dashed absorption curve is in ether.

Fig. 15. Absorption and MCD spectra of chlorophyll a in ether.(11)

Fig. 16. Transition monopoles for near infra-red and visible Q_y and Q_x transitions in simulated bacteriochlorophyll. Monopoles are in thousands of an electronic charge, dipoles in e-Å. All numbers are normalized to give experimental oscillator strengths when experimental energies are used. (β_{CO} = -2.36 eV, CI to 150 nm, SCMO-PPP calculations.)

Fig. 17. Ground state bond orders and charge densities for simulated bacteriochlorophyll a and chlorophyll a. (β_{CO} = -2.36 eV, SCMO-PPP calculation.)

Fig. 18. Coefficients of highest occupied and lowest empty orbitals in simulated bacteriochlorophyll a and chlorophyll a. (β_{CO} = -2.36 eV, SCMO-PPP calculation.) Coefficients for meso carbons are inside the ring, for α carbons outside.

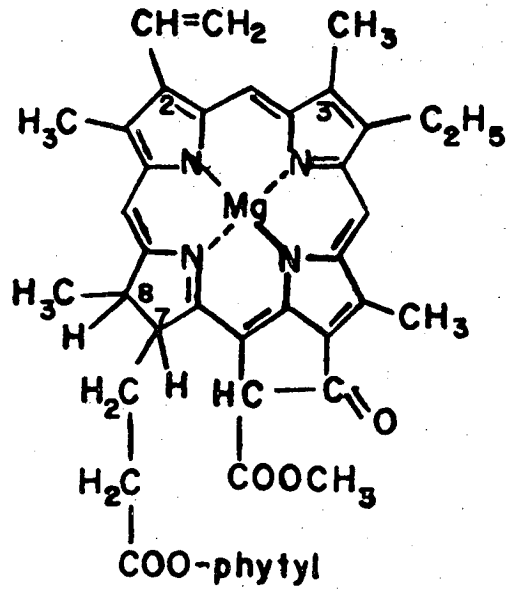

Chlorophyll a
Chlorophyll b: 3-CHO
Chlorophyll d: 2-CHO
Protochlorophyll:
7,8-dehydrochlorophyll
Pheophytin a, b, d: H_2 replaces Mg
Methyl Pheophorbide a, b, d: CH_3 replaces phytyl in pheophytin

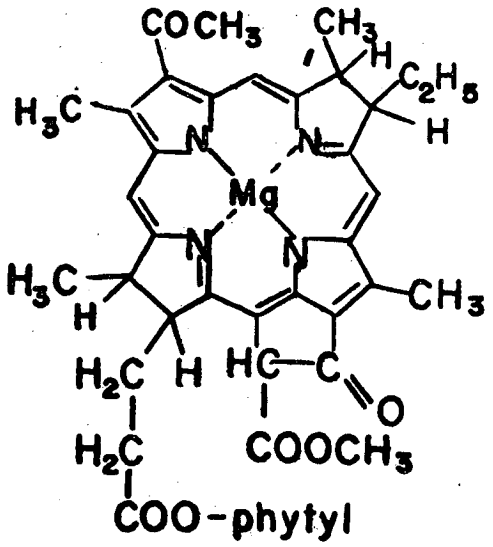

Bacteriochlorophyll

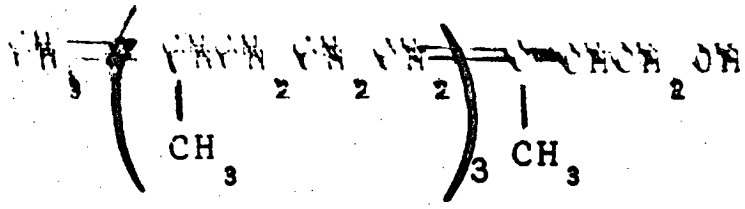

Phytol

Fig. 1

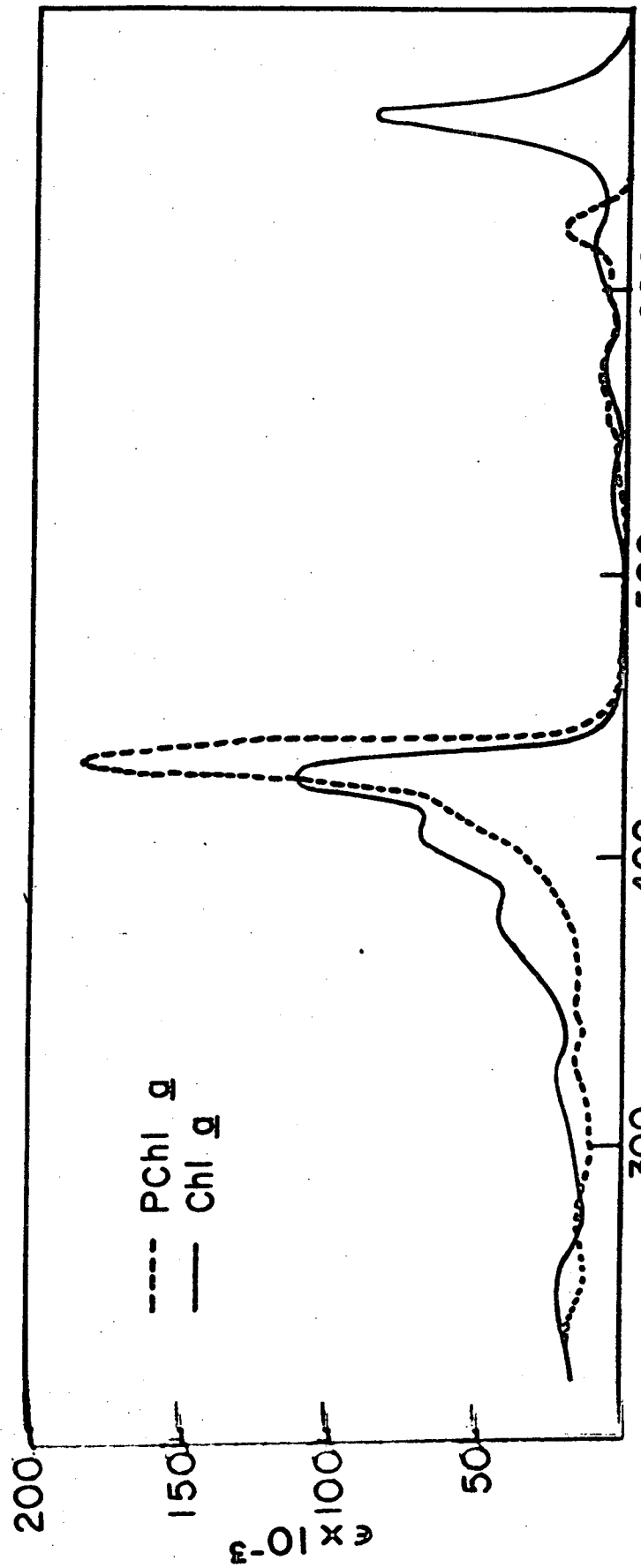

Fig. 2

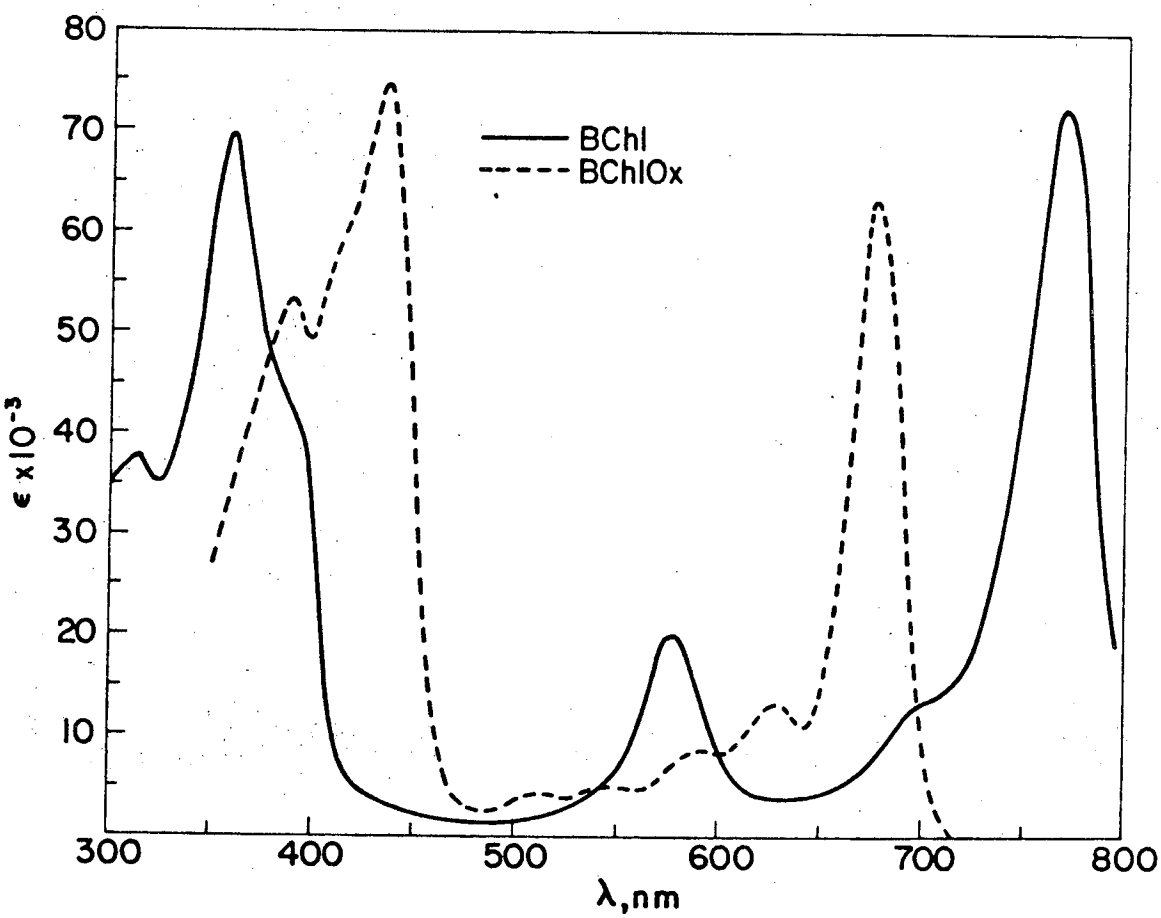
80
70
60
50
40
30
20
10
ε x10⁻³
300
400
500
600
700
800
λ,nm
BChl
BChlOx

Fig. 3

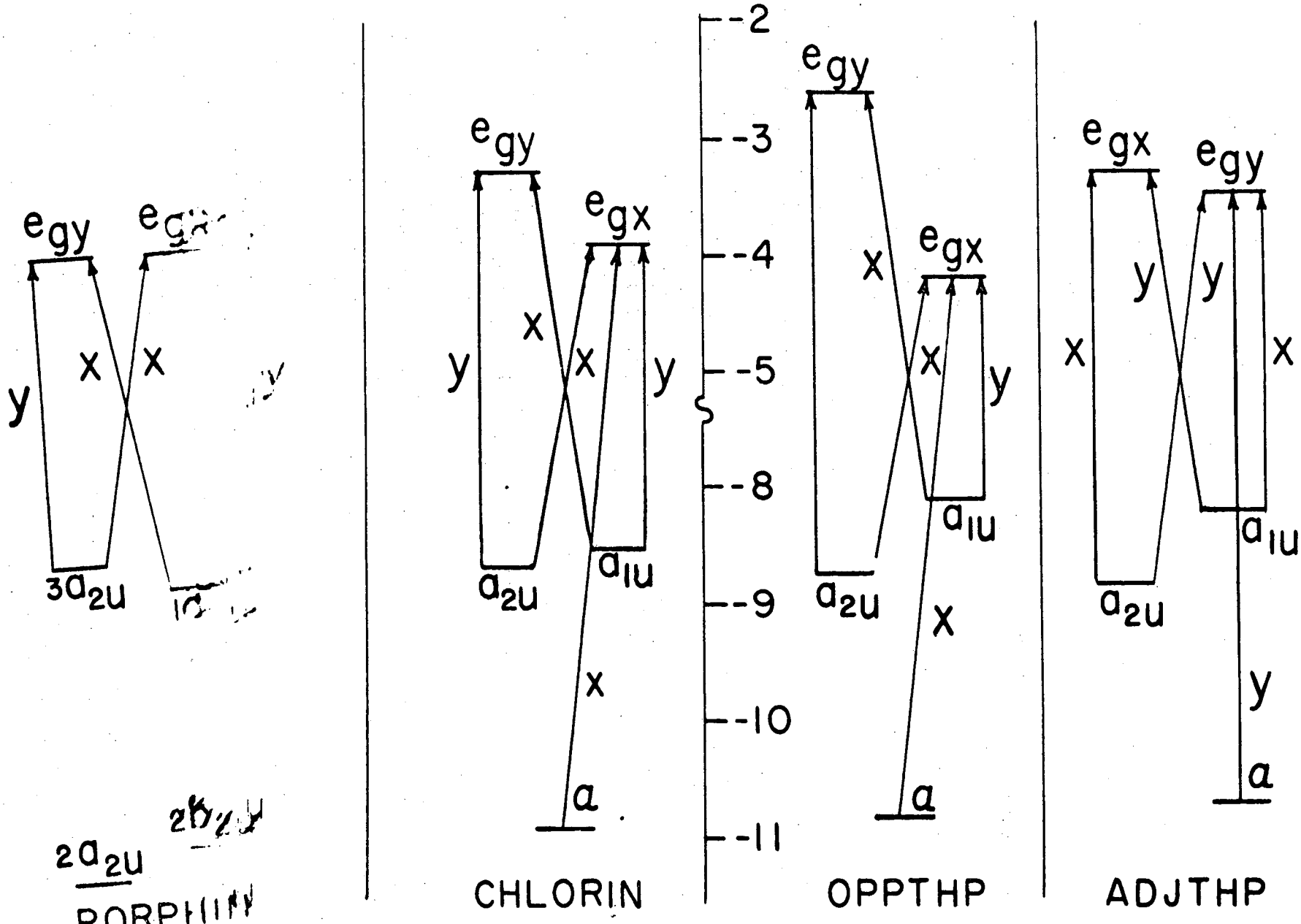
egy
egx
x
y
3a2u
2a2u
PORPHIN
CHLORIN
OPPTHP
ADJTHP
a2u
a1u
a
-2
-3
-4
-5
-8
-9
-10
-11

Fig. 4

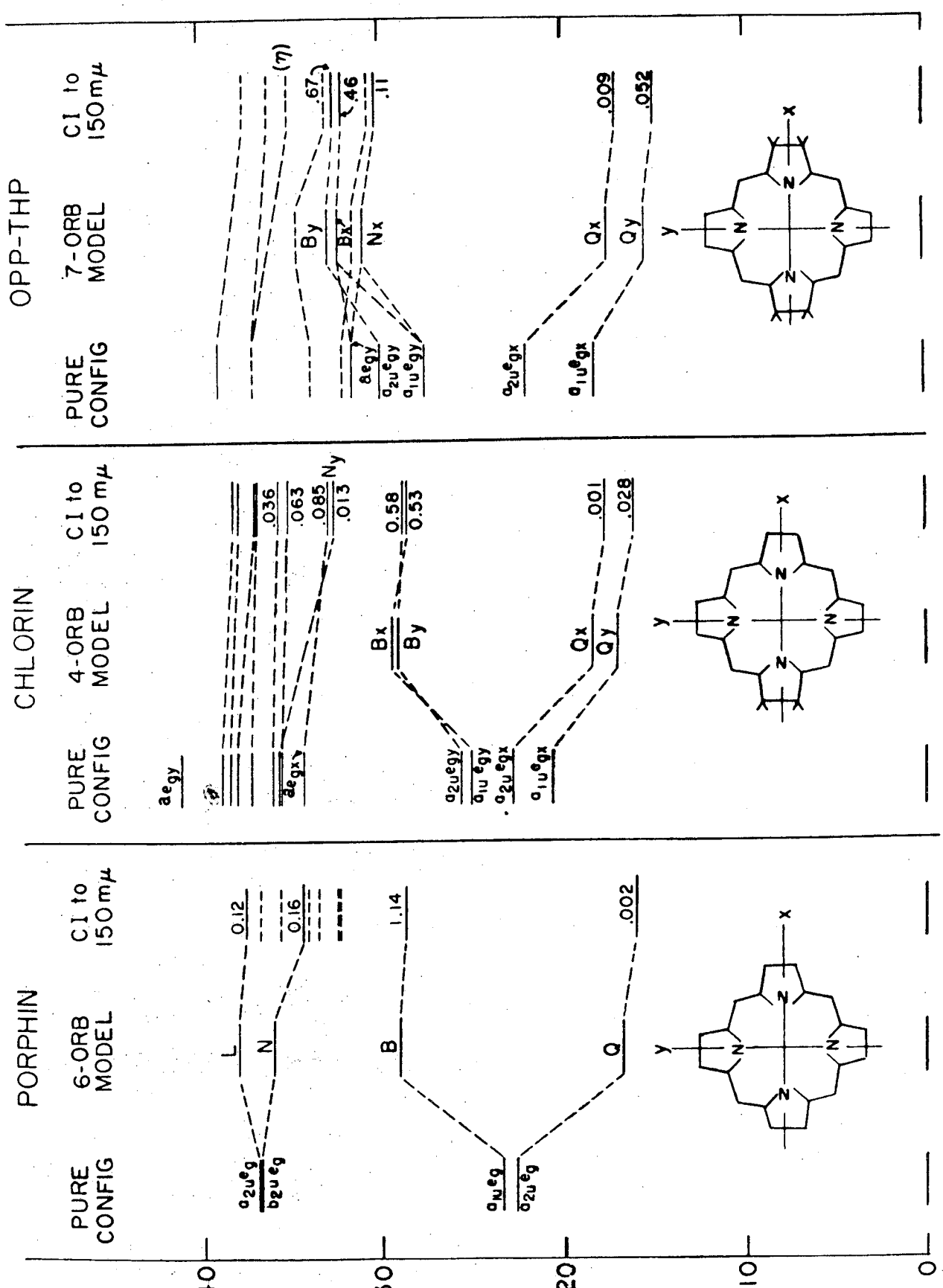
PORPHIN
6-ORB MODEL
CI to 150mμ
PURE CONFIG
CHLORIN
4-ORB MODEL
CI to 150 mμ
PURE CONFIG
OPP-THP
7-ORB MODEL
CI to 150mμ
PURE CONFIG
cm⁻¹ x 10⁻³
40
30
20
10
0
L
N
B
Q
Bx
By
Nx
Ny
Qx
Qy
0.12
0.16
1.14
.002
0.58
0.53
.036
.063
.085
.013
.001
.028
.67
.46
.11
.009
.052
x
y
N

Fig. 5

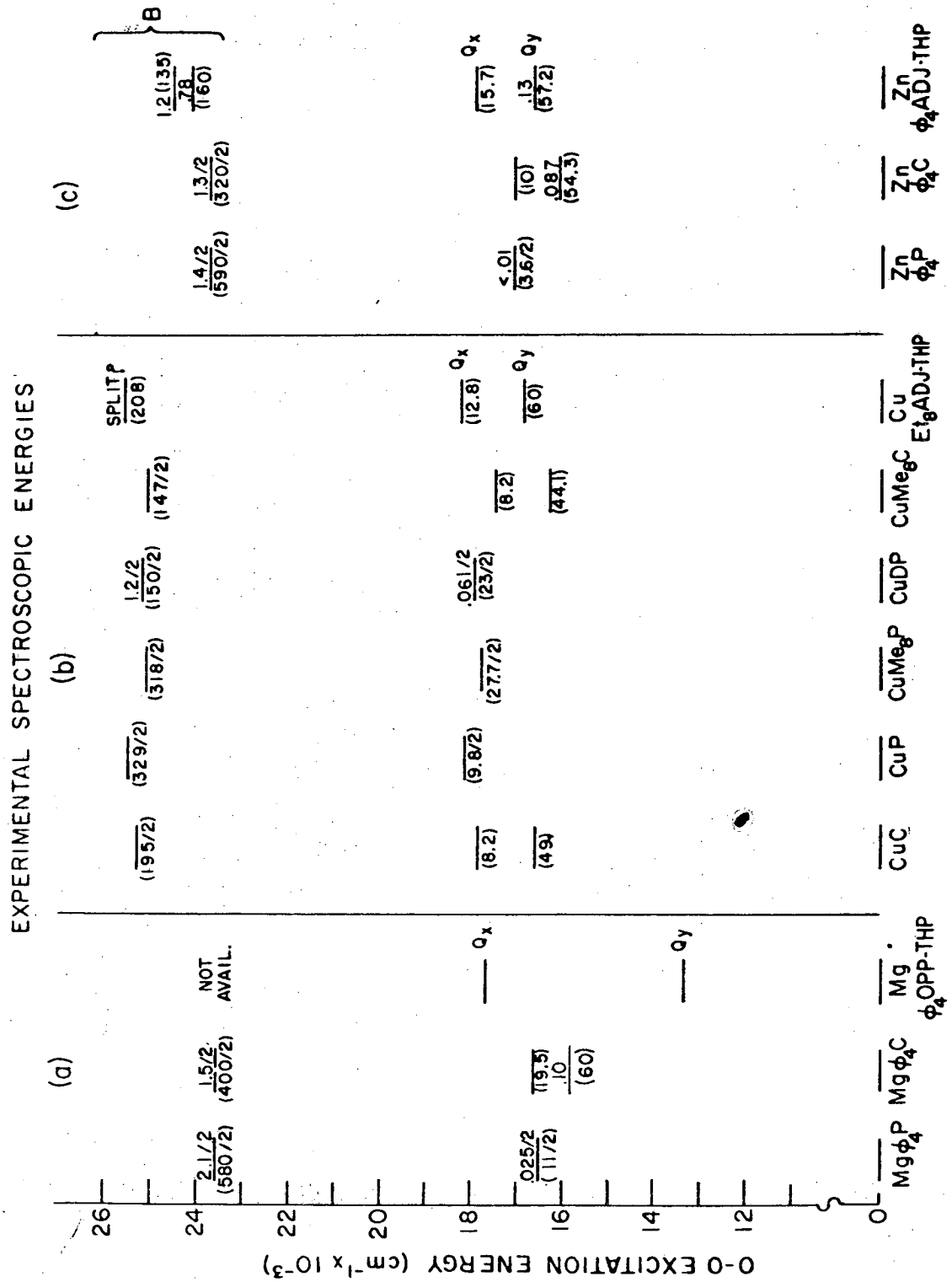
EXPERIMENTAL SPECTROSCOPIC ENERGIES
0-0 EXCITATION ENERGY (cm⁻¹ x 10⁻³)
(a)
(b)
(c)
Mgφ4P
Mgφ4C
Mg φ4OPP-THP
CuC
CuP
CuMe8P
CuDP
CuMe8C
Cu E't8ADJ-THP
Zn φ4P
Zn φ4C
Zn φ4ADJ-THP
Qx
Qy
NOT AVAIL.
SPLIT?
B

Fig. 6a, b, c

BACTERIOCHLOROPHYLL ABSORPTION IN DIFFERENT SOLVENTS

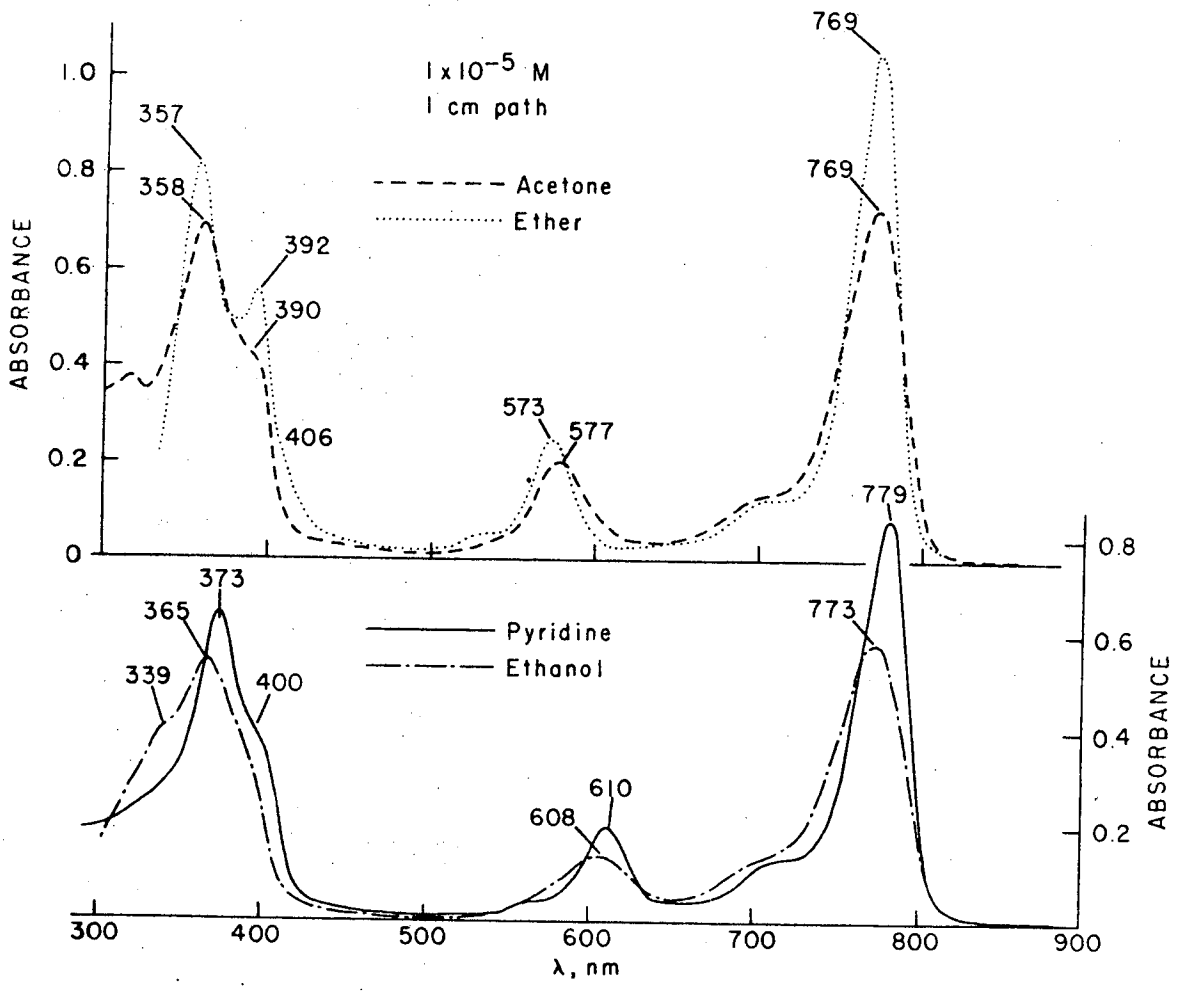

Fig. 7

XBL 6911-5365

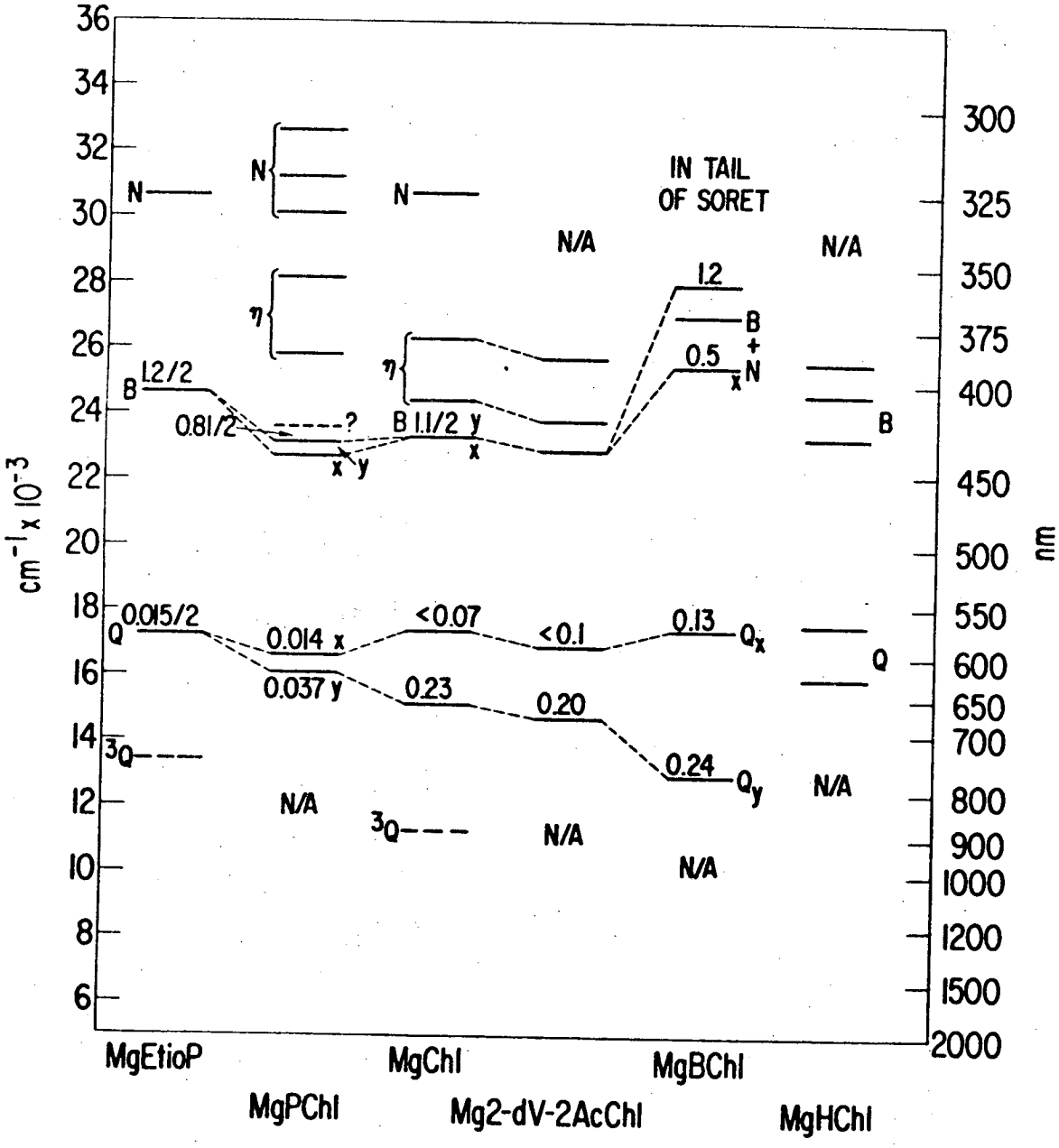
36
34
32
30
28
26
24
22
20
18
16
14
12
10
8
6
cm⁻¹ x 10⁻³
300
325
350
375
400
450
500
550
600
650
700
800
900
1000
1200
1500
2000
nm
N
N
N
IN TAIL
OF SORET
N/A
N/A
η
η
1.2
B
0.5
N
B 1.2/2
0.81/2
?
B 1.1/2 y
x
y
x
B
Q 0.015/2
0.014 x
<0.07
<0.1
0.13
Qx
Q
0.037 y
0.23
0.20
0.24
Qy
3Q
N/A
3Q
N/A
N/A
N/A
MgEtioP
MgChl
MgBChl
MgPChl
Mg2-dV-2AcChl
MgHChl

Fig. 8

Optical activity of PChl-a in ether

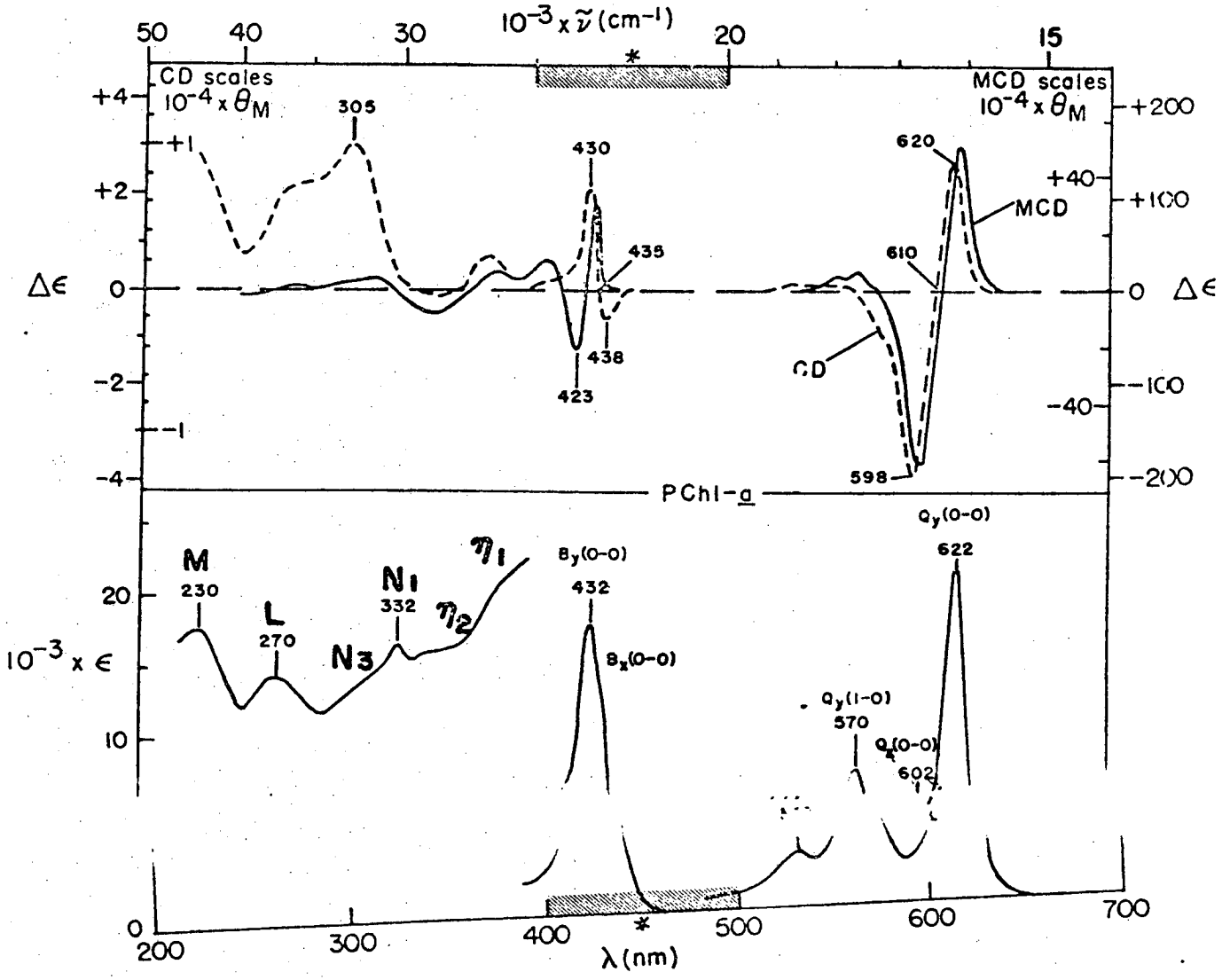

Fig. 9

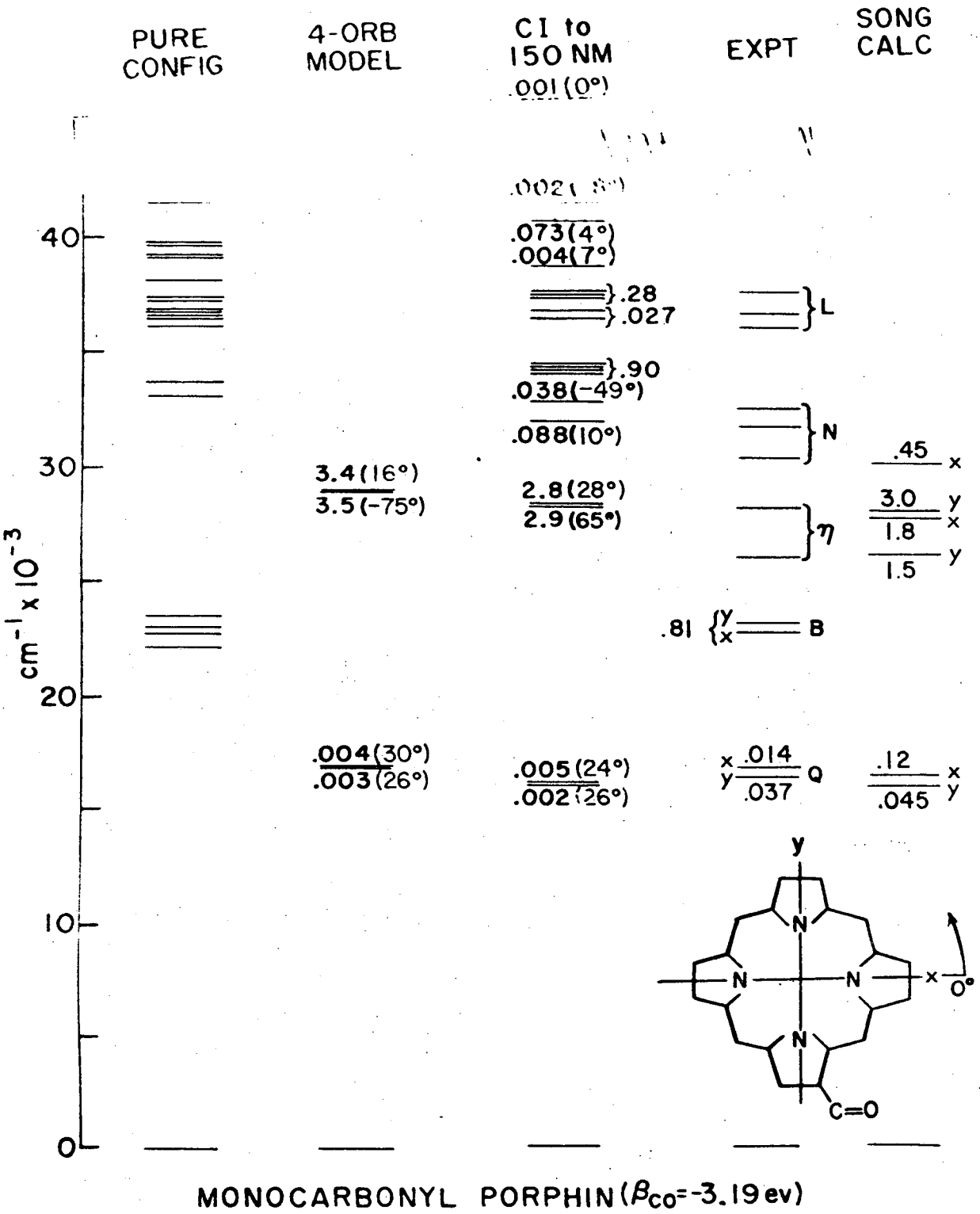
PURE CONFIG
4-ORB MODEL
CI to 150 NM
EXPT
SONG CALC
.001(0°)
.002(8°)
.073(4°)
.004(7°)
.28
.027
L
.90
.038(-49°)
.088(10°)
N
.45 x
3.4(16°)
3.5(-75°)
2.8(28°)
2.9(65°)
3.0 y
1.8 x
1.5 y
η
.81 y x B
.004(30°)
.003(26°)
.005(24°)
.002(26°)
x .014 y .037 Q
.12 x
.045 y
cm⁻¹ x 10⁻³
40
30
20
10
0
y
N
N
N
x
0°
C=O
MONOCARBONYL PORPHIN (βCO=-3.19 ev)

Fig. 10

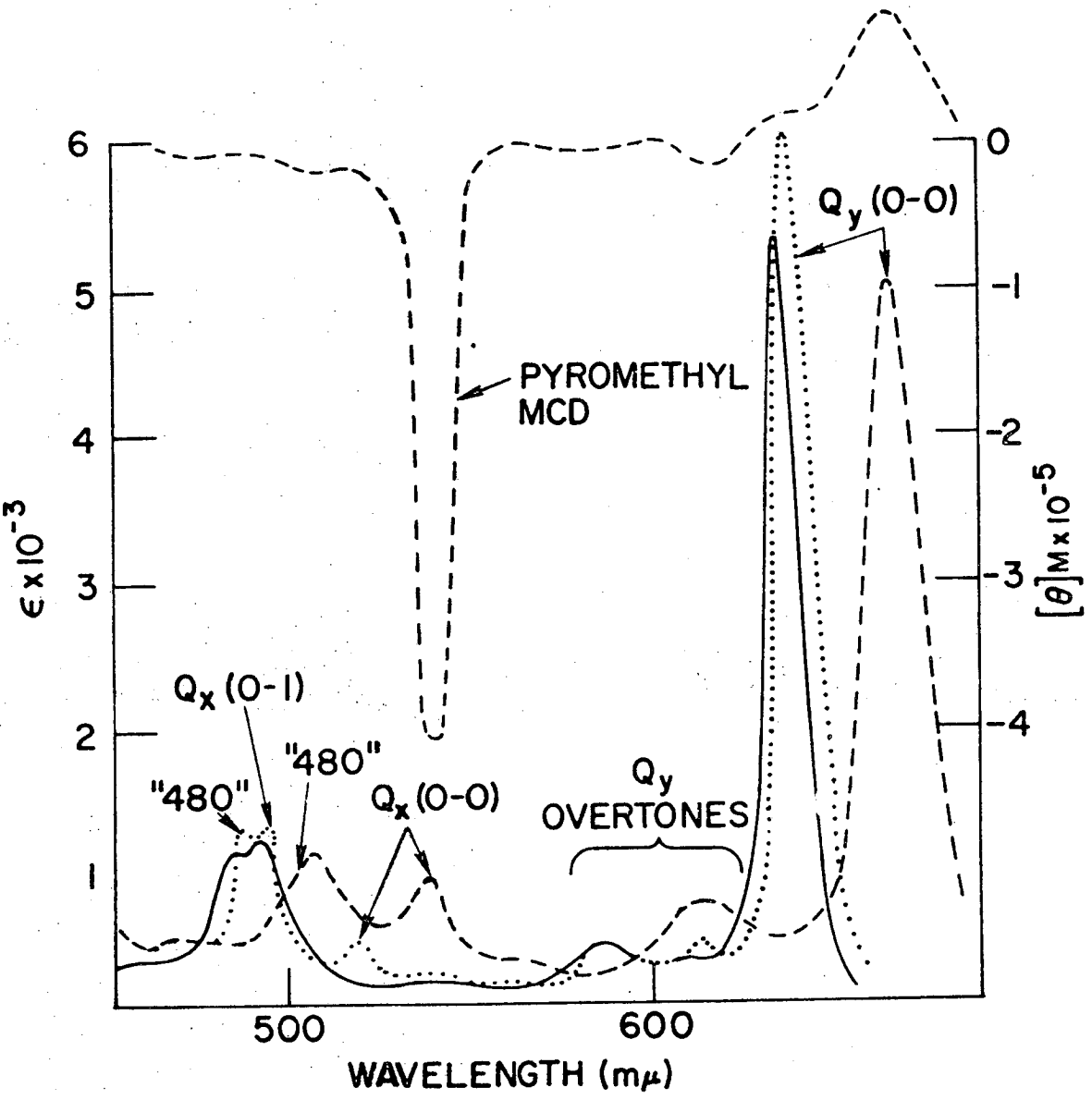
6
5
4
3
2
1
0
-1
-2
-3
-4
$\epsilon \times 10^{-3}$
$[\theta]M \times 10^{-5}$
Q_y (0-0)
PYROMETHYL MCD
Q_x (0-1)
"480"
"480"
Q_x (0-0)
Q_y OVERTONES
500
600
WAVELENGTH (mμ)

Fig. 11

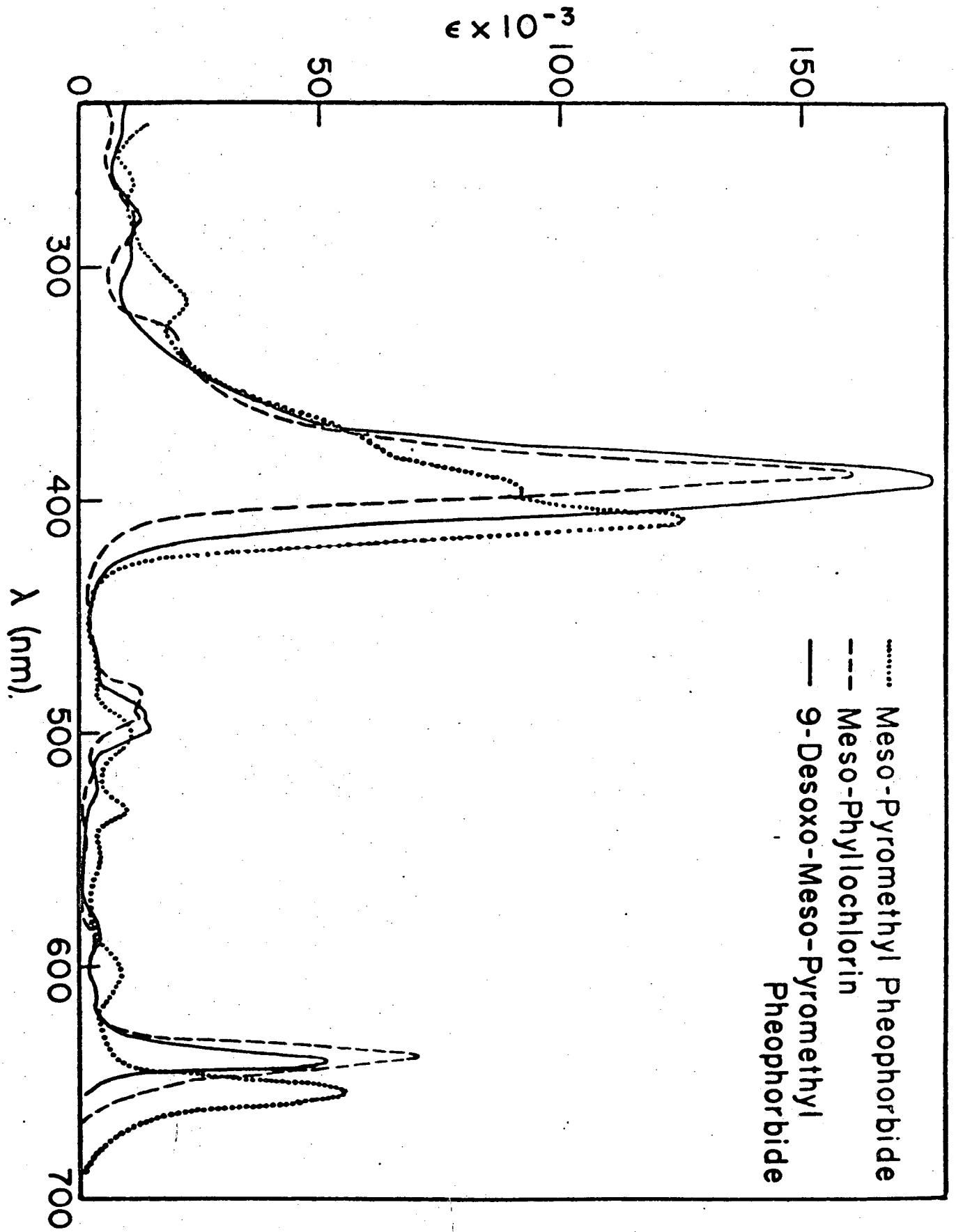
ε x 10⁻³
0
50
100
150
300
400
500
600
700
λ (nm)
Meso-Pyromethyl Pheophorbide
Meso-Phyllochlorin
9-Desoxo-Meso-Pyromethyl Pheophorbide

Fig. 12

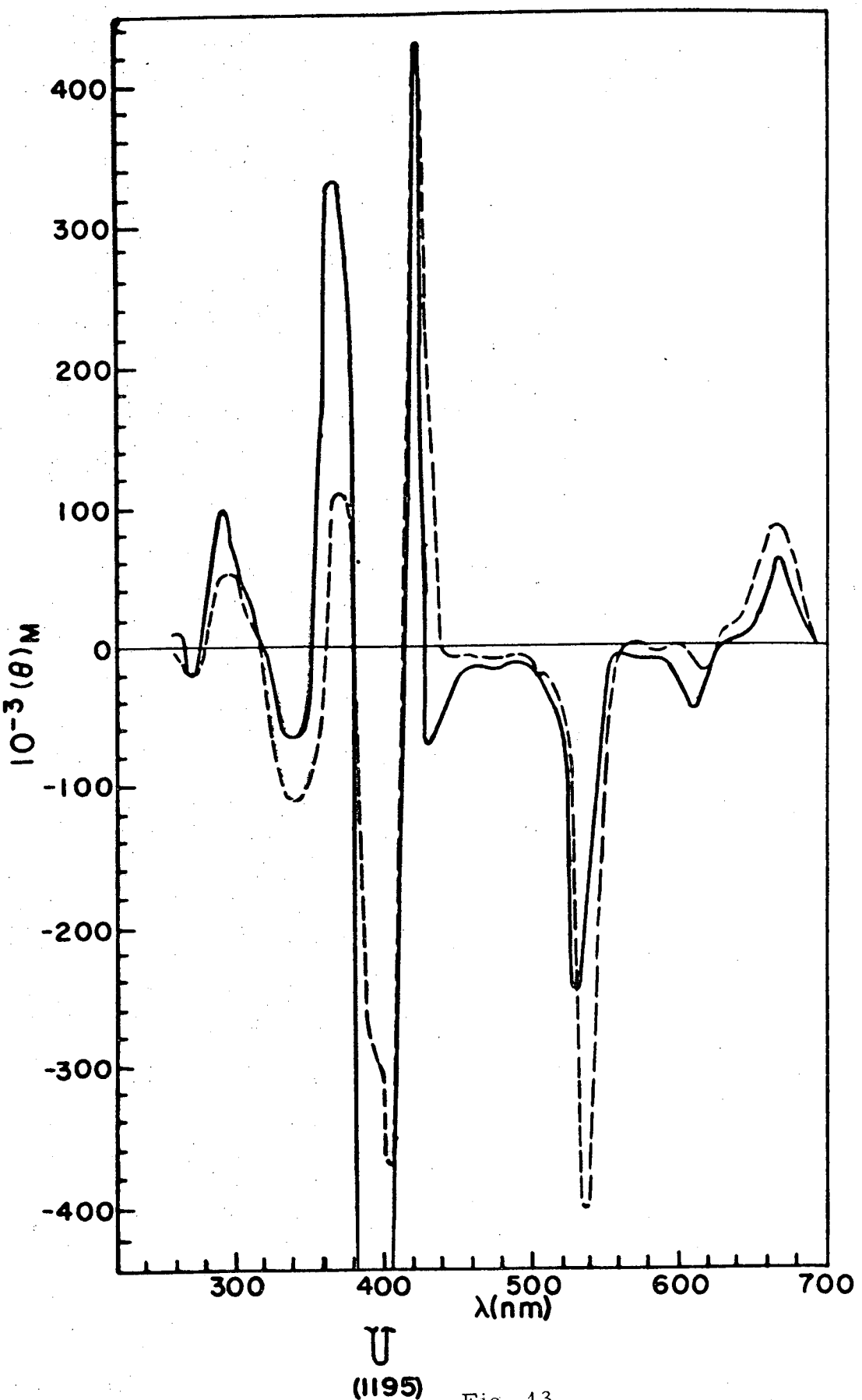
400
300
200
100
0
-100
-200
-300
-400
$10^{-3}(\theta)_M$
300
400
500
600
700
λ(nm)
U
(1195)

Fig. 13

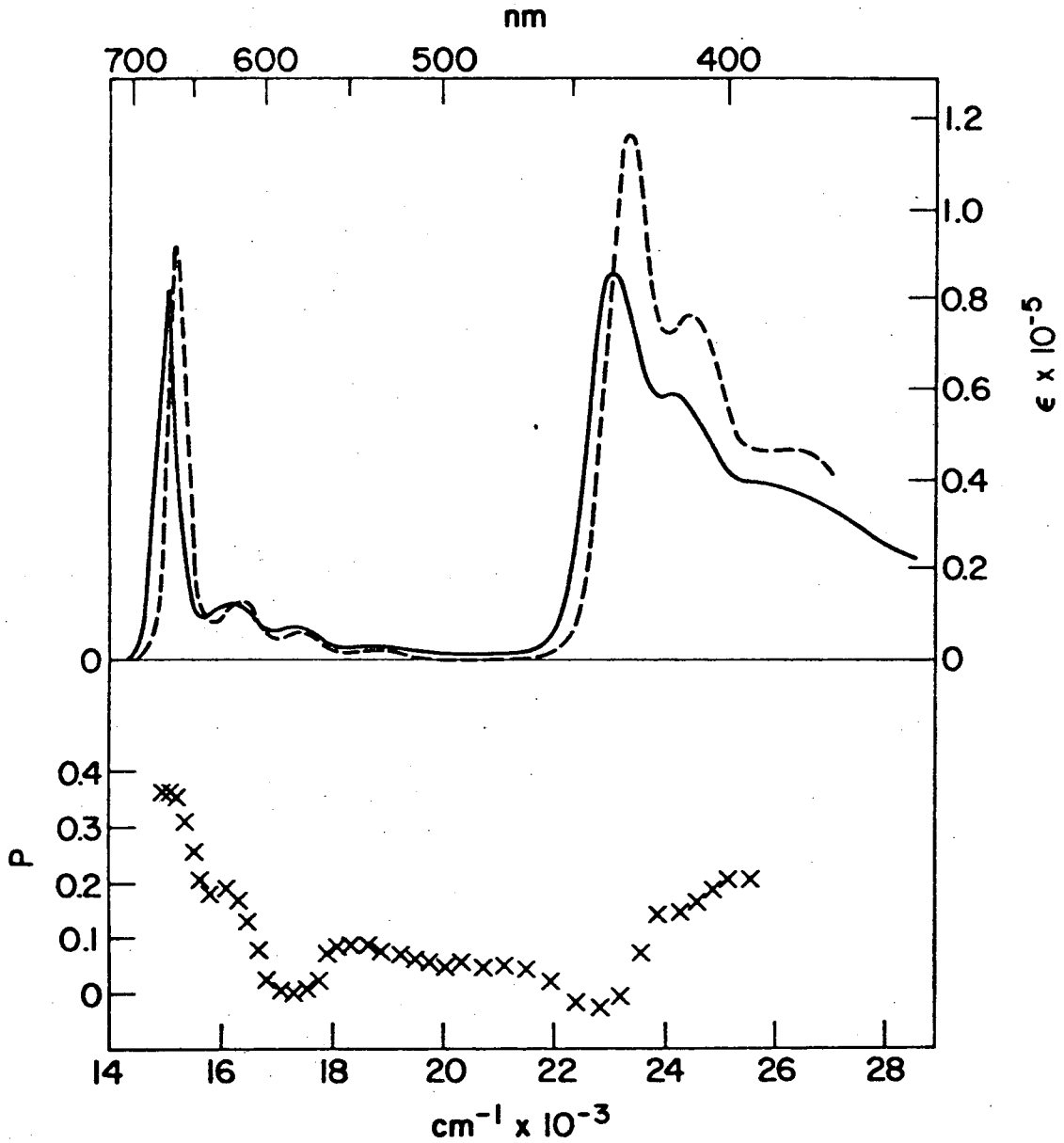
nm
700
600
500
400
1.2
1.0
0.8
0.6
0.4
0.2
0
ε x 10⁻⁵
0
0.4
0.3
0.2
0.1
0
P
14
16
18
20
22
24
26
28
cm⁻¹ x 10⁻³

Fig. 14

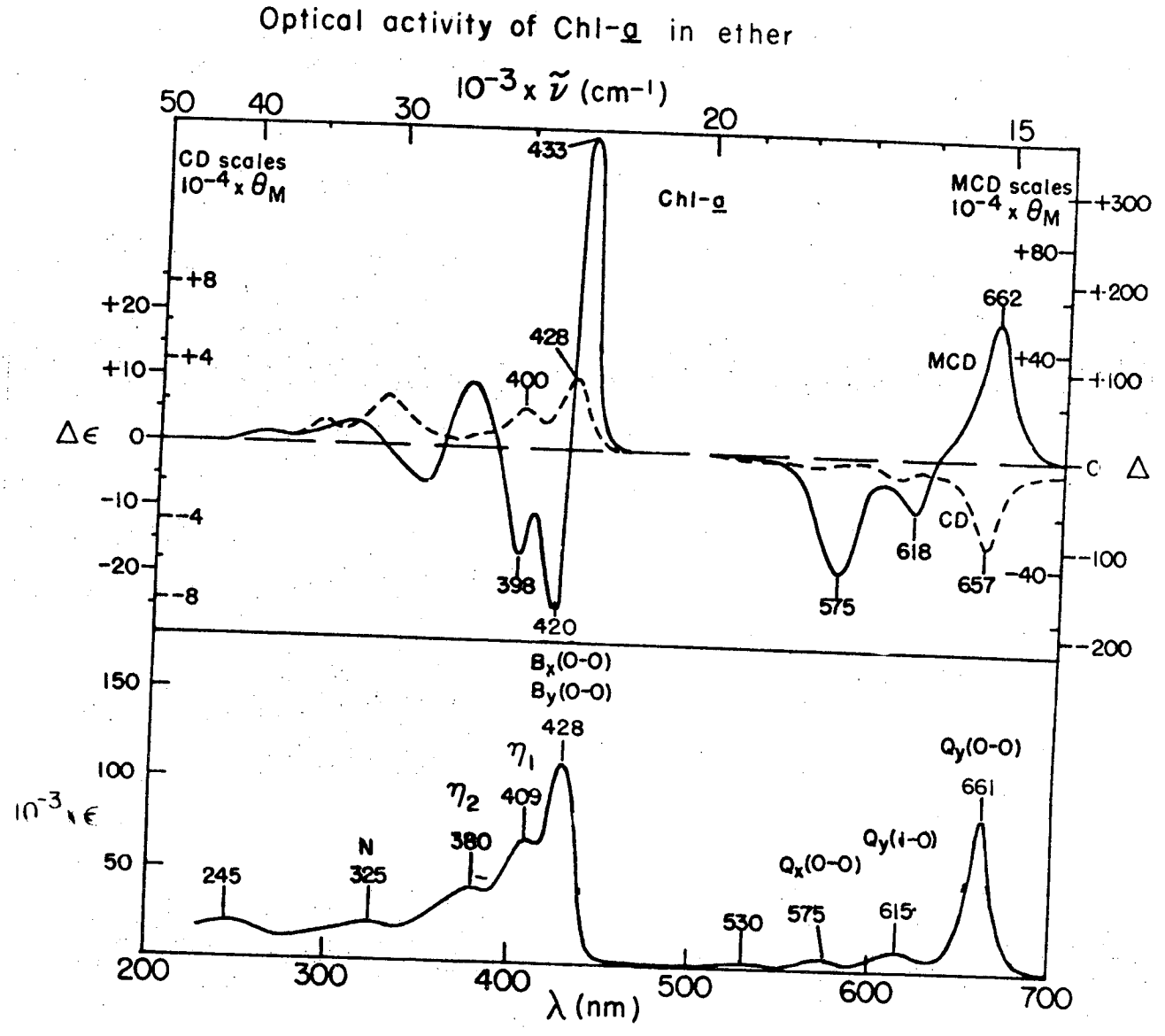

Fig. 15

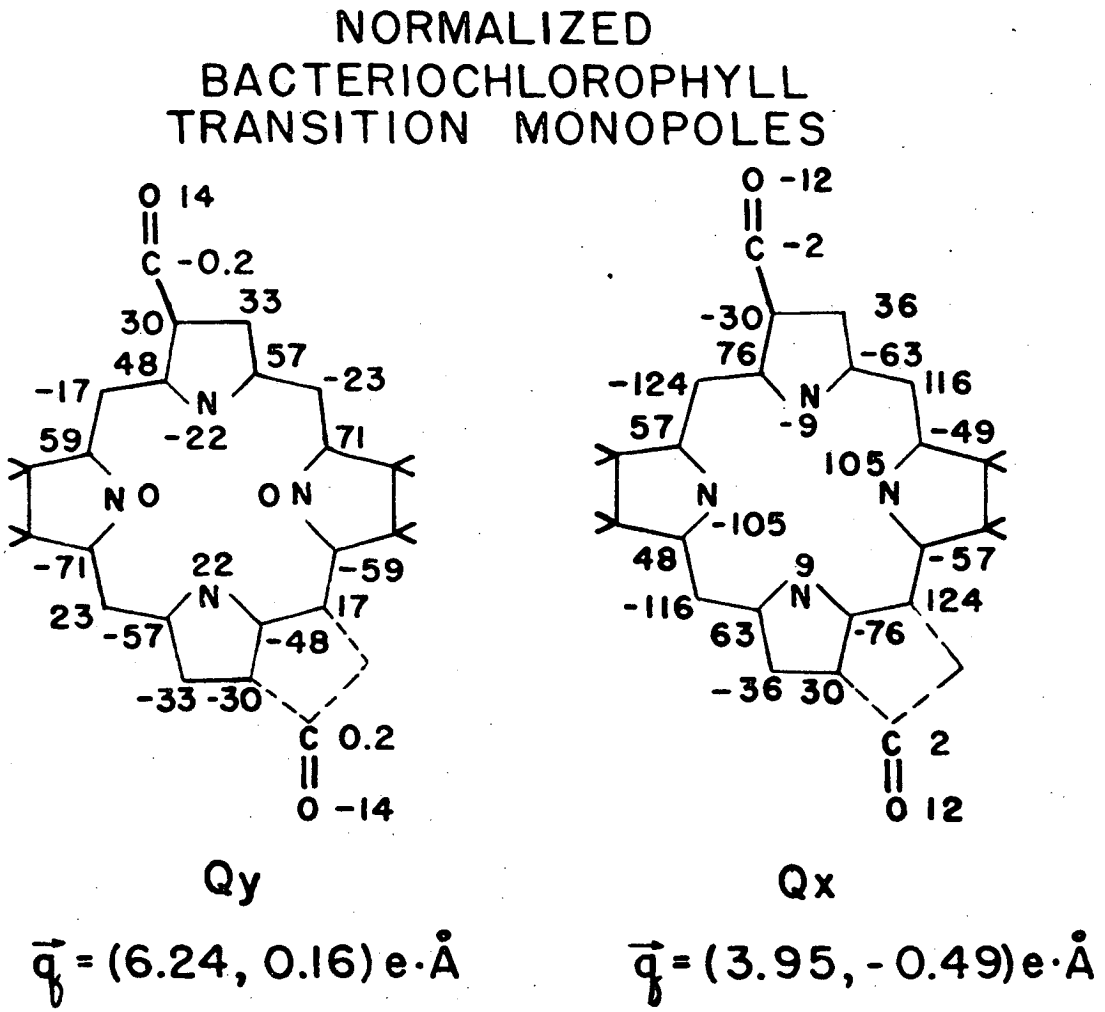
NORMALIZED
BACTERIOCHLOROPHYLL
TRANSITION MONOPOLES
O 14
C -0.2
30
33
48
57
-23
-17
N
-22
59
71
NO
ON
-71
22
N
-59
23
-57
17
-48
-33 -30
C 0.2
O -14
Qy
$\vec{q}$ = (6.24, 0.16) e·Å
O -12
C -2
-30
36
76
-63
-124
N
-9
116
57
-49
105
N
N
-105
48
9
-57
-116
N
124
63
-76
-36 30
C 2
O 12
Qx
$\vec{q}$ = (3.95, -0.49) e·Å

Fig. 16

$\beta_{CO} = -2.36$

2,6 DICARBONYL OPP-THP (BACTERIOCHLOROPHYLL)

2-VINYL-6-CARBONYL CHLORIN (CHLOROPHYLL A)

CHARGE DENSITIES:

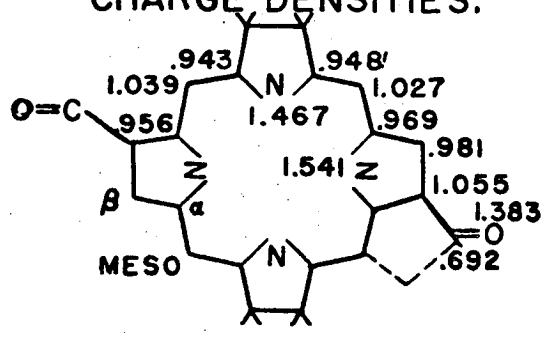

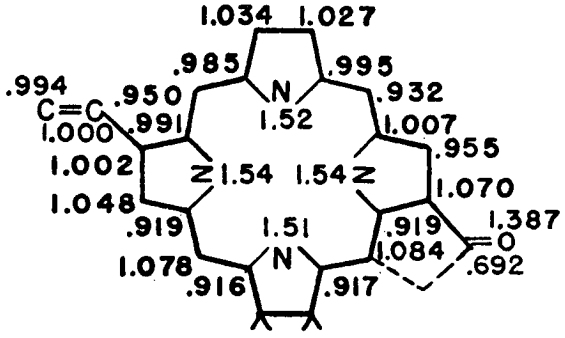

BOND ORDERS:

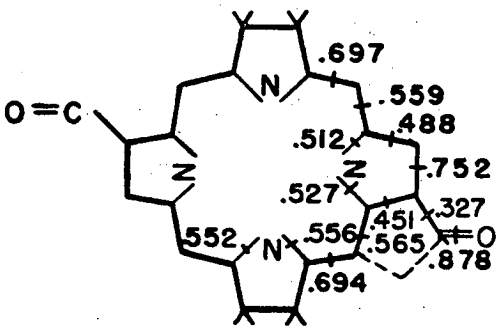

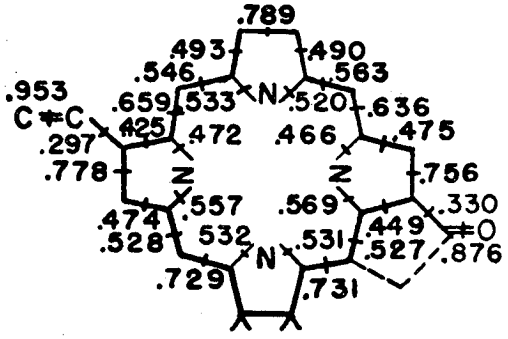

Fig. 17

$\beta = -2.36$

2-VINYL-6-CARBONYL CHLORIN

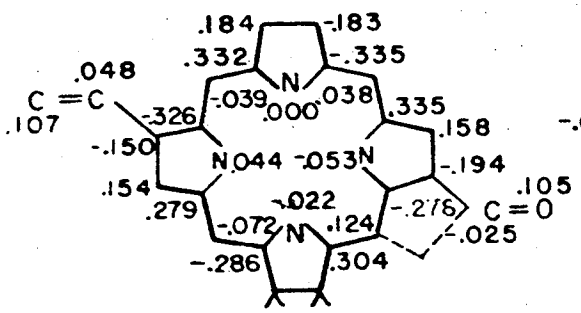

2,6-DICARBONYL OPP-THP

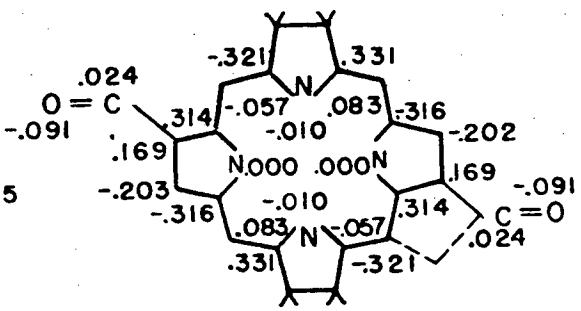

HIGHEST FILLED

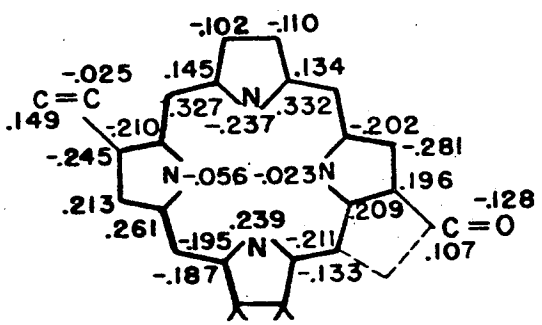

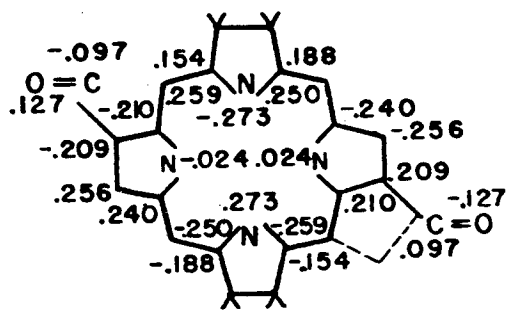

LOWEST UNFILLED

Fig. 18

Table I. Structure of Chlorins

(a)

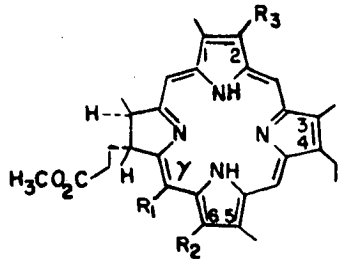

No.	R_1	R_2	R_3	Compound
1	$CH_2CO_2CH_3$	CO_2CH_3	$CH{=}CH_2$	Chlorin e_6 trimethyl ester
2	H	CO_2CH_3	$CH{=}CH_2$	Rhodochlorin dimethyl ester
3	H	CO_2CH_3	CH_2CH_3	Meso-rhodochlorin dimethyl ester
4	H	H	CH_2CH_3	Meso-pyrrochlorin methyl ester
5	H	H	$CH{=}CH_2$	Pyrrochlorin methyl ester
6	CH_3	H	$CH{=}CH_2$	Phyllochlorin methyl ester
7	CH_3	H	CH_2CH_3	Meso-phyllochlorin methyl ester
8	H	CH_2CH_3	CH_2CH_3	Etiochlorin free base
9	$COCO_2CH_3$	CO_2CH_3	$CH{=}CH_2$	Purpurin 7 trimethyl ester

(b)

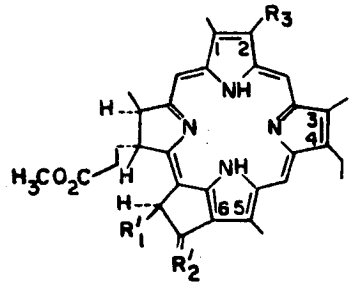

	R'_1	R'_2	R_3	
10	CO_2CH_3	O	$CH{=}CH_2$	Methyl pheophorbide a
11	H	O	$CH{=}CH_2$	Pyromethyl pheophorbide a
12	H	O	CH_2CH_3	Meso-pyromethyl pheophorbide a
13	H	H_2	CH_2CH_3	9-desoxo-meso-pyromethyl pheophorbide a

Table I. Continued

(c)

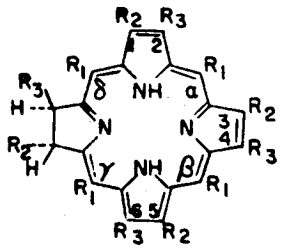

No.	R_1	R_2	R_3	Compound
14	H	CH_3	CH_2CH_3	Etiochlorin free base
15	H	H	H	Chlorin free base
16	C_6H_5	H	H	Tetraphenyl chlorin free base

(d)

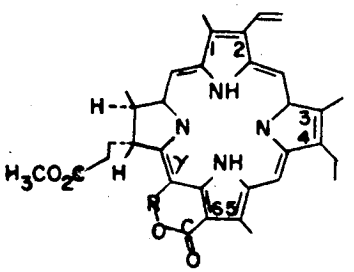

No.	R	Compound
17		Purpurin 18-methyl ester
18	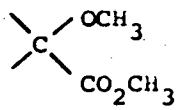	Purpurin 7-lactone methyl ether methyl diester

Table II* Spectra of Reduced Porphyrins - Comparison of Theory & Experiment

Compound	CI	β_{CO} (eV)	E_{Qy} (cm^{-1})	f_{Qy}[d]	θ_{Qy}[c]	ΔE_Q	E_{Qx}	f_{Qx}[d]	θ_{Qx}[c]	E_{B_1}[f]	f_{B_1}[d]	θ_{B_1}[c]	ΔE_B	f_{B_2}[d]	θ_{B_2}[c]
Chlorin: Theory	4-orb	-	17030	.195	90°	1410	18440	.030	0°	29100	2.55	90°	260	2.95	0°
	CI to 150	-	16170	.14	90°	1540	17710	.027	0°	28580	2.32	0°	170	2.33	90°
Expt[2]	-	-	16390	(56)[g]	b	1280	17670	(7.7)[g]	b	24880	(309)[g]	b	0?[i]	-	-
6-carbonyl chlorin: Theory	4-orb	-3.19	16900	.23	92°	1560	18460	.043	11°	29010	2.60	71°	190	2.81	-15°
	CI to 150	-3.19	16010	.17	92°	1690	17700	.037	9°	28350	2.36	29°	210	2.32	61°
	CI to 150	-2.36	15960	.18	92°	1740	17700	.042	12°	28100	2.45	47°	360	2.21	-47°
Expt[p]	-	-	15150	.13	b	2150	17300	(9.0)[g]	b	23150	1.4[h]	b	0[j]	-	b
2-Vinyl-6-Carbonyl Chlorin: Theory	4-orb	-3.19	16820	.26	91°	1580	18400	.051	24°	28660	2.59	85°	210	2.76	-4°
	CI to 150	-3.19	15990	.21	90°	1770	17760	.046	24°	27440	1.78	-65°	690	2.34	17°
	CI to 155	-2.36	15980	.22	91°	1780	17760	.052	27°	27330	1.92	-83°	610	2.16	23°
Chlorophyll a: Theory	Song Calc.[51]	-3.00	15720	.33	∥	2490	18210	.08	⊥	24760	3.07	∥	1700	3.28	⊥
													2500	3.38	∥
Expt[q]	-	-	15100	.23[n]	∥	2200	17300	(9.5)[g]	⊥	23260	1.1[h]	m	0[j]	-	m

Compound	CI	E_{B_x}[u]	f_{B_x}	θ_{B_x}[c]	E_{B_y}	f_{B_y}	θ_{B_y}[c]	E_{N_x}	f_N
OPP-THP: Theory	7-orb	32310	1.49	0°	32810	2.90	90°	32310	1.17
	CI to 150	32010	1.93	0°	32570	2.91	90°	30230	.65
	Otten Calc.[46]	29980	2.24	0°	31190	2.07	90°	26100	.08
Expt[r]	-	b	b	b	b	b	b	b	b
2 6 Dicarbonyl OPP-THP: Theory	4-orb	31030	2.48	9°	32450	2.94	-82°	-	-
	CI to 150	31290	2.19	32°	31960	2.66	-73°	29720	.54
	CI to 160	30790	2.41	41°	31580	1.96	-68°	29450	.66
Mg Bacteriochlorophyll: Theory	Song Calc.[51]	28310	1.36	⊥	29920	0.62	∥	26800	.02
					30080	0.18	⊥		
Expt[s]	-	25580	.5	⊥	27930	1.2[k]	∥	25500	e

* All spectroscopic energies in wave numbers. x axis passes through the reduced double bond(s). Note that in Table IV of Ref. 6, the headings Q_x and Q_y are reversed.

[a] Degenerate

[b] not available

[c] angle of polarization measured from +x axis

[d] oscillator strength

[e] unresolved

[f] B_1 and B_2 are the Soret daughters that are lower and higher in energy, respectively

[g] extinction coefficient

[h] includes Soret and η_1 band

[i] shape of spectrum not given but band assumed not split

[j] assuming that shoulder represents a separate transition (see text)

[k] relative intensities depend on solvent

[m] net polarization of overlapping B_x and B_y is ⊥

[n] Oscillator strength in ether[15] and in carbon tetrachloride[13]. Ref. 11 gives f = .16 for Q_y, .03 for Q_x, in ether

[o] Mg Chlorin in benzene[38]

[p] Mg Chlorobium Chlorophyll in ether[15]

[q] Mg Chlorcpyll a in ether[15]

[r] Mg Tetraphenyl OPP-THP in benzene[37]

[s] Mg bacteriochlorophyll in ether[15]

Table III - Effects of Perturbations in Chlorin Spectra ∓

1	2a	2b	3	4	5a	5b	6	7a	7b
Ref.	Compounds Compared		Perturbation		Q_y		Q_x	B	
	#1	#2			ΔE	ϵ_1/ϵ_2	ϵ_1/ϵ_2	ΔE	ϵ_1/ϵ_2
38,76	(15)	(4)	H_7 → alk$_7$ [d]	Expt	-185	0.81	0	-190	.99
76,57	(4)	(8)[e]	H → alk	Expt	+80	1.05	.80	+60	.87
57,77	(8)[e]	(3)	6-alk → 6-CO [a]	Expt	-255	.94	1.32	*	*
59	(13)	(12)	6-alk → 6-CO [b]	Expt	-400	.90	0.35	-1010	1.30
			H_2 → CO	Theory	-170[f]	.81[c]	.68[c]	-270	1.00[c]
77,9	(3)	(2)	2-alk → 2-V	Expt	-300	1.06	.64	*	*
76,77	(4)	(5)	2-alk → 2-V	Expt	-300	1.37	1.45	*	*
9	(12)	(11)	2-alk → 2-V	Expt	-300	1.06	1.03	-300	1.08
57,77	(7)	(6)	2-alk → 2-V	Expt	-350	1.03	0.74	*	*
			H_2 → V_2	Theory	+20	.84[c]	.82[c]	-430[c]	1.10[c]
9	(2)	(1)	γ-H → γ-Me	Expt	+20	1.15	.94	-60	.97
76,57	(4)	(7)	γ-H → γ-Me	Expt	+50	1.22	1.38	+130	1.13
77	(5)	(6)	γ-H → γ-Me	Expt	-130	.92	.61	*	*
9	(1)	(10)	close pentenone isocyclic ring	Expt	-50	.96	.49	-550	1.29
57	(7)	(13)	Close pentene isocyclic ring	Expt	+120	.96	.67	-130	.92

∓ Explanation: This table compares the spectra of pairs of closely related compounds in column 2. These are chosen to exemplify the substituent perturbations listed in column 3. (Here alk refers to any α-saturated substituent, 6-CO to any α-carbonyl substituent in the 6-position, V to vinyl.) ϵ_1/ϵ_2 is the ratio of the extinction coefficients of the two compounds. Theoretical predictions are based on SCMO-CI calculations on chlorin with only the indicated substitution (average of available calculations). $f_B = f_{B_x} + f_{B_y}$. ϵ_B is the experimental Soret maximum whether or not the band is split. For numbering of atoms see Table I. All spectra in dioxane except as noted by [d].

Notes:
- * spectrum not available
- a no isocyclic ring
- b with isocyclic ring
- c ratio of oscillator strengths
- d benzene solvent
- e Soret band is octamethyl chlorin free base[39]
- f Should be compared with $-360 = -185 + 80 - 255$

TABLE IV. Predicted Energy of Lowest Triplet Configurations

Compound	β_{co}(eV)	$^3E_1$	$^3E_2$	$^3E_3$	$^3E_4$ (cm^{-1})
Porphin	---	11160	11160	14540	14540
Carbonyl Porphin	-2.36	10870	11370	14230	14770
	-3.19	10910	11330	14290	14710
Protochlorophyll	(Song)	12740		15080	
Chlorin		11070	11440	15850	16970
6-Carbonyl Chlorin	-2.36	11040	11500	16150	17240
	-3.19	11040	11470	16090	17190
Chlorophyll a	(Song)	11050		15729	
ADJ-THP		11210	14390	16780	17050
OPP-THP		5630	9810	17030	22050
2,6-Carbonyl OPP-THP	-2.36	5520	9540	17290	22190
	-3.19	5540	9570	17210	22120
Bacteriochlorophyll a	(Song)	7100		14040	

TECHNICAL INFORMATION DIVISION
LAWRENCE BERKELEY LABORATORY
UNIVERSITY OF CALIFORNIA
BERKELEY, CALIFORNIA 94720